Experimental and numerical modeling of waves routing on permeable soils

POLITECNICO DI TORINO

Ph.D. in Water and Land Management Engineering

Experimental and numerical modeling of waves routing on permeable soils

Stefania Grimaldi
matr. 169411

Advisor:
Prof. Davide Poggi

Ph.D. Dissertation

March 2013

I would like to thank my advisor, Prof. Davide Poggi, for his guidance.
I wish to extend my warmest thanks to Dr. Edoardo Daly for his support during my visits at Monash University (Clayton, Australia).
A simple "thanks" would not be enough for all my colleagues, friends more than colleagues.

Summary

Introduction 1

1. A review on coupled surface and subsurface flows..... 6
1.1 Surface flow..... 7
1.2 Subsurface flow..... 9
1.2.1 Soil definition..... 9
1.2.2 Energy state of soil water and soil water retention curve 9
1.2.3 Hydraulic conductivity..... 13
1.2.4 Moisture profiles during infiltration and percolation..... 14
1.2.5 Flow of water in saturated soil..... 15
1.2.6 Flow of water in unsaturated soil..... 15
1.2.6.1 Richards equation 15
1.2.6.2 Physically based models..... 16
1.2.6.3 Semi-empirical models..... 18
1.2.6.4 Empirical models..... 19
1.2.6.5 Empirical *vs* physical models 20
1.3 Coupling strategies for surface-subsurface flow 21
1.3.1 Internal iterative coupling..... 23
1.3.2 External iterative coupling..... 26

2. Infiltration of overland flow: experimental and numerical modeling
2.1 Introduction....28
2.2 Flume tests, experimental setup....30
2.3 Sand parameters assessment....38
2.3.1 Density....38
2.3.2 Porosity....38
2.3.3 Grain size distribution....39
2.3.4 Saturated hydraulic conductivity....40
2.4 Soil Water Retention Curve....41
2.4.1 Traditional approaches....43
2.4.2 Our approach....45
2.4.3 Column tests, experimental set up....49
2.4.3.1 Tap water....51
2.4.3.2 Tracers....51
2.4.3.3 Soil moisture sensors....57
2.4.4 Implementation of the numerical strategies....60
2.4.5 Results....62
2.4.5.1 Critical issues....62
2.4.5.2 Main drying curve....63
2.4.5.3 Main wetting curve....64
2.5 Numerical model....69
2.6 Conclusions....72

3. Overland flow and infiltration in near horizontal plots: numerical modeling.....

3.1 Introduction 74

3.1 Case study: the biofiltration trench installed at Monash university (Melbourne, Australia) 82

3.2 Hydrologic performances 87

3.3 Hydraulic parameters of the filter media 95

3.3.1 Saturated and residual water contents.....95

3.3.2 Saturated hydraulic conductivity 95

3.3.3 Soil Water Retention Curve.....100

3.4 Numerical model 104

3.5 Analysis of "large" storm events 108

3.5.1 Event "A": clogging of the filter media.....108

3.5.2 Event "B": anomalous functioning.....111

3.5.3 Saturated hydraulic conductivity as a bulk parameter 113

3.6 Numerical analysis of "small" events.....133

3.7 Soil water repellency 141

3.7.1 Origin.....142

3.7.2 Preferential flow pathways 143

3.7.3 Moisture effect on infiltration patterns 146

3.7.4 Concluding remarks.....148

3.7.5 Management strategies 149

3.8 Discussion on the implementation of a lumped model....150

3.9 From diagnosis to prognosis.....154

3.9.1 Assessment of the soil water retention curve.....154

3.9.2 Assessment of the saturated hydraulic conductivity..154

3.10 Conclusions and further developments.....164

References... ……I

Introduction

In the natural hydrologic cycle, water fluxes between the atmosphere, the surface, and the subsurface are continuous regardless of the water phase. Atmospheric water is the source for both surface runoff and vadose zone water through direct infiltration. Surface water infiltrates into the vadose zone or, in cases of shallow groundwater, directly into the saturated zone. Groundwater, whether perched or regional, is a source for surface streams through springs.

Of the freshwater on Earth, nearly 70% is stored in the ground (Shiklomanov, 1993). Groundwater is recharged from, and eventually flows to, the surface naturally; it provides a vital contribute to the streams, springs, wetlands, and surface vegetation during droughts and dry periods.
It is currently recognized as the world's most extracted raw material. Global abstraction grew from a base level of 100–150 km^3 in 1950 to 950–1000 km^3 in 2000. Nowadays, groundwater extraction meets one fifth of current world water needs (Burke, 2007). Future projections state that groundwater exploitation will further increase as climate change will deplete other sources of supply (e.g. Taylor, 2012).
At world level groundwater exploitation roughly covers:

- 50% of drinking water needs;
- 20% of the demand for irrigation water;
- 40% of the needs of self-supplied industry.

In most of the industrialized world, groundwater is the chief drinking-water supply source. Agriculture tends to be the largest exploiter in nearly every country outside the humid intertropical zone, where surface-water resources are scarce. The irrigated areas supplied by groundwater are officially reported at 69 million hectares, up from approximately 30 million hectares during the 1950s (Shah, 2007).

Beside the widely recognized risk of groundwater overdraft, not appropriate application of irrigation techniques could have negative feedbacks on groundwater. In particular, *surface irrigation* techniques may cause deep drainage, pollution, salinization. The term *surface irrigation* refers to a broad class of irrigation methods (mainly, flood plain irrigation, border-strip irrigation, level-basin irrigation, furrow irrigation) in which a surge wave routes from an inlet and water gradually covers the field. This practice is thousands of years old and currently represents as much as 95% of irrigation activity (International Commission on Irrigation and Drainage, 2011).
Overirrigation may cause water to move below the root zone (deep drainage) resulting in rising water tables and, in case chemical additives are used, groundwater pollution. In regions with naturally occurring saline soil layers or saline aquifers, these rising water tables may bring salt up into the root zone (salinization). Careful scheduling of irrigation timing and quantities is beneficial to prevent this issues.

Nevertheless, human induced changes in the infiltrability of the soil surface often causes significant alteration of the natural groundwater recharge regime.
Urban development, roadways, and associated infrastructure highly increase impervious surfaces in a watershed and generally result in reduced infiltration and base flow, while stormwater runoff volumes, peak flows, flood frequency, and flood wave celerity are sensibly enhanced (e.g. Wang et al., 2001; Davis 2003).
These hydrologic changes, termed *hydromodification*, result in groundwater storage depletion; widening and increased instability of stream channels; increased sediment loads, erosion and degradation of both fish habitat and riparian life cycle (e.g. MacRae 1992; Annear et al. 2004; Asleson 2009). In addition to sediments, urban runoff often contains a wide variety of pollutants including nutrients, oxygen-demanding substances, pathogens, road salts, petroleum

hydrocarbons, heavy metals (e.g. Hatt et al., 2004; Leopold, 1968; Meyer et al., 2005).
Low impact development (LID) is a urban planning approach that aims at mimicking the conditions of an initial undeveloped land.
Biofiltration systems are one of the most prominent technologies to mitigate the environmental impacts of urban stormwater runoff (e.g. Davis, 2005; Wong, 2006). Runoff from impervious areas is diverted to a vegetated, close area (the biofiltration facility); surface waves routes while infiltrating into the soil. These facilities provide detention storage and promote water retention through infiltration and evapotranspiration thus reducing volume, peak discharge, and celerity of stormwater runoff while enhancing groundwater recharge. Pollutant removal is achieved via a number of processes including sedimentation, fine filtration, sorption, and biological uptake.

An adequate understanding of surface-subsurface flow interactions is thus essential for water management both in rural and in urban areas.
Analysis have been conducted over a range of scales, from field (e.g. Schmitz & Seuss, 1989; Bautista et al., 1998; Wohling et al., 2007), to hillslope and streambed (e.g. Harvey & Bencala, 1993; Fan & Bras, 1998; Storey et al., 2003), to watershed (e.g. Nikolaidis et al., 1993; Michaud & Sorooshian, 1994; Blasch et al., 2006; Rigon et al. 2006).
Quite different modeling approaches have been typically used at small (field to hillslope) and large (watershed to continental) scales.
At finer scales, a detailed physical insight on both surface and subsurface processes is essential.
Such a study may be of great interest for several purposes, e.g. (a) the optimal use of water for surface irrigation; (b) the analysis of the exchanges between surface and underground water resources; (c) the optimization of innovative solutions for urban runoff mitigation and treatment.

Referring to surface irrigation techniques, a physically based modeling of (i) the celerity of the surface wave, (ii) the relative quantities of water routing on the surface and moving downwards through the ground, (iii) the subsurface flow patterns, (iv) water distribution and residence time in the soil could provide a useful planning tool to (1) enhance water use efficiency; (2) manage ground

water recharge; (3) avoid deep percolation of fertilizers or other chemical products.
Water use efficiency is a term commonly used to describe the relationship between water (input) and agriculture product (output). Lack of water could lead to low production or event to the wilting of the plants. On the contrary, waterlogging can cause the plant to shut down delaying further growth until sufficient water drains from the rootzone. On this topic A.Deakin in 1890 stated "*It is not the quantity of water applied to a crop, it is the quantity of intelligence applied which determines the result - much more is due to intelligence than water in every case*".

A physically based hydraulic modeling of the functioning of an biofiltration facility is essential for the assessment of (i) the outflow hydrograph resulting from a given input; (ii) the soil moisture patterns in the filter media. The latter have a crucial impact on both hydrologic and pollutant removal performances of a facility (e.g. Li et al., 2009; Lintern et al. 2011). Improving the system understanding could thus provide a valuable tool for both design and management purposes.

Our study on waves routing on permeable boundaries focused on the finer scale of near horizontal plots. In particular, it involved two phases: a first, propaedeutic experimental and numerical modeling of the infiltration process was completed by the complete numerical modeling of the coupled phenomena observed in an infiltration trench.
The experimental activity was completed in the *Hydraulics Laboratory "G.Bidone"* of the Polytechnic University of Turin. The routing of surges on a permeable bottom boundary was modeled in a prismatic flume; complementary experimental activities were completed to assess the parameters required for a coherent modeling of the sampled data. Surface and subsurface flow data were recorded and used for the complete numerical modeling of the infiltration process. The main objectives of these activities were (a1) the analysis of the experimental issues connected with the modeling of the infiltration process consequent to the routing of a surface wave; (b1) the analysis of the numerical issues connected with the physical modeling of a 2D infiltration flow due to a surge wave; (c1) the

analysis of simple, parsimonious methods for the assessment of soil parameters.

The complete analysis of overland flows on permeable soils in near horizontal plots was then achieved through the numerical modeling of a specific case study, i.e. the infiltration trench installed at Monash University in Melbourne. Interesting insights on the interactions of the main parameters (i.e. inflow hydrographs, infiltration trench geometry, soil features) leading the hydraulic behavior of an biofiltration trench were pointed out.

The resulting numerical model (a2) improved the system understanding; (b2) documented hydrologic performances; (c2) provided a valuable tool for design and management purposes.

A short outcoming of this study will be the analysis of the behavior of the infiltration trench during a complete hydrological cycle. This analysis is beneficial for the definition of optimal design parameters (mainly, geometry, soil type, vegetation type) and management protocols for both quantitative and qualitative treatment of stormwater runoff according to site specific conditions (mainly, frequency, intensity, and volume of precipitation; temperature).

Chapter 1

A review on coupled surface and subsurface flows

A complete coupled surface-subsurface flow system includes the surface component, the subsurface component, interfacial (i.e., between the surface and the subsurface) boundary conditions, external boundary conditions, and initial conditions. Water flow in both domains, above and below the soil surface, obeys the basic physical laws of conservation of mass and momentum. However, each domain has seen a different development through history leading the surface component to the Saint-Venant equations and the subsurface component to the Richards equation.

1.1 Surface flow

The Saint Venant equations are a set of hyperbolic partial differential equations that describe one-dimensional flow below a pressure surface in a fluid (usually, but not necessarily, a free surface) In particular, Eq. 1a is a mass balance equation, while Eq. 1b**Errore. L'origine riferimento non è stata trovata.** is a momentum conservation equation.

$$\frac{\partial \Omega}{\partial t} + \frac{\partial Q}{\partial x} = q_r - q_s \qquad \text{Eq. 1a}$$

$$\begin{aligned} & c_1 \frac{1}{g\Omega}\frac{\partial Q}{\partial t} \\ & + c_2 \left\{ \frac{1}{g\Omega}\frac{\partial}{\partial x}\left(\frac{Q^2}{\Omega}\right) + \frac{1}{g\Omega}\left[u_{rx} q_r - u_{sx} q_s - (q_r - q_s)\frac{Q}{\Omega}\right] \right\} \\ & + c_3 \frac{\partial h}{\partial x} - c_4 (S_0 - S_f) = 0 \end{aligned} \qquad \text{Eq.1b}$$

The independent variables are time, t [T], and the space coordinate, x [L]. The dependent variables are the fluid discharge, Q [L^3/T], and the fluid velocity field, U [L/T]. The force acting on the fluid is gravity, represented by the gravitational constant, g [L/T^2]. Ω [L^2] is the flow cross-sectional area, q_s [L^2/T] is a sink term (e.g., infiltration or lateral losses, in terms of volume per unit length per unit time), q_r [L^2/T] represents channel sources (due to, e.g., rain, in terms of volume per unit length per unit time), u_{sx} [L/T] and u_{rx} [L/T] are x components of the channel sinks and sources, S_0 and S_f (both dimensionless) are channel and friction slopes, respectively, and c_1 through c_4 (dimensionless) are parameters used to reduce the general equation to its subversions. All subversions leave large space for empiricism, especially with regard to the way the friction slope, S_f, is modeled, where Manning's equation is typically used.

The sink–source terms are worth a short discussion. While for the mass balance equation both rain and infiltration are well understood, this is not the case for momentum transfer. When horizontal surface flow is considered the horizontal component of the rain (due to wind speed) can be significant, especially if the surface area of the surface

water is large. On the other hand, the infiltration horizontal component of momentum transfer is hardly evident and indeed hardly accounted for. It is speculated that it should be used only when modeling very steep flow. Setting different values to the parameters, leads to different versions of the surface flow models, namely,

- the kinematic wave when $c_1 = c_2 = c_3 = 0$ and $c_4 = 1$
- the zero inertia (or diffusion wave) approximation if $c_1 = c_2 = 0$ and $c_3 = c_4 = 1$;
- the gravity wave approximation when $c_1 = c_2 = c_3 = 1$ and $c_4 = 0$;
- the quasi-steady dynamic wave if $c_2 = c_3 = c_4 = 1$ and $c_1 = 0$;
- the (hydro) dynamic wave, i.e. the full partial differential equation $c_1 = c_2 = c_3 = c_4 = 1$.

1.2 Subsurface flow

Subsurface flow, in hydrology, is the flow of water beneath earth's surface. Rigorously speaking, *infiltration* is the process of water penetration from the ground surface into the soil. The subsequent movement of infiltrated water in the unsaturated zone of a soil is called *redistribution*. This can involve *exfiltration* (evaporation from the upper layer of the soil), *capillary rise* (movement upward from the saturated zone to the unsaturated zone due to surface tension), *recharge* (movement of water in the unsaturated zone towards the saturated zone) and *interflow* (flow that moves downslope). *Percolation* is a general term for the downward flow in unsaturated or saturated zone. The term *infiltration* is often used to address both the process of water penetration from the ground surface into the soil and the downward flow in unsaturated or saturated zone.

1.2.1 Soil definition

Soil is a three-phase system comprised of minerals and organic matter (solid phase), water, and air. The composition and proportion of these components greatly influence soil physical properties, including texture, structure, and porosity. Soil texture is the proportion of three mineral grain size categories, i.e. sand, silt and clay. Soil structure is the arrangement and binding together of soil particles into larger clusters, called aggregates or ‘peds.’ Porosity is the fraction of pore space in a soil. Soil texture, structure, and porosity, directly affects water and air movement in the soil.

1.2.2 Energy state of soil water and soil water retention curve

Soil water can contain energy in varying quantities and forms. Classical physics recognizes two principal forms of energy, kinetic and potential. Because the movement of the water in the soil is quite slow, its kinetic energy is generally negligible. On the other hand, the

potential energy is of primary importance in determining the state and movement of water in the soil.

Philipp (1960) defined the total soil-water potential as "minus the work required, isothermally and reversibly, per unit quantity of water, to completely remove the water from the soil and to transform it into pure, free water at some specified datum level". Force fields result from the mutual attraction between the solid matrix and water, from the presence of solutes in the soil solution, as well as from the action of external gas pressure and gravity. Accordingly, the total potential of soil water can be thought of as the sum of the separate contributions of these various factors (Eq. 2):

$$\Phi_t = \Phi_g + \Phi_p + \Phi_o + \cdots \qquad \text{Eq. 2}$$

where Φ_t [M/(LT^2)] is the total potential, Φ_g the gravitational potential, Φ_p the pressure potential, Φ_o the osmotic potential, and the ellipsis signifies that additional terms are theoretically possible.

The gravitational potential of soil water at each point is determined by the elevation of the point relative to some arbitrary reference level.

The pressure potential of soil moisture is also termed as capillary potential or matric potential. It results from the interactive capillary and adsorptive forces between water and the soil matrix, which bind water in the soil. The pressure potential is considered positive when soil water is at hydrostatic pressure greater than atmospheric, otherwise it is negative and it is commonly known as tension or suction. Tension and suction are thus semantic devices to avoid the use of the negative sign.

The osmotic potential express the lowering effect of solutes on water potential energy.

The soil-water potential can be expressed in terms of an equivalent head of water h (commonly called potential or hydraulic head) [L], which is the height of a liquid column corresponding to the given pressure (Eq. 3).

$$h = z + \psi + \Phi_o/g + \cdots \qquad \text{Eq. 3}$$

were z is the gravitational head, ψ is the soil water pressure head, Φ_o/g is the osmotic head.

In a saturated soil at equilibrium with a body of free water at the same elevation, soil water is at atmospheric pressure, hence the hydrostatic

pressure is zero. If a slight suction (i.e. a water pressure slightly sub-atmosperic) is applied to water in a saturated soil, no outflow occurs until, as suction is increased, a critical value is exceeded at which the largest surface pore begins to empty and its water content is displaced by air. This critical suction is called the *air-entry* suction. As suction is applied incrementally, the first of the pores to be emptied are the relatively large ones. Increasing suction is thus associated with decreasing soil wetness. The amount of water remaining in the soil at equilibrium is a function of the sizes and volumes of the water filled pores and of the amount of water adsorbed to the particles, hence it is a function of the matric suction. This function is represented graphically by a curve called soil water retention curve (SWRC), also known as the soil-moisture release curve or the soil-moisture characteristic (Childs, 1940; Klute, 1986; Bruce and Luxmoore, 1986). Although the characterization and estimation of the SWRC has been a major focus of research for more than 60 years, no universal theory exists for prediction of the matric suction versus wetness relationship from basic soil properties (i.e., texture and structure). The adsorption and pore-geometry effects are generally too complex to be described by a simple model. As a consequence, the SWRC is usually obtained experimentally in either one of these two ways: (1) in desorption, by starting with a saturated sample and applying increasing suction, in a step-wise manner, to gradually dry the soil while taking successive measurements of wetness versus suction; and in (2) sorption, by gradually wetting an initially dry soil sample while reducing the suction incrementally. Each of these protocols yields to a different continuous curve. This dependence of the equilibrium content and state of soil water upon the direction of the process leading up to it is called hysteresis (Haines, 1930; Miller and Miller, 1955-56; Philip, 1964).

Many empirical models (e.g. Gardner, 1958; Brooks and Corey, 1964; Campbell, 1974; Clapp and Hornberger, 1978; van Genuchten, 1980; Hutson and Cass, 1987; Russo, 1988) have been developed for modeling both the SWRCs. In particular, the soil-moisture characteristic commonly reported in literature is the desorption curve, more easy to determine.

Four different phenomena are responsible for the occurrence of hydraulic hysteresis, namely, (i) air entrapment in “blind” or “dead-

end" pores, which further reduces the water content of newly wetted soils (Poulovassilis 1970; Vogler et al.1999); (ii) inkbottle effect resulting from the geometric nonuniformity of the individual pores (see for example, Sharma 1998); (iii) contact angle effect by which the contact angle and the radius of curvature are greater in the case of an advancing meniscus than in the case of a receding one (Bear 1979); (iv) swelling, shrinking, or aging phenomena which result in differential changes of soil structure, depending on the wetting and drying history of the sample (Hillel and Mottes, 1966).

The two complete characteristic curves, from saturation to dryness and vice versa, are the main branches of the hysteretic soil moisture curve. When a partially wetted soil commences to drain, or when a partially desorbed soil is rewetted, the relation of suction to moisture content follows some intermediate curve named *scanned curve*; cyclic changes often entail wetting and drying scanning curves, which may form loops between the main branches.

In the past, hysteresis was generally disregarded in the practice of soil physics because of the lack of good data. This may be justifiable in the treatment of processes involving monotonic wetting (e.g., infiltration) or monotonic drying (e.g. evaporation). Nevertheless hysteresis is important in cases of composite processes where wetting and drying occur simultaneously or sequentially in various parts of the soil profile (e.g. Liu *et al.*, 1995; Ritsema *et al.*, 1998; Di Carlo *et al.*, 1999; Pham et al., 2003).

Measurement of soil water hysteresis is deeply time consuming. Experimental generation of a complete data set may require several months or even years. Therefore a number of attempts have been made to describe the interrelationships between hysteretic water retention curves. The various models used to predict hysteretic SWCCs can be classified into two categories: domain models and empirical models.

Domain models (e.g. Poulovassilis, 1962; Mualem, 1972-1977-1984; Parlange, 1976-1980; Hogarth, 1988) assume that there are two states, i.e. when soil suction increases to a certain suction value then the pore is drained spontaneously, and when soil suction decreases to a certain value then the pore is filled spontaneously.

Empirical analytical models (e.g. Scott et al., 1983; Kool & Parker, 1987; Nimmo, 1992; Feng and Fredlung, 1999; Pham, 2003; Wheeler

et al., 2003) assume that the primary, secondary, and higher-order scanning curves can be scaled from the main hysteresis curve; different analytical expressions describing the soil water characteristic curve were used in these studies.
The same models may also be classified according to the measured data required (for instance, boundary hysteresis loop and one family of primary scanning curves; boundary hysteresis loop; one branch of boundary hysteresis loop and two meeting points; two parallel boundary curves; one boundary curve and one specified point on the other boundary curve).

1.2.3 Hydraulic conductivity

The hydraulic conductivity of a soil is a measure of the soil's ability to transmit water when submitted to a hydraulic head gradient.
Perhaps the most important difference between unsaturated and saturated flow lies in the hydraulic conductivity. When the soil is saturated , all the pores are water-filled and conducting; the water phase is then continuous and the conductivity is maximal. When the soil desaturates, some of the pores become air filled so that the conductive portion of the soil’s cross-sectional area diminishes. As suction develops, the first pores to empty are the largest ones, which are the most conductive, thus relegating flow to the smaller pores. At the same time, the large, empty pores must be circumvented, so that, with progressive desaturation, tortuosity increases. Water flow in an unsaturated soil may occur either as film creep along the walls of wide pores, or as tube flow trough narrow water-filled pores. The transition from saturation to unsaturation generally entails a steep drop in hydraulic conductivity. The conductive properties of unsaturated soils depend greatly on their texture and structure. Generally speaking, for a given degree of soil saturation, the hydraulic conductivity increases by several orders of magnitude going from clay to silty clay loam to sand. The steep decline of hydraulic conductivity with rising matric suction carries important implications regarding soil-water dynamics. It suggests that processes taking place in wet soil conditions are generally inherently faster than those occurring in drier soil conditions. The relation of conductivity to suction is slightly affected by hysteresis.

Various empirical equations have been proposed for the relation of conductivity to suction or wetness, e.g. Gardner (1960), Corey (1977), Mualem (1976), Van Genuchtne (1980).

1.2.4 Moisture profiles during infiltration and percolation

The typical moisture profile during infiltration was described by Bodman and Colman (1944) and is shown schematically in Fig. 1.
The examination of an initially dry, texturally uniform soil profile at any moment during infiltration under ponding generally shows the surface zone to be saturated to a depth of several millimeters or centimeters. Beneath this saturated zone is a less-than-saturate, lengthening zone of apparently uniform wetness, known as the *transmission zone*, beyond which occurs a *wetting zone*. In the latter zone, soil wetness increases with time at each point, but at any given time wetness decreases with depth at a steepening gradient, down to a *wetting front*. At the *wetting front* the gradient is so steep that there appears to be a sharp boundary between the moistened soil above and the initially dry soil beneath. The transmission zone becomes larger and the wetting zone moves downwards into the soil.

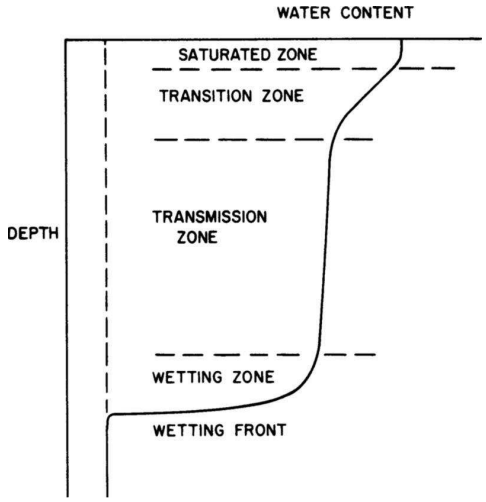

Fig. 1 – Moisture profiles during percolation, Bodman and Colman (1944)

1.2.5 Flow of water in saturated soil

In 1856, Henri Darcy derived an empirical formula for the behavior of water flow through saturated soils.
The instantaneous downward discharge rate Q [L^3/T] through a porous medium is proportional to the product of the saturated hydraulic conductivity of the medium k_s [L/T], the cross-sectional area to flow Ω [L^2] and the head drop ($h_B - h_A$) [L], all divided by the length L_{AB} [L] over which the head drop is taking place (Eq. 4).

$$Q = k_s \Omega \frac{(h_B - h_A)}{L_{AB}} \qquad \text{Eq. 4}$$

Darcy's law is valid for laminar flow of water through saturated soils, which is typical for fine grained soil types, and coarse grained soils proveded hydraulic gradients are low.

1.2.6 Flow of water in unsaturated soil

1.2.6.1 Richards equation

In 1907 Edgar Buckingham presented data and a theoretical conceptualization of soil moisture movement. His work constitutes a milestone in the history of soil physics and more generally, of movement of multiple fluid phases in porous media. Central to his model were the notion of (i) capillary potential, (ii) soil moisture retention curve, and (iii) potential-dependent hydraulic conductivity. In particular, he extended Darcy's law to describe unsaturated flow by generalizing the relationship between soil water pressure head Ψ and hydraulic conductivity k. The mathematical representation of Buckingham's intuition would be given by Richards in 1931 (Eq. 5):

$$\frac{\partial \theta}{\partial t} = \nabla \cdot [k(\psi) \nabla h] \qquad \text{Eq. 5}$$

θ [-] is the moisture content; k [L/T] is the hydraulic conductivity, expressed as a function of the matric suction head ψ [L]; h [L] is the total potential head, usually evaluated using only gravitational and matrix components (Eq. 6).

$$h = \psi + z \qquad \text{Eq. 6}$$

Richards equation (Eq. 5) can be used to predict infiltration, redistribution of moisture, percolation, and other forms of subsurface flows.

Despite considerable efforts, analytical solutions to Richards' equation can be obtained only under simplifying assumptions (e.g. Philip, 1957; Parlange et al., 1997, 1999). Although these solutions give valuable insights into patterns of soil moisture movement, they cannot adequately address problems of the natural soil environment.

For general cases, the Richards equation can only be solved numerically, and presents significant computational challenges, even when dealing with uniform soil and initial conditions. A variety of finite difference, finite element, finite volume solution techniques have been proposed. (e.g. Neuman, 1973; Narashima and Witherspoon, 1976; Haverkamp et al., 1977; Haynoe, 1978; Huyakorn et al., 1986; Zarba, 1988; Celia et al., 1990; Rathfelder 1994; Berniger, 2000; Azizi Pour, 2011). Among these, the finite element, "mass conservative" method proposed by *Celia et al.* (1990) has known a wide diffusion, and it is the protocol implemented in Hydrus (Šimůnek et al., 1999), i.e. one of the most widespread commercial software for the analysis of 1D, 2D, and 3D water, heat, and multiple solute flow in variably saturated porous media.

To overcome the issues of a complete numerical solution of Richards equation, simplified physical models, semi-empirical and empirical models based on specific hypothesis were also proposed. A quick review on these models is here presented.

1.2.6.2 Physically based models

Examples of simplified, physical models were proposed by Green and Ampt (1911), Philip (1957, 1969), Mein and Larson (1971, 1973), Smith (1972), Smith and Parlange (1978).

Green and Ampt model (1911)

The main assumption of the Green and Ampt approach are that (a) there exist a distinct and precisely definable wetting front during infiltration; (b) the soil is uniformly wet and of constant conductivity in the transmission zone behind the wetting front. The wetting front is

thus viewed as a plane separating a uniformly wetted infiltrated zone from an as-yet totally uninfiltrated zone; gives no information about details of the soil moisture profile during infiltration is given. In effect, this supposes the k-ψ relation to be discontinuous. These assumptions simplify the flow equations making it amenable to analytical solution (Eq. 7):

$$i = \frac{dI}{dt} = k_s \left(\frac{h_0 - h_f}{L_f} \right) \qquad \text{Eq. 7}$$

where i [L/T] is the flux into the soil and through the transmission zone, I [L] the cumulative infiltration, k_s [L/T] is the saturated hydraulic conductivity of the transmission zone, h_0 [L] the pressure head at the entry surface, h_f [L] the effective pressure head at the wetting front, and L_f [L] the distance from the surface to the wetting front (the length of the wetted zone).
Green and Ampt has been found to apply particularly to infiltration into uniform, initially dry, preferably coarse textured soils, which exhibit a sharp wetting front (Hillel and Gardner, 1970).

Philip (1957)

Philip developed an approximate solution of Richard's Equation. In particular, his original solution pertained to the case of an infinitely deep uniform soil of constant initial wetness θ_i, assumed at time $t = 0$ to be submerged under a thin layer of water that instantaneously increase soil wetness at the surface from its initial value θ_i to a new value θ_{nS} (near saturation) that is thereafter maintained constant. Referring to these hypothesis, he converted the Richard's equation into an ordinary differential equation yielding to a solution in the form of a power series. Cumulative infiltration I [L] is given by Eq. 8:

$$I(t) = \sum_{n=1}^{\infty} j_n(\vartheta) t^{\frac{n}{2}} = s t^{\frac{1}{2}} + (A_2 + K_0)t + A_3 t^{\frac{3}{2}} + \cdots + A_n t^{\frac{n}{2}} \qquad \text{Eq. 8}$$

in which the coefficients $j_n(\theta)$ [L/T$^{n/2}$]are calculated from the relationships $k(\psi)$ and $\psi(\theta)$, and the coefficient s [L/T$^{0.5}$] is called sorptivity and it as a measure of the capacity of the medium to absorb or desorb liquid by capillarity.

This solution suggests that at small times the advance of any soil moisture value proceeds as $\sqrt{t}$; whereas at longer times the downward advance of soil wetness approaches a constant rate

$$(k_{nS}\text{-}k_i)/(\vartheta_{nS} - \vartheta_i) \quad \text{Eq. 9}$$

where k_{nS} and k_i are the conductivities at the wetness value of ϑ_0 and ϑ_{nS}, respectively.

1.2.6.3 Semi-empirical models

Semi-empirical models were proposed, for example, by Horton (1938), Holtan (1961), Overton (1964), Singh and Yu (1990), Grigorjev and Iritz (1991).

Horton model (1938)

Horton developed the following infiltration equation (Eq. 10) :

$$i = i_c + (i_0 - i_c)e^{-dt} \quad \text{Eq. 10}$$

in which i_c [L/T] is the steady state value of the infiltration rate, i_0 [L/T] is its value initial value, and *d* (dimensionless) is the infiltration decay factor (i.e. it states how quickly i will decrease from i_0 to i_c). Despite the simplicity of the mathematical expression, the practical implementation of this model is deeply cumbersome because it contains three site and event specific constants that must be evaluated experimentally.

Holtan model (1961)

Using a storage exhaustion concept, Holtan (1961) derived an infiltration equation expressed as (Eq. 11):

$$I = I_c + a(M - W)^n \quad \text{Eq. 11}$$

where a and n are adimensional constants dependent on soil type, surface and vegetation conditions, and (*M-W)* is the storage available (total porosity M minus the antecedent soil moisture W(t) expressed in units of equivalent depth) [L]. This model can be applied provided that $0 \leq W \leq M$; $i = i_c$ can only occur at the single point $W = M$. When W>M, $i = i_c$ must be imposed, since there is no reason to suppose that infiltration should decrease once W=M. Despite the

simplicity of the mathematical expression, the practical implementation of this model is deeply cumbersome because it contains three site and event specific constants that must be evaluated experimentally.

1.2.6.4 Empirical models

Empirical models are based on data derived from either field or laboratory experiments. Mathematical expressions were built in order to have the correct qualitative shape. The parameters of these models are event and site dependent and require specific calibration. Examples were proposed by Kostiakov (1932), Huggins and Monke (1966), SCS (1974), Collis-George (1977).

Kostiakov model (1932)

The general form of the infiltration equation given by Kostiakov (1932) is (Eq. 12):

$$i = at^{-b} \qquad \text{Eq. 12}$$

where a [LT^{b-1}] and b (dimensionless, $0<b<1$) are constants.
This formulation provides an infinite initial infiltration rate and implies that as time t increases, i approaches to zero. This is relevant to horizontal water absorption (in the absence of a gravity gradient) but is clearly deficient for downward infiltration. Observation of long irrigation events as well as theoretical considerations showed that downward infiltration rate declined to a positive minimum value i_c. This led to the developing of Modified Kostiakov equation (also known as Kotiakov-Lewis or Mezencev variant, 1948) expressed as (Eq. 13):

$$i = at^{-b} + i_c \qquad \text{Eq. 13}$$

Collis-George model (1977)

Collis-George argued that the Green and Ampt model did not mimic the observed behavior of simple soils at long times while the Horton model did not at short times. He therefore proposed a model which would work well at all times (Eq. 14) :

$$i = i_c + \frac{0.5 \cdot f_0 \cdot [1 - \tanh\,(\frac{t}{t_c})^2}{\tanh\,(\frac{t}{t_c})^{0.5}} \qquad \text{Eq. 14}$$

where i_c is the final infiltration rate; $f_0 = s(t_c)^{1/2}$, t_c is a time parameter, s is soil sorptivity [L/T$^{0.5}$].

1.2.6.5 Empirical *vs* physical models

When dealing with coupled surface-subsurface flow models, empirical models have often been preferred to physical models or to the complete numerical solution of Richards equation.

Except for simplified conditions, only numerical solutions to the unsteady surface flow equations are possible; empirical functions allow infiltration to be calculated explicitly at a point as a function of time and, therefore, simplify the solution strategies. As previously stated, the parameters of all the empirical functions are event specific, hence they cannot account for the effects of changes in flow depth and antecedent soil moisture content. In addition, empirical functions can describe the rate of infiltration and cumulative infiltration but they lack the capability to describe the dynamics of soil water once it enters the soil and, consequently, the spatial and temporal patterns of soil moisture (Furman et al. 2006).

The use of a physically based model to describe infiltration is advantageous in terms of wider applicability and higher reliability. Subsurface distribution of water and soil moisture patterns can be predicted. A deep insight on the importance and impacts of (a) soil hydraulic properties, (b) boundary conditions and (c) initial conditions on subsurface flows is possible.

1.3 Coupling strategies for surface-subsurface flow

The problem of modeling the surface and subsurface flow processes as separate domains is further exacerbated by the problem of coupling the models of the individual domains.
Generally, a complete system of coupled surface–subsurface flows involves a mathematical description of (1) the surface process, (2) the subsurface process, (3) the external boundary conditions, and (4) the internal boundary conditions (i.e. at the soil surface). Flow depth and discharge computations for the surface-flow must take into account infiltration losses, while the subsurface flow must take into account the effect of variable pressure at the soil surface (flow depth).
This computational problem has been examined over a range of scales, from field (e.g. Schmitz & Seuss, 1989; Bautista et al., 1998; Wohling et al., 2007), to hillslope and streambed (e.g. Harvey & Bencala, 1993; Fan & Bras, 1998; Storey et al., 2003), to watershed (e.g. Nikolaidis et al., 1993; Michaud & Sorooshian, 1994; Paniconi and Putti, 1994; Blasch et al., 2006; Rigon et al. 2006).
Quite different modeling approaches have been typically used at small (field to hillslope) and large (watershed to continental) scales.
A significant, although not exhaustive, reference for surface-subsurface flows models at watershed scale is GEOtop (Ringon et al., 2006). GEOtop is a complete distributed, physically based model that exhaustively treats both water and the energy balance on a landscape defined by three-dimensional grid boxes, whose surfaces come from a digital elevation model (DEM). It allows to describe the interaction and the feedbacks between soil and atmosphere at watershed scale, where the complex topography and the heterogeneity of the territory require an accurate spatial distribution of the driving variables and of the parameters. In particular the model, given the meteorological data and soil parameters in input, allows to know in each point of the domain and in each time (a) the evaporation of the soil; (b) the transpiration of the vegetation; (c) the radiation and energy fluxes at the soil surface; (d) the pore water pressure in the soil; (e) the water-table movements in the saturated zone; (f) the water discharge in an outlet; (g) the temperature and ice content in the soil; (h) the height and density of the snow. Furthermore, thanks to the post-process software GEOtopFS (GEOtop Factor of Safety), it is also able to

calculate the dynamic probability of slope instability during a precipitation event.

In this study we focused on small spatial scales. Fields and plots often have an almost flat, trivial topography. At the time scales of irrigation or storm events, many energy fluxes are negligible. Coupled overland-infiltration flows have been widely examined in the context of irrigation modeling. Each inflow event involves an advance phase followed by a depletion phase caused by a cut-off event. The spatial domain is usually limited and a storage phase may exist before the depletion phase. A summary on these models is here presented.

In particular three surface-subsurface flows coupling strategies were identified (Morita and Yen, 2002); Furman, 2008).

The simplest strategy was labeled degenerate coupling, or external coupling. It solves each process separately at a given time step, without iteration between the models. This approach ignores the influence of one or more of the dependent variables on one of the flow processes. This strategy is employed by irrigation models with empirical infiltration functions, which solve the surface-flow equations iteratively at each time step, but with infiltration computed explicitly as a function of time. The influence of flow depth and initial soil water content on the subsurface flow is embedded in the parameter estimates, making the parameters specific to an irrigation event. The time step of the calculations is dictated exclusively by the surface flow calculations.

The second strategy is called full-coupling. It is highly expensive in computational terms as it solves the full combined system of equations for the overland and subsurface flow processes. Many models (e.g. Van der Kwaak,1999; Panday and Huyakorn, 2004) were developed to study the problem at the watershed scale. No smaller scale (i.e. the field scale) models have been implemented using this approach.

The third strategy was named internal iterative coupling. It consists in solving the surface and subsurface flow equations separately, but with the models iterating on the dependent variables sequentially at the level of the time step.

Internal iterative coupling and external coupling strategies were both applied to solve surface-subsurface problems at the field scale.

1.3.1 Internal iterative coupling

Internally coupled models are computationally complex and require special strategies to ensure model convergence and accurate results. The specific coupling algorithm depends on the computational schemes employed to solve the surface and subsurface-flow components. Analytical and semi-analytical as well as numerical solutions were proposed.

A further classification is based on (a) the degree of complexity and accuracy incorporated to simulate surface flow; (b) the strategy employed to describe subsurface flow.

The models proposed for the solution of de Saint-Venant equations are normally categorized into four major classes, namely, (a1) the full hydrodynamic model; (a2) the zero inertia model; (a3) the kinematic wave model; (a4) the volume balance model.

The volume-balance model is based on the solution of the spatially and temporally lumped form of the continuity equation.

A number of studies was performed to check the performances of these four classes of models adopted in coupled surface-subsurface flow problems. The outcomes are here summarized.

The volume balance technique (a4) is suitable for rough, preliminary solutions in simple computational domains.

The kinematic-wave model (a3) is reasonable with relatively large slopes and open-ended systems; on the contrary it yields to unacceptable errors in case of subcritical flows on flat slopes or when the downstream boundary condition is an important factor (e.g. Tayfur et al., 1993).

Coupled surface-subsurface problems are often characterized by low flow velocities (i.e. Froude<0.2, Strelkoff & Katopodes, 1977) and the inertial terms in the momentum equation seem to have little effect on the final results. In those cases, the zero-inertia model (a2) is numerically stable and its results are as accurate as the complex and complete full hydrodynamic model (a1) while computational efforts are sensibly reduced (e.g. Strelkoff and Katopodes 1977; Zerihun et al. 1996; Vlipour, 2011).

As explained in par.1.2, subsurface flow may be described by (b1) physical models; (b2) semi-empirical models; (b3) empirical models.

Tabel 1 – Analysis of surface-subsurface flow at small scales. Literature review on the main models based on the internal iterative coupling strategy.

Analytical and semi-analytical models	
Surface flow	**Subsurface flow**
Kinematic wave solution	*Empirical model* Henderson (1966)
Zero-Inertia solution	*Empirical model* Schmitz and Seus (ZIMBA, 1990,1992); Arasteh 1995; Schmitz et al. (2002) ; Wohling et al. (2004 2005); Wöhling and Mailhol (2007); Mailapalli (2006) ; Philipp et al. (2010).
	*Physical model (*Green & Ampt) Maiapalli, Singh and Raghuwanshi (2009)
Numerical models	
Surface flow	**Subsurface flow**
Kinematic wave solution	*Empirical model* Akan (1981), Sunada and Hong (1988), Govindaraju et al. (1988), De Lima and Van der Molen (1995)
	Physical model Smith and Woolhiser (1971)
Zero-Inertia solution	*Empirical model* Strelkoff and Katopodes (1977); Strelkoff (1985); Walker and Skogerboe (1987); Oweis and Walker (1989); Hromadka et al (1985); Todini and Venutelli (1991); Zerihun et al. (2008)
	Physical model Wöhling et al. (2004; 2006); Zerihun et al. (2005); Wöhling and Schmitz (2007) coupled the quasi-analytical zero-inertia (Schmitz and Seus, 1992) model of the surface-flow with the numerical sub-surface physical model Hydrus (1D or 2D) (Šimůnek et al., 1999). HYDRUS simulations are conducted at every time step of the surface-flow computations. Preissmann and Zaoui; Govindaraju and Kavvas (1991).
Hydro-dynamic solution	*Empirical model* Woolhiser and Liggett ; Lin *et al. ;* Chow and Ben-Zvi; Kawahara and Yokoyama; Zhang and Cundy 37; Tayfur et al. (1993)
	Physical model Akan and Yen; Schmitz et al.(1985); Tabuada et al.(1995); Singh and Bhallamudi(1996, 1997); Bradford and Katopodes (1998)

Focus on the numerical solutions: software simulation tools

Although development of improved simulation tools has long been the objective of many research projects, the models implemented so far provide a numerical solution of the unsteady gradually varied open channel flow problem in which infiltration is described by empirical models or, rarely, by Green & Ampt (1911) model.
In particular, SIRMOD (Walker 1997) and WinSRFR (Bautista et al. 2009) appear to be the most widely used simulation models (Furman, 2008).
SIRMOD (surface irrigation simulation, evaluation and design) is a comprehensive, commercial simulation software package for simulating basin and border irrigation hydraulics. The software is based on the numerical solution of the full hydrodynamic model but is also capable of applying the volume balance model. Surface roughness effects are taken into account using the Manning empirical coefficient. The infiltration process is described by the Kostiakov empirical model.
Since the late 1970s, The USDA-Agricultural Research Service has been involved in the development of hydraulic simulation models and related software tools for analyzing surface irrigation systems. WinSRFR is an open source modeling tool resulting from the integration of the previous surface irrigation program SRFR (Strelkoff et al., 1998), the design tool for sloping, open-ended border strip systems BORDER (Strelkoff et al., 1996), and the design tool for level-basin systems BASIN (Clemmens et al.,1995). WinSRFR can simulate surface irrigation hydraulics with both the zero-inertia and kinematic wave formulations. The equations describing the surface flow are discretized with the Preissmann implicit finite-difference scheme, and the resulting system is solved iteratively using the Newton-Raphson procedure. Channel roughness is modeled by Manning empirical coefficient. The simplified physical model proposed by Green and Ampt (1911), and a number of empirical (e.g. Kostiakov, 1932) infiltration models are available.
This brief review on the simulation models is completed quoting SISCO (Gillies et al. 2010), a simulation engine based on the complete hydrodynamic equations; ZIGASED (Maiapalli, Singh and Raghuwanshi, 2009) a physically based model for simulating flow in irrigated furrows under both uniform and layered soils.

1.3.2 External iterative coupling

Bautista et al. (2010) proposed an external iterative strategy which operates at the time scale of an inflow event. Although the overall strategy could be used to couple any surface and subsurface flow model, it was prototyped using the free software packages WinSRFR (Bautista et al. 2009) and Hydrus-1D (Šimůnek et al., 1999).
Infiltration into the soil and water movement through the soil profile are treated as a one-dimensional process described by the Richards equation, any flow through cracks and macropores is hence ignored.
WinSRFR and Hydrus-1D are run sequentially and iteratively at the time scale of the inflow event. It is worth noting that the modeling is limited to the advance phase of any inflow event. The protocol is here described.

(1) Hydrus-1D is run with an assumed constant depth as the upper boundary condition. This simulation yields to the values of cumulative infiltration as a function of time; numerical fitting allows the assessment of the site and event dependent values of the modified Kostiakov infiltration formula.
(2) These parameters of the modified Kostiakov infiltration formula are used to conduct a complete simulation with WinSRFR, assuming spatially uniform soil-infiltration properties. Flow depth hydrographs generated at a selected number *n* of nodes along the field length are extracted from WinSRFR results. These user defined locations are identified as calibration nodes. The WinSRFR simulation also yields estimates of final infiltration depth at the calibration nodes.
(3) A HYDRUS-1D simulation is conducted at each calibration node using the hydraulic head hydrographs generated in the previous step as the upper-boundary condition. These simulations yield *n* cumulative-infiltration time series.
(4) The Hydrus-1D results of the previous step are fitted to modified Kostiakov equations.
(5) A new WinSRFR simulation is conducted with infiltration given at each calibration node by its corresponding fitted

function from step (4). This simulation yields a new set of hydrographs and final infiltration depths.

(6) An error term is defined as the mean relative difference (MRD) between the WinSRFR simulated final cumulative infiltration depths at the calibration nodes and the corresponding Hydrus-1D. A possible convergence criterion requires the absolute difference between MRD values computed for two subsequent iterations to be lower than 1%.

(7) Steps 3 to 5 are iterated until the convergence criterion expressed in (6) is achieved.

The accuracy of the proposed strategy was assessed by comparison with results from the internally coupled model of Zerihun et al. (2005). In all the examples provided, the procedure converged in just a few iterations.

The original Hydrus package does not allow mass accumulation at the upper boundary of the domain and any water excess is instantaneously removed (Šimůnek et al., 1999). Consequently, the external coupling strategy applied exclusively to the advance phase of the routing of a surge wave on a permeable boundary.

Chapter 2

Infiltration of overland flow: experimental and numerical modeling

2.1 Introduction

Generally, a complete model of coupled surface–subsurface flow phenomena involves an appropriate mathematical description of (a) the surface process, (b) the subsurface process, (c) the external boundary conditions, (d) the internal boundary conditions (i.e., at the surface–subsurface interface).

The not-negligible interactions between the mutually dependent surface and sub-surface flow domains exacerbate the challenges intrinsically connected to the modeling of these flow processes conceived as separate phenomena.

Adopting a scaling-up approach, we first focused on the subsurface flow consequent to the routing of a surge wave on a permeable boundary.

Experimental and numerical modeling activities were planned to decouple the phenomenon. Planned conditions in an artificial environment allowed a total control on all the parameters involved.
The experimental activities were completed in the *Hydraulics Laboratory "G.Bidone"* of the Polytechnic University of Turin.
Two-dimensional flume tests modeled water infiltration of overland flows in order to investigate the interdependence of surface and subsurface flows. One-dimensional column tests focused on the temporal and spatial patterns of soil moisture as a consequence of infiltration flows.
In particular, the first aim was achieved using a prismatic, horizontal flume. Perfectly clean, homogeneous sand modeled the infiltration domain. A spatially homogeneous mattress of reticulated foam depicted the effects of surface roughness and vegetation. Issues commonly faced in field case studies, such as clogging, cracking, swelling, shrinkage of the soil; spatial heterogeneities of the infiltration domain due to roots dieback or burrows; spatial and temporal heterogeneity of the vegetation cover were thus avoided.
Surface and subsurface flow data were recorded and used for the complete numerical modeling of the infiltration process. The numerical model was based on the solution of the Richards equation provided by the commercial software Hydrus 2D (Šimůnek, 1998).
One dimensional infiltration column tests investigated the temporal and spatial patterns of soil moisture providing a valuable methodology for the assessment of the soil parameters required by the numerical model.
Recorded time series of water depth values of the surface flow were used as upper boundary conditions to decouple the problem.
Recorded time series of the position of the wet/dry interface in the porous media allowed the calibration of the numerical model and the validation of the experimental soil parameters values.
The main objectives of these activities were the analysis of (i) the experimental issues connected with the modeling of the infiltration process consequent to the routing of a surfeace wave; (ii) the numerical issues connected with the physical modeling of a 2D infiltration flow due to a surge wave; (iii) simple, parsimonious methods for the assessment of soil parameters.

2.2 Flume tests, experimental setup

The experimental modeling of waves routing on permeable boundaries was performed in the hydraulic laboratory "Giorgio Bidone" of DIATI (Polytechnic University of Turin).
The experimental setup is represented in Fig. 2. It consisted of a closed hydraulic circuit composed by a pump, a small reservoir, a flume , a connecting underground channel.

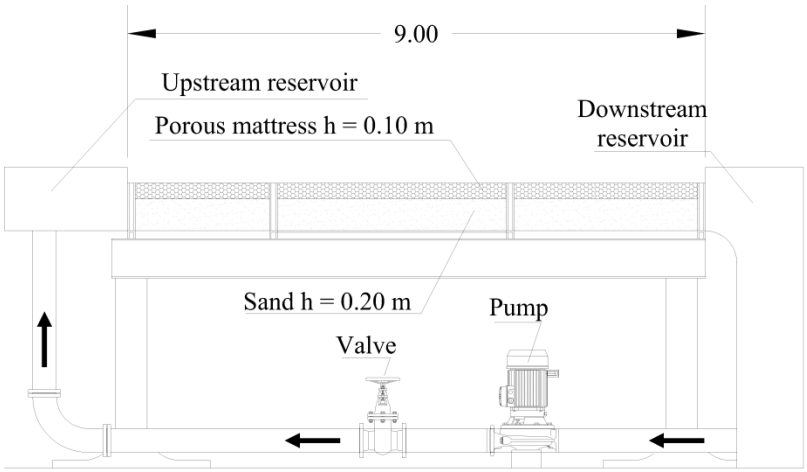

Fig. 2 – Flume tests, scheme of the experimental setup

The experimental flume was horizontal, prismatic, 0.30m wide, 0.30m deep,9m long. It had 4mm thick, trasparent plexiglass walls. It represented the domain of the phenomenon of interest.
A 0.20m constant deep layer of sand modeled the bottom permeable boundary. In order to achieve a two-dimensional flow (longitudinal and vertical dimensions) and to avoid preferential flow paths a small trolley was used to overlap several 2mm deep sand layers.
A 0.10m thick mattress of reticulated foam was carefully laid on the sand surface in order to (i) model the effect of surface roughness on waves routing; (ii) avoid scouring phenomena; (iii) enhance the visibility of the surface wave.

A rectangular sharp-crested weir without lateral contraction (i.e. as large as the flume) allowed water flowing from a prismatic (0.3m wide, 0.6m long, 0.8m deep) upstream reservoir into the experimental flume. The overflow edge was at the interface between the sand layer and the porous mattress. A rectangular gate prevented water to flow into the channel while filling the upstream reservoir. A surge wave was then originated by a quick manual rising of the gate. Consequently to the system geometry, the surge wave routed through the mattress and infiltrated in the sand. Fig. 3 is a scheme of the experimental set-up.

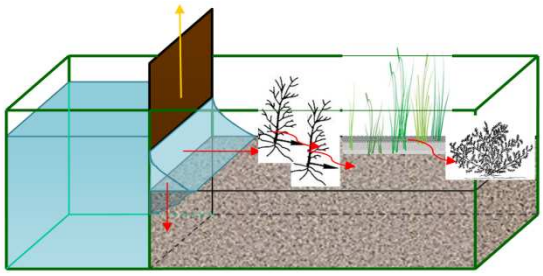

Fig. 3 – Sketch of the experimental set-up

The bottom of the channel was impervious and the system was "air confined", i.e. air was allowed to escape only from the soil surface through a horizontal flow. Consequently, an appropriate calibration of the experimental parameters (i.e. sand and porous mattress textures, flow regime) was required in order to avoid water flow instabilities due to air entrapment (e.g. Wang et al., 2000).

Three sensibly different sand textures were tested; preliminary to a specific description, we referred to them as (1) "coarse", (2) "medium" and (3) "fine".

Three different textures of the reticulated foam were available; after Clifton et al. (2009) they were named (a) regicell 10 foam, (b) regicell 30 foam, (c) regicell 60 foam. Their parameters were measured by Neumann, Courville, Schneebeli (Clifton et al., 2009). In particular, the parameters of interest are porosity; pores' average characteristic dimension (d); specific surface area (SSA), i.e. the surface area of the medium per unit volume; hydraulic conductivity k_s (see Tabel 2).

Tabel 2 – Characteristics of the three reticulated foam tested

Reticulated foam	Porosity [%]	d [mm]	SSA [mm^{-1}]	k_s [m/s]
Regicell 10 foam	96.4	3.9	0.37	1.57
Regicell 30 foam	97.0	1.5	0.82	0.38
Regicell 60 foam	98.0	0.5	1.70	0.06

An illustrative image obtained by X-ray tomography (Schneebeli & Sokratov, 2004) of the microstructure of the polyester foam used is shown in Fig. 4

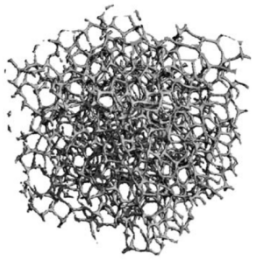

Fig. 4 – Microstructure of the polyester "Regicell 60" reticulated foam obtained by X-ray tomography (M. Schneebeli)

Three flow regimes were hypothesized: (i) a wave pulse obtained by quickly closing the gate 5 seconds after its complete opening; (ii) a dam break flood wave leading to the emptying of the upstream reservoir; (iii) a constant head value of 0.10 m at the inlet cross section was achieved operating the butterfly valve (Fig. 2).
Many experimental schemes were tested by combining sand textures, reticulated foam textures, flow regimes.
Every test was recorded by five high resolution video cameras (spatial resolution 768x576 pixel; temporal resolution 25 frames/s). In particular, four cameras were installed on the right side of the channel, one on the left side. One camera on the left side was used to check the effective bi-dimensionality of the flow: its recordings proved the negligibility of gradients in the transversal direction. Four cameras on the right side could thus be used to record surface and subsurface flows.

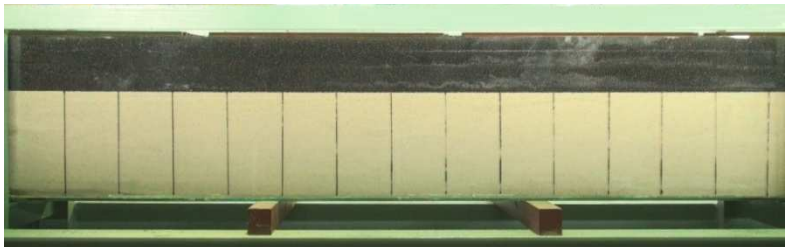

Fig. 5 – Frame, example

Three cameras framed three, 1.20m long sections of the channel; one camera framed one, 0.60m long section next to the inlet of the channel in order to provide higher resolution data of the establishment of the flow. Recordings were stopped as soon as the subsurface flow reached the impervious bottom of the channel.
An original image processing protocol based on the digital number of each pixel and developed in Matlab environment allowed the interpretation of each frame. In particular, the wet/dry interface was located both in the sand and in the porous bed. A metric scale fixed at the bottom of the channel was used as reference to compute metric distances taking into account the variability in the aperture angle of the camera. The exact wet/dry interface position was then computed according to Snell's law describing the relationship between the angles of incidence and refraction of light waves passing through a boundary between two different isotropic media (i.e. air and plexiglass).
Fig. 6 shows an example of the detection of the wet/dry interface in the porous bed and in the sand.

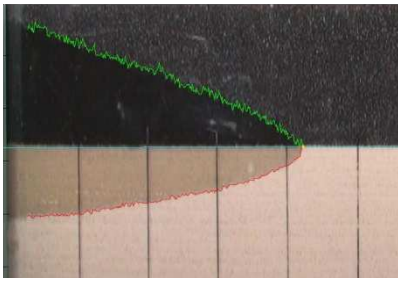

Fig. 6 – Numerical detection of the wet/dry interface position in the porous bed (green line) and in the sand (red line), example.

Time series of front wave position, front wave celerity, wetted area in the sand, and wetted area in the porous mattress were also computed.
Regardless the flow regime and the reticulated foam adopted, when the coarsest sand was used the downward water flow quickly reached the impervious bottom of the channel and a preferential horizontal flow was observed. On the contrary, when the finest sand was used surface flow significantly prevailed on subsurface flow. The downward movement of the wetting front was extremely slow, and water ponded on top of the sand layer. Furthermore, the low permeability value highly hampered the horizontal flow of water-displaced air; soil air pressure increased below the wetting front causing water flow instabilities (Wang et al., 2000). Upward air preferential flow paths were observed in many points of the sand domain (Fig. 7)

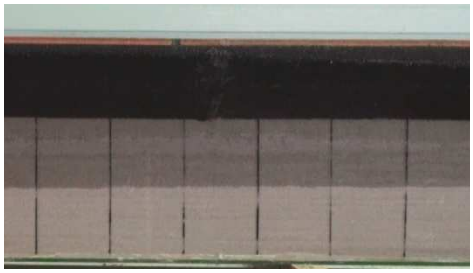

Fig. 7 – Sand "fine", regicell 10 foam, constant inflow regime: air preferential flows.

The medium textured sand showed optimal results: in appropriate conditions not disturbed coupled surface-subsurface flow could be observed for hundreds of seconds and large part of the horizontal spatial domain was used before the infiltration flow reached the bottom of the channel.
Instable, fingered flow (occurred during the depletion phase following the pulse flow regime and the reservoir emptying phase, i.e. when the quickly decreasing hydraulic head became lower than the gauge air pressure below the wetting front (details on this topic can be found in par. 3.7.2). Fig. 8 shows the instable flow regime occurred during the depletion phase following a pulse flow that routed through the middle textured reticulated foam and infiltrated into the middle texture sand.

Fig. 8 – Sand "medium", regicell 30/60 foam, pulse flow: instable infiltration flow during the depletion phase

The constant head regime allowed an extended observation of a stable, regular surface-subsurface coupled flow. Surface or subsurface flow slightly and interchangeably prevailed depending on the permeability of the porous mattress used. For instance, a smaller porosity value obviously lowered the celerity of the front wave, enhanced the water depth of the surface wave, fastened the subsurface flow. Tabel 3 lists the values of the final mean celerity of the front wave $\overline{v_f}$, the maximum distance d_{max} travelled by the surface flow before the subsurface flow reached the impervious bottom of the channel, the time employed t_{dmax} as a function of the reticulated foam used.

Tabel 3 – Impact of the texture of the reticulated foam on the main features of a constant flow regime

Reticulated foam	$\overline{v_f}$ [m/s]	d_{max} [m]	t_{dmax} [s]
Regicell 10 foam	0.02	3	120
Regicell 30 foam	0.0125	3	170
Regicell 60 foam	0.01	1.3	75

The two, extreme conditions provided by the finest and the coarsest porous mattress were worth a further analysis.
Fig. 9 represents the front wave position as a function of time.
Fig. 10 represents (a) the temporally increasing total wetted area detected in the surface flow domain (M) and in the surface flow

domain (S); (b) the values of the total wetted area evaluated in both the flow domains at the same position of the front wave.
These analysis highlighted the bigger importance of the infiltration process as a consequence of a finer porous mattress. Stating the extremely large values of porosity and permeability of the porous mattress, a uniform, instantaneous saturation condition was reasonable; on the contrary, the detection of the wetted area in the sand domain allowed merely qualitative conclusions.

Aiming at a study on the infiltration process, spatial and temporal variations in sand moisture profiles were of great interest.
Although many lighter areas in the wetted sand domain were detected in some video-recordings, image processing techniques weren't of any help in the assessment of soil moisture gradients and a different approach was required.
Recorded time series of the wet/dry interface in the porous mattress allowed to decouple the problem and thus to focus on the infiltration process. Recorded time series of the wet/dry interface were the hydraulic head values required as upper boundary condition by a physical infiltration model.
Experimental lab activities were carried out to assess the hydraulic parameters of the uniform sand layer.

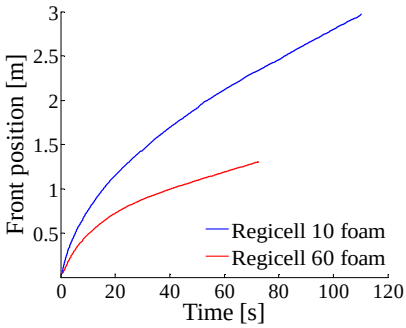

Fig. 9 – Sand “medium”, constant flow regime: front wave position.

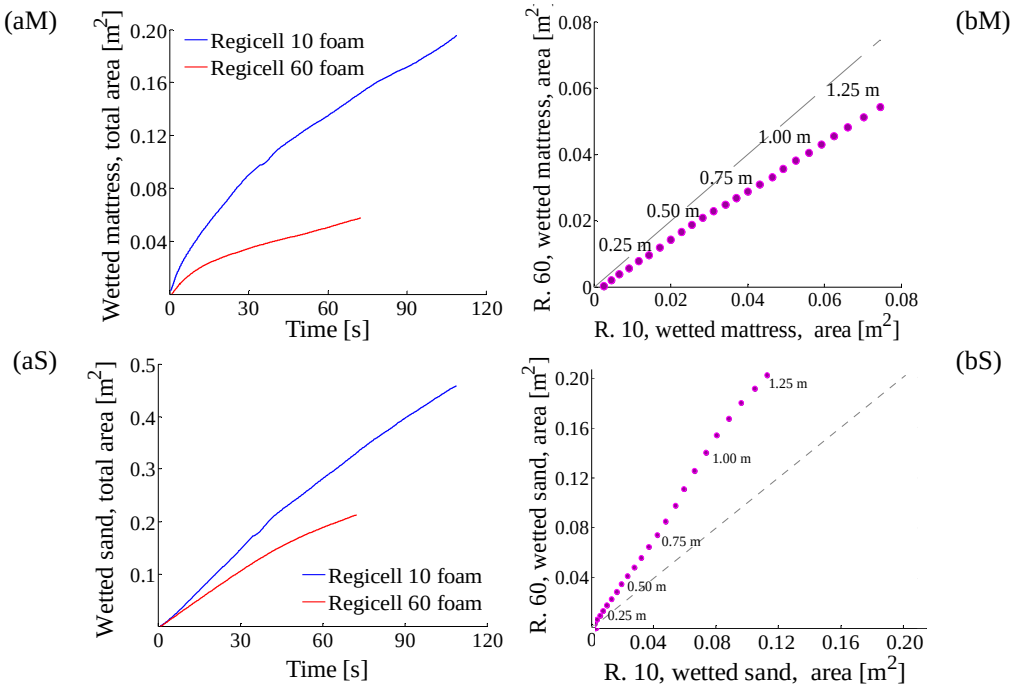

Fig. 10 – Sand “medium”, constant flow regime, Regicell10 and Regicell 60: (a) total wetted area of the surface domain (M) and of the subsurface domain (S); (b) total wetted area of the surface domain (M) and of the subsurface domain (S) evaluated for discrete positions of the front wave.

2.3 Sand parameters assessment

Laboratory tests were performed to measure the main parameters of the sand "medium" used for both experimental and numerical modeling of the infiltration process; in particular:

- density;
- porosity;
- grain size distribution;
- hydraulic conductivity;
- soil moisture characteristic curve.

A comprehensive study on soil moisture characteristic curve is presented in the next paragraph (2.4).

2.3.1 Density

Density represents mass per unit volume of a substance.
We accurately filled a bucket of known volume with dry sand, the ratio between its net weight and its volume yielded to the density value (Eq. 15):

$$\rho = \frac{Net\ Full\ bucket\ Weight}{Bucket\ Volume} \cdot \frac{1}{g} = 1665\ kg/m^3 \qquad \text{Eq. 15}$$

2.3.2 Porosity

Two types of porosity were defined: *total or absolute porosity* and *effective porosity*. Total porosity is the ratio of all the pore spaces of a sample to its bulk volume of the rock. Effective porosity is the ratio of interconnected void spaces to the bulk volume. For granular materials, the effective porosity approaches the total porosity.
We accurately filled a bucket of known volume with dry sand, we checked its net weight. We used bottles of known volume to pour water into the bucket; this phase was very slow in order to allow the gradual rise and escape air bubbles small enough to prevent the origin of cavities or preferential paths. We stopped as soon as a thin water

film was formed on top of the sand. The total volume of water introduced was the pore volume of the sand sample. It straightly yielded to the porosity value (Eq. 16).

$$porosity = \frac{Water\ volume}{Bucket\ volume} = 0.3 \qquad \text{Eq. 16}$$

2.3.3 Grain size distribution

The distribution of different grain sizes defines the soil texture, i.e. the proportion of four mineral particles, clay (d<0.002mm), silt (0.002<d<0.05mm), sand (0.05<d<2mm), gravel (d>2mm).
Furthermore, particle size distribution affects the magnitude of soil permeability, i.e. its ability to transmit fluids.
A Particle Size Distribution analysis (PSD) is a measurement designed to determine and report information about the size and range of a set of particles representative of a material. Sieve techniques are suitable when performing analysis on coarse materials such as sand. Sieves are screens made from wires of standard diameters, the most common scale used to classify particle sizes is the US Sieve Series; each sieve is identified by the number of openings per linear inch.

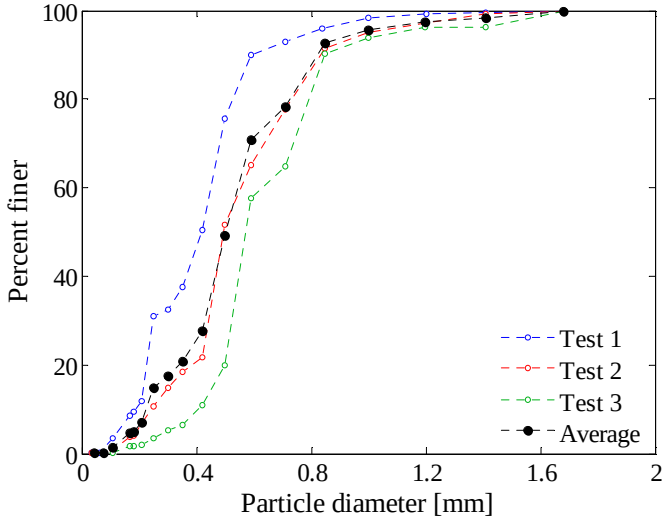

Fig. 11 – Sand “medium”, grain size distribution

In our laboratory tests 18 sieves having decreasing opening size were stacked up and placed on a mechanical shaker. Three samples of sand were weighted, poured into the top sieve, shaken for about 2 minutes. The material retained by each sieve as well as by the bottom pan was carefully weighted. The computation of the percent passing through each sieve yielded to the grain size distribution curve, its narrow shape highlighted the textural uniformity of the sand "medium". Fig. 11 shows the results of three trials, as well as average values; the sand

2.3.4 Saturated hydraulic conductivity

Saturated hydraulic conductivity was measured during a previous research project. In particular, c*onstant head tests* and the *falling head test*s were performed.
During constant head testing, a fixed hydraulic gradient *h/L* was established through a cross-sectional area A_{flow} of soil and water flow was continued until a steady-state flow rate was obtained. Outflow water was then collected for a period of time, with the total volume of flow *V* collected over time period *t* used to determine the saturated hydraulic conductivity of the soil by a re-arrangement of Darcy's equation as (Eq. 17):

$$k_S = \frac{(V/t)\,L}{A_{flow}(h+L)} \qquad \text{Eq. 17}$$

During falling head tests initial and final water heads h_1 and h_2 were recorded at many time steps t_1 and t_2 and used to calculate the saturated hydraulic conductivity by a re-arrangement of Darcy's equation (Eq. 18), where A_{surf} is the area of the ponded surface:

$$k_S = (ln\ h_2 - ln\ h_1)\frac{A_{surf}}{A_{flow}}\frac{L}{(t_2 - t_1)} \qquad \text{Eq. 18}$$

Tabel 4 – Sand "medium", measured values of k_S (previous project)

	Constant head test	Failing head test
Mean [m/s]	$1.050 \cdot 10^{-4}$	$1.054 \cdot 10^{-4}$
Standard deviation [m/s]	$6.650 \cdot 10^{-6}$	$8.576 \cdot 10^{-6}$

2.4 Soil Water Retention Curve

The description, quantification and study of soil water flow processes requires the consideration of the hydraulic properties of unsaturated soils. This involves the relationship between the soil water content, θ, the pressure potential ψ, and the hydraulic conductivity, *k.* Details on this topic can be found in par. 1.2.2.
Among the various empirical models proposed to describe the relationship between soil water content and pressure head, i.e. the Soil Water Retention Curve, Van Genuchten model (1980) is presently the mostly used in numerical models because of its ability to accurately fit data from the main drying and wetting paths (see, for example, Sharma and Mohamed, 2003). Van Genuchten model is mathematically represented by Eq. 19:

$$Se = \frac{\theta - \theta_r}{\theta_s - \theta_r} = \frac{1}{[1 + (\alpha\psi)^n]^m} \qquad \text{Eq. 19}$$

In which:

- S_e is called *effective saturation;*
- θ is the volumetric water content;
- θ_r is the residual water content;
- θ_s is the saturated water content;
- ψ is the pressure head;
- α, n, m are specific parameters and $m = 1/(n-1)$, $n > 1$

Measuring the unsaturated hydraulic conductivity during wetting and drying cycles would be practically difficult and time consuming.
A common alternative is the implementation of the predictive model for the unsaturated hydraulic conductivity function in terms of soil water retention parameters proposed by van Genuchten (1980) and based on the statistical pore-size distribution model of Mualem (1976).

$$k(\psi) = k_s S_e^{0.5} \left[1 - \left(1 - S_e^{1/m}\right)^m\right]^2 \qquad \text{Eq. 20}$$

When using Eq. 19 and Eq. 20 the problem of defining soil behavior is solved by the definition of 5 parameters:

- saturated water content θ_s and residual water content θ_r ;
- saturated hydraulic conductivity k_s ;
- Van Genuchten model's parameters *α*, *n*.

Saturated water content θ_s was assumed equal to porosity; assessing the residual water content value was a bit more challenging.
Van Genuchten (1980) defined the residual water content as the water content at a soil suction of 1500 kPa. This is suction limit of measurement for most soil suction testing equipment. Also, a suction value of 1500 kPa is defined as the wilting point. Eleven years later, Van Genuchten (1991) provided a more general description defining the residual water content as the water content at which the slope of the soil-water characteristic curve (i.e., $d\theta/d\psi$)) and coefficient of permeability go to zero when soil suction becomes large. This definition is still open to interpretation, since the slope of the soilwater characteristic curve does not become zero until a soil suction of 10^6 kPa when the water content reaches zero. According to Luckner et al (1989), the residual water content specifies the maximum amount of water in a soil that will not contribute to liquid flow because there is a blockage in flow paths or a strong adsorption onto the solid
phase. According to Luckner et al (1989), the residual water content specifies the maximum amount of water in a soil that will not contribute to liquid flow because there is a blockage in flow paths or a strong adsorption onto the solid phase. Nitao and Bear (1996) noted that calculated residual water contents are more a function of the instrumentation used to measure the soil-water characteristic data (i.e., the maximum suction measurable by the instrument) than an actual physical constant. Sillers (1997) more recently defined residual water content as the water content where the soil-water goes from being held within the soil primarily by capillary action to soil-water being held in the soil primarily by adsorptive forces.
The soil-water characteristic curve is a continuous function and there is no specific point that can be called the residual water content. Currently, most investigators treat residual water content as a fitting parameter with no real physical significance (van Genuchten, 1991;

Kosugi, 1994; van Genuchten, 1988; Siddroupoulos and Yannopoulos, 1988; Luckner et al, 1989; Nimmo, 1991; Nielsen and Luckner, 1992; Kosugi, 1994). One reason for treating residual water content as a fitting parameter is that the residual water content is not the lowest possible water content within soil. Through evaporation, centrifuging or oven drying it is possible for water content to be less than residual water content. Adopting the latter approach, a first estimate of the residual water content was based on a literature review; in particular, after Carsel & Parrish (1998) it was related to the water content at saturation. The selected value was checked for coherence during the analysis aiming at the definition of the Soil Moisture Retention Curve.
The value of saturated hydraulic conductivity was provided by laboratory experiments completed in a previous project.
Recalling the results of the experimental measures (see par.2.3.2), we assumed the values listed in Tabel 5.

Tabel 5 – Saturated and residual water content values

θ_s	θ_r	$k_s[m/s]$
0.30	0.03	$1.050 \cdot 10^{-4}$

Van Genucthen model parameters α, n were still missing for a complete description of unsaturated soil behavior. Stating the purpose of this study, the parameters of the main wetting phase were required.

2.4.1 Traditional approaches

A first approach to determine the soil water retention curve rely on direct laboratory measurements of the behavior of undisturbed or disturbed soil samples. All the slightly different protocols proposed (e.g. Dirksen, 2000; Dane and Topp, 2002; Dane and Hopmans, 2002; Klute, 1986) are based on the use of a tension plate assembly in the low suction (<1 bar) range, and of a pressure plate or pressure membrane apparatus in the higher suction range. Aiming at the definition of the main drying curve, these instruments allow the application of successive suction values and the repeated

measurement of the equilibrium soil wetness at each suction (Klute, 1986). A modified apparatus is required for the measurement of wetness versus suction during sorption (Tanner and Elrick, 1958). Uncertainties arising near water saturation where multiphase phenomena may be expected to be important were highlighted by Bayer et al (2004). In order to overcome these difficulties they suggested a X-ray absorption technique to measure the distribution of water in porous media. X-ray measures can be made with high spatial and temporal resolution, nevertheless high spatial resolution demands long exposure times and thus reduces temporal resolution.

Generally speaking, experimental methods are expensive in terms of money, time, personal skills (e.g. Wösten et al., 2001). Furthermore, they are often limited to a relatively narrow range of water contents, and usually pertain to relatively restrictive initial and boundary conditions.

A second approach consists in indirect methods based on the premise that the hydraulic properties can be related to more easily measured or more readily available soils data (e.g. Bouma, 1989; Wösten et al., 2001; Van Genuchten and Leij, 1992; Timlin et al., 1996; Pachepsky et al., 1999). Pedotransfer functions represent the most widespread indirect method. They relate the hydraulic properties to particle size distribution, bulk density and/or organic matter content (e.g. Bouma and van Lanen, 1987; Bouma, 1989; Cosby et al., 1984; Saxton et al., 1986; Vereecken et al., 1989; Wosten et al., 1995; Wosten, 1997; Rawls et al., 2001). Comprehensive reviews on pedotransfer functions have been recently published (Wosten et al., 2001; McBratney et al., 2002; Pachepsky and Rawls, 2004). Although the development of many databases, e.g. UNSODA (Leij et al., 1996), HYPRES (Lilly, 1997; Wösten et al., 1999), WISE (Batjes, 1996) and USDA-NRCS database (Soil Survey Staff, 2010), the very specific data requirements often hampers the practical application of PTFs. The Rosetta package (Schaap et al., 2001) was an attempt to overcome this issue; it implements five hierarchical PTFs to predict the SWRC, as well as the saturated and unsaturated hydraulic conductivity. The hierarchy in PTFs allows prediction of the hydraulic parameters using limited (soil textural class only) to more extended (texture, bulk density, and one or two water retention points) input data. Nevertheless, many authors (e.g. Williams et al.,

1992; Gimenez et al, 1997; Tietje and Tapkenhinrichs, 1993; Kern, 1995; Wosten et al., 2001) highlighted the limited portability of
An alternative indirect method for estimating the SWRC is based on the premise of shape similarity between the water retention curve and the cumulative pore-size distribution (e.g. Arya and Paris, 1981; Haverkamp and Parlange, 1986; Fredlund et al., 2002; Haverkamp et al., 2005; Leij et al., 2005). Although some progress based on tomography has been achieved (i.e., Mooney, 2002), measurement and characterization of soil pore spaces is expensive and limited in its capabilities (Pachepsky et al., 2006)
A third approach for assessing SWRC is to design appropriate transient experiments and to analyze the data with a suitable numerical model. The effort of determining hydraulic properties can thus be shifted from experimentation to computation (Kool and Parker, 1988).

2.4.2 Our approach

Aiming at the development of a simple, rapid, money-saving methodology for the assessment of the soil water retention curve the third, expedient approach was selected.
A series of transient experimental tests with known initial and boundary conditions were carried out to provide the calibration data for the numerical modeling of both main wetting and main drying behavior of the sand employed in the flume experiments.

Two, possible numerical strategies are available for the assessment of the soil water retention curve : (A) inverse parameter estimation techniques; (B) fitting of the main drying curve based on sampled data.
In particular, the analysis of the drainage phase of an initially saturated column supports (B1) a direct approach for the computation of the main drying branch; (B2) an indirect approach for extrapolating the main wetting branch.
Further details on these approaches are provided in the following paragraphs.

2.4.2.1 Inverse parameter estimation techniques

Inverse parameter estimation techniques have been extensively used for this purpose. Transient experiments are simulated using the governing water flow equations and selected analytical functions representing the soil hydraulic properties. Starting with initial estimates, the parameters are further adjusted in repeated solutions until deviations between measured and computed water flow attributes (such as water contents, pressure heads, or fluxes) are minimized. The parameter updates can be done manually (trial-and-error calibration) or by using an automated minimization algorithm.

2.4.2.2 Analysis of the drainage phase

The problem of the vertical one-dimensional transient gravity drainage from soils has been widely investigated both theoretically and experimentally (e.g. Liakopoulos, 1964; Whisler & Watson, 1968; Kastanek, 1971). During drainage, a non steady state exists and it is described by the three equations of motion, continuity and state. The resulting equivalent problem in mathematical terms is a non-linear parabolic partial differential equation in which the dependent variable is the pressure of the water or the volumetric water content of the soil and the independent variables are the time and the position along the vertical direction. Stating the strong non-linearity in its terms, the equation cannot be solved by analytical methods and therefore numerical integration is employed. Both explicit and implicit schemes were used.
The bottom of the soil layer is constantly at atmospheric pressure and, therefore, the pressure of the water leaving the soil stratum is zero (i.e.Ψ=0). The top boundary condition follows from the absence of flow across the upper soil surface boundary (i.e. $\frac{\partial \psi}{\partial z} = -1$). The initial condition results from the fact that when the gravity drainage starts (time when the final increment of the ponded water has entered the soil surface) the pressure is zero, so that the drainage is under the effect of the gravity pull only. After this initial stage, the pressure will start attaining negative values; these negative values decrease at all height and times, until an equilibrium condition, at which the pressure is equal to the elevation, is achieved.

Fig. 12 shows the experiments completed by Liakopoulos (1964): the experimental setup of the column tests (a) and the distribution of pressure head values in relation to elevation above the bottom atmospheric boundary during the gravity drainage of a column filled with saturated sand.

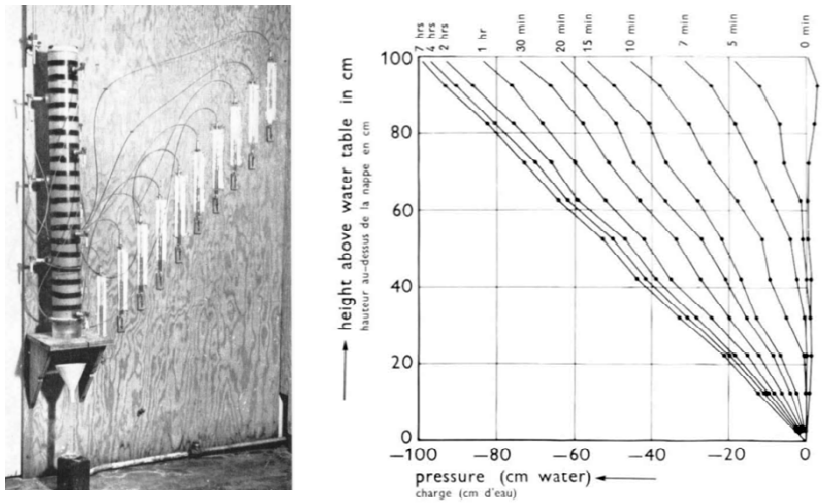

Fig. 12 - Column tests performed by Liakopoulos (1964): (a) general view of the experimental setup; (b) distribution of pressure head in relation to elevation (colums one meter height)

It is worth noting that as soon as the equilibrium condition has been achieved, pressure head values are known at any point of the flow domain. Measures of soil moisture content values straightly yield to the reconstruction of the main drying branch of the soil water retention curve.

Furthermore, many physical or numerical models predict the main wetting phase from the main drying curve. These models were developed to benefit of the more common experimental measures of the drainage phase (Hillel, 1998). In particular, the main contributions were due to Parlange (1976), Mualem (1977), Hogarth et al. (1988), Feng and Fredlund (1999) and Pham et al. (2003). All the models listed require the boundary drying curve and two meeting points (i.e. the coalescence points of the main drying and wetting curves) to

predict the entire boundary wetting curve. Reliability analysis of these models were performed by comparing their results with many experimental datasets. Viaene et al. (1994), Si and Kachanoski (2000), and Maqsoud et al. (2004) selected the model proposed by Parlange (1976); while Pham et al. (2003) argued that an originally modified version of the Feng and Fredlund (1999) model provides the best results.

Braddock et al. (2001) introduced the Van Genuchten (1980) model of the soil water characteristic function into the Parlange (1976) hysteresis model, which was originally based on the Brooks and Corey function. They obtained a first order ordinary differential equation which can be integrated to give simple closed form expressions for the main wetting function $\theta_{w,main}$ (Eq. 21)

$$\theta_{w,main}(\psi) = -\theta_s \alpha\psi + \theta_s[1 + (\alpha\psi)^n]^{1/n} \qquad \text{Eq. 21}$$

The general solution of the same first order ordinary differential equation leads to a pair of formulae for the wetting and drying scanning curves (see par. 3.3.3).

Maqsoud et al. (2004) demonstrated that the Braddock et al. (2001) version of the model of Parlange (1977) was the best one to predict the wetting and drying hysteretic behavior of silty sand and fine sand textures.

The Feng and Fredlund (1999) model is based on the empirical equation (Eq. 22) used to represent both the boundary drying and the boundary wetting curve.

$$\theta_{main}(\psi) = \frac{\theta_{d,\psi=0} b + c\psi^d}{b + \psi^d} \qquad \text{Eq. 22}$$

Where $\theta_{d,\psi=0}$ is the water content on the boundary drying curve at zero soil suction; and *b*, *c*, *d* are curve-fitting parameters. The residual water content ant the water content at zero soil suction are assumed to be the same for both boundary curves: once the boundary drying curve has been defined, two curve fitting parameters are known ($\theta_{d,\psi=0}$ and *c*).

Two additional curve-fitting parameters, i.e. b_w and c_w , are required to predict the boundary wetting curve. In order to achieve this aim, two additional points on the boundary drying curve are required.

Pham et al. (2003) suggested that the position of the first point on the boundary wetting curve could be defined as a point having a soil suction of ψ_1 such that:

$$\psi_1 = \left(\frac{b}{10}\right)^{1/d} \quad \text{Eq. 23}$$

where *b* and *d* are best-fit parameters of the boundary drying curve (Eq. 22).
The soil suction at the second additional point, ψ_2 (corresponding to a water content θ_2) , can be determined from the following equation (Eq. 24):

$$\psi_2 = \psi_1 - 2\left\{\left[\frac{b(\theta_{d,\psi=0} - \theta_1)}{\theta_1 - c}\right]^{1/d} - b^{1/d}\right\} \quad \text{Eq. 24}$$

where *b*, *c*, *d* are curve-fitting parameters of the boundary drying curve, θ_1 is the water content at the first additional point.
The two parameters b_w and c_w can then be calculated using Eq. 25 and Eq. 26

$$d_w = \frac{log\left[\frac{(\theta_1 - c)(\theta_{d,\psi=0} - \theta_2)}{(\theta_{d,\psi=0} - \theta_1)(\theta_2 - c)}\right]}{\log(\Psi_2/\Psi_1)} \quad \text{Eq. 25}$$

$$b_w = \frac{(\theta_1 - c)\,\psi_1}{\theta_{d,\psi=0} - \theta_1} \quad \text{Eq. 26}$$

2.4.3 Column tests, experimental set up

Column tests were performed in the *Hydraulics Laboratory "G.Bidone"* of the Polytechnic University of Turin in order to achieve one-dimensional water movement into the porous medium.
The experimental setup consisted in a plexiglass colum 1.50m high, 0.012 cm thick, having a circular, 0.10m diameter cross section. 0.10m vertically distant ticks provided an undistorted spatial reference. The column was packed uniformly with perfectly dry sand

from the bottom up to 1.15m; 0.35 m was the maximum hydraulic head value allowed: the corresponding water volume assured the complete saturation of the sand column before the end of the depletion phase. Water pouring was performed manually, as quickly as possible, using a bucket and a funnel. A layer of Regicell 30 reticuated foam 0.04 m thick avoided scouring and promoted a water uniform distribution during the early phases. A wire mesh filter was installed at the bottom of the column to retain sand while allowing air to flow.

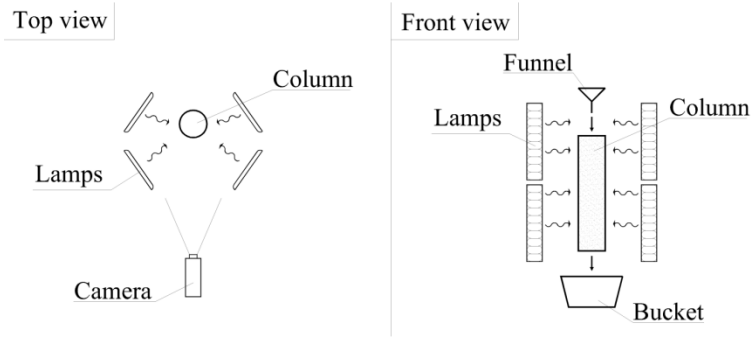

Fig. 13 – Column tests: sketch of the experimental setup

A transition phase lasted untill the water level reached the maximum value and was followed by a merely infiltration phase up to a zero value of the water level. Every trial was recorded using a camera (spatial resolution 768 x 576 pixel; temporal resolution 25 frames/sec). A original image interpretation protocol developed in Matlab environment allowed the analysis of each frame and the detection of (i) water level, i.e. the hydraulic head above the sand column and (ii) wet/dry downward moving interface in the porous media. The metric scale reference provided by the 0.10 m vertically dinstant ticks allowed to take into account the variability in the aperture angle. The exact water level or wet/dry interface position were then computed according to Snell's law describing the relationship between the angles of incidence and refraction of light waves passing through a boundary between two different isotropic media (i.e. air and plexiglass). Different techniques were

subsequently applied to detect time-dependent soil moisture profiles during infiltration under ponding and drainage phases.

2.4.3.1 Tap water

Tap water was manually poured in the column as quickly as possible using a bucket and a funnel. Fig. 14 shows the time series of (i) water level and (ii) wet/dry moving interface retrieved using our Matlab code for image processing.
The quasi-dichotomous distribution of color intensity in the wet and dry areas prevented the assessment of time dependent soil moisture profiles and demanded a more sophisticated solution.

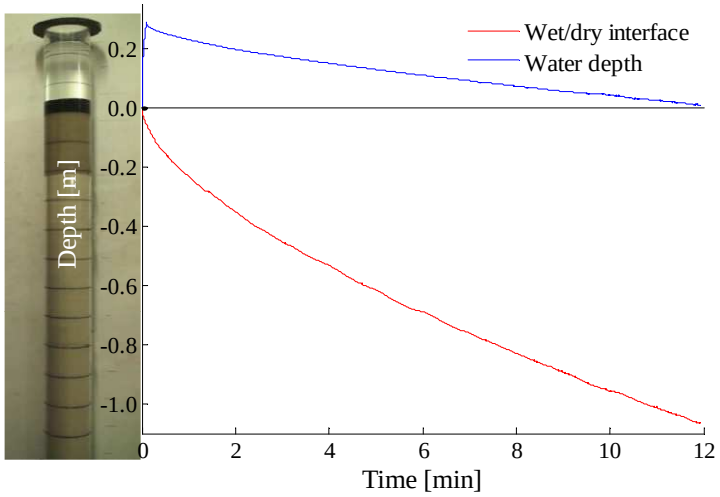

Fig. 14 – Column test, tap water: detection of the time dependent values of water depth and wet/dry interface position.

2.4.3.2 Tracers

In general, a tracer is a substance or entity that is experimentally measured in a system for deducing process information. To be detected by a measuring device, a tracer must be distinctively different from other substances or entities within the system of study.
In subsurface hydrology, tracers have played a significant role in elucidating flow pathways, velocities and travel times, hydrodynamic

dispersion, recharge, and discharge, flow and transport processes, flow connections, flow velocities, and hydrodynamic dispersion.
An ideal water tracer should have the following characteristics (Kaufman and Orlob, 1956; Church, 1974; Davis et al., 1980; McLaughlin, 1982):

1. conservative behavior, i.e. the tracer moves in a manner similar to water, that is, (1) without sorption to soils, sediments, or rocks and (2) without degradation during the time frame of interest;
2. low background concentration, i.e. the tracer is clearly discernible from the background of the system;
3. insensitivity to changes in solution chemistry, i.e. the tracer's fate and transport behavior are unaffected by changes in pH, alkalinity, or ionic strength of the aqueous solution;
4. detectability either by chemical analysis or by visualization;
5. low toxicological impact on the study environment.

Nevertheless, the same authors pointed out the inexistence of such an ideal water tracer. In fact, the tracer closest to an hypothetical ideal one are stable isotopes of the water molecule itself.
Although a wide variety of tracers have been used in subsurface hydrology (e.g. temperature, inorganic anions, sulfur hexafluoride, spores and particles, microorganisms) dyes are recognized as the most prominent; their popularity is due to their low detection limits, visualization potential, and ease of quantification by chemical analysis (Flury et al., 2003).
Dyes are usually classified either by their chemical structure or coloristic features; the most comprehensive catalogue of dyes is the Colour Index (The Society of Dyers and Colourists, 1971, 1999).
In particular, fluorescent dyes are especially attractive tracers because of their (1) detectability at very low concentrations (0.1 to 0.01 μg/l and, in some cases, even 0.001 μg/l); (2) low cost; (3) non-toxicity; (4) non-mutagenetic behavior (e.g. Gasper, 1987; Sabatini and Austin, 1991). Fluorescence generally refers to any emission of light not directly ascribable to heat (Wilson, et. al. 1986). Upon irradiation from an external source, a fluorescent substance will emit radiation (light) of lower energy (longer wavelength). When irradiance ceases, fluorescence ceases. Each fluorescent substance is characterized by a specific excitation spectrum and specific emission spectrum. The

concentration of the dye is proportional to its fluorescence. Fluorescence intensity could be measured through image processing thus leading to the detection of time dependent soil moisture profiles during both wetting and drying phases.

There are a number of physicochemical factors that must be considered when performing dye fluorometry hydrologic studies: mainly concentration, temperature, and quenching (Wilson et al. 1986).

Dye fluorescence varies directly with dye concentration. An adequate volume of dye must be used to permit accurate and precise measurements for the duration and extent of the study while avoiding over-exposition problems.

Fluorescence activity increases as water temperature decreases thus indicating an apparent higher dye concentration.

Quenching is the suppression of fluorescence resulting from the action of other substances. Quenching agents may act (1) absorbing excitation energy; (2) absorbing emission (fluorescence) energy; (3) degrading excitation-state energy; and (4) chemically altering the dye molecular structure (Williams and Bridges 1964). Chlorine is an example of a quenching agent that changes fluorescent properties of many dyes by altering their molecular structure; great care must consequently be taken to use distilled or deionized water when preparing dye dilutions. Photochemical decay results from exposure of the dye to bright sunlight for extended periods of time. Water tracing dyes have a tendency to adhere to (adsorption) or to be incorporated in (absorption) suspended matter, sediments. As a rule, organic sediments tend to adsorb more dye than inorganic sediments.

The most prominent fluorescent dyes used as hydrological tracers are Rhodamine WT and Fluorescein (Flury et al., 2003).

In our tests we used distilled water at 22°C and great care was taken to avoid direct sunlight exposition. Dilution tests were performed to prove fluorescence detectability while avoiding overexposure problems. The standard concentration of 10 mg/L (see, for example, Chua et al., 2007) was verified and adopted.

Fluorescence detectability of saturated samples was also checked.

Based on the absorption spectrum of both these fluorescent dyes, for black lights provided the only external source for irradiation (Fig. 13, Fig. 16) .

A black light is a lamp that emits long wave ultraviolet UV-A light (wave length range: 315 to 400 nm) essential in observing fluorescence. The lamps we used had a dark purple glass filter in the lamp housing, which blocked most visible light and allowed UV, they had a dim purple glow when operating.

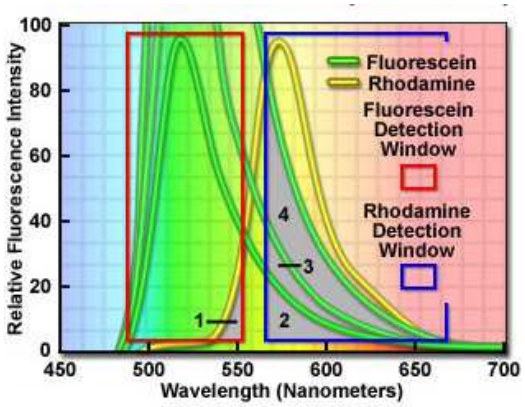

Fig. 15 – Fluorescein and Rhodamine emission spectra

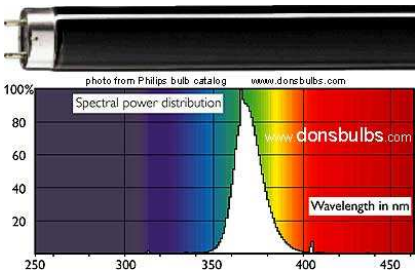

Fig. 16 – Black light: lamp and spectral power distribution

Rhodamine

Rhodamine WT, also known as Acid Red #388, is a synthetic red to pink colored water soluble dye having brilliant fluorescent qualities. Its molecular formula is $C_{29}H_{29}N_2O_5ClNa_2$ and its Colour Index is 37299-86-8.

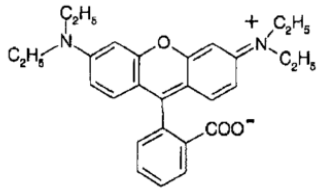

Fig. 17 – Rhodamine: structural formula

Rhodamine has been largely used in dye fluorometry hydrologic studies thanks to its ease of use, relatively low cost, low adsorptive tendency, strong fluorescence, high diffusity, chemical stability, and benign character in the aquatic environment (e.g. Parker 1973, Smart and Laidlaw 1977, Wilson, et. al. 1986, Kilpatrick and Wilson 1988). It is often preferred to fluorescein as it offers longer wavelength emission maxima and provides opportunities for multicolor labeling or staining.

Fluorescence detectability of saturated samples was checked; the standard concentration of 10 mg/L (see, for example, Chua et al. (2007)) was verified and adopted.

Unluckily, when we performed our laboratory test, fluorescence quenching occurred as soon as the dilution traveled downwards in the sand column (Fig. 18).

Fig. 18 – Column test, rhodamine quenching

In fact, several researches previously observed fluorescent dyes sorption behavior on aquifer media (e.g. Smart and Laidlaw, 1977; Bencala et al., 1983; Behrens, 1986; Sabatibi and Austin, 1991; Mikulla, 1997).
Fluorescent dyes are large molecules that would not be water soluble without ionic functional groups (e.g. COO^- and SO_3^- groups). These ionic groups not only increase the dye water solubility but can also interact with oppositely charged surface sites thus increasing dye sorption. In particular, Kasnavia et al. (1999) discussesed the interaction of dye and media properties of four fluorescent dyes (fluorescein, rhodamine B, rhodamine WT, and sulforhodamine B) and two oppositely charged mineral surfaces (alumina and silica). Fluorescein, which has only negative functional groups, sorbed least onto negatively charged silica but most onto positively charged alumina. The rhodamine dyes, with a permanent positive charge and negatively charged functional groups, sorbed onto both alumina and silica.

Fluorescein

Fluorescein, also known as Acid Yellow 73, is a synthetic organic yellow to green colored water soluble dye having brilliant fluorescent qualities. Its molecular formula is $C_{20}H_{12}O_5{}^{-}{}_2Na$ and its Color Index is 518-47-8.

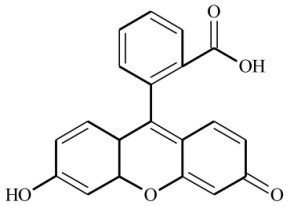

Fig. 19 - Fluorescein: structural formula

Fluorescence detectability of saturated samples was checked; the standard concentration of 10 mg/L (see, for example, Chua et al. (2007)) was verified and used.
Unluckily, the dilution wetted the inner surface of the plexiglass column creating a uniform opaque film which prevented the detection

of fluorescence intensity gradients (and thus soil moisture variations) in the sand media (Fig. 20).

Fig. 20 – Column test: fluoresceine dilution wetted the inner surface of the plexiglass column.

2.4.3.3 Soil moisture sensors

One common technique to assess soil moisture is to measure the dielectric constant, that is, the capacitive and conductive parts of a soil's electrical response. Since the dielectric constant of water is much higher than that of air or soil minerals, the dielectric constant of the soil is a sensitive measure of water content. Through the use of appropriate calibration curves, the dielectric constant measurement can be directly related to soil moisture (Topp et al. 1980).
Dielectric constant may be measured by commercially available probes, designed to be buried and left in-situ. In this study, three EC-5 Soil Moisture Sensors produced by Decagon Devices were used (Fig. 21).
These small sensors (8.9cm x 1.8cm x 0.7cm) can detect from zero to saturation water content. They are powered by 2.5 to 3.6 V at 10mA, the output signal is 10-40% of excitation voltage (i.e. 250-1000mV at 2500mV excitation). Measured data are provided every 10ms and recorded by a datalogger.

Fig. 21 – EC-5 Soil Moisture Sensor produced by Decagon Devices.

Volumetric water content were computed from measured values of the dielectric constant using experimental calibration curves specifically derived for the soil textures used in our laboratory experiments. In particular, a minimum square fitting method yielded to an empirical relationship between known values of soil water content and sensor's output data.

Three small holes were dug in the column 0.20, 0.40,0.80 m below the water/sand interface. Sensors were introduced, any void space in the side wall of the column was accurately filled with mastic (Fig. 22) . When installing the sensors, it was important to remember that the soil adjacent to the sensor surface has the strongest influence on the sensor readings, any air gaps or excessive soil compaction around the sensor can profoundly influence the readings. Although the sensor could theoretically be oriented in any direction, the flat side was perpendicular to the surface of the soil in order to minimize disturbing effects on downward water movement.

Data recordings were performed during the wetting phase and the subsequent drainage phase of three experimental trials (Test2, Test3, Test4). Time dependent soil moisture values at three point of the sand domain were useful for the implementation of the numerical strategies selected for the assessment of Van Genuchten parameters.

Fig. 23 shows the data sampled during the wetting phase of one experimental trial.

The experimentally detected wet/dry interface provided a good approximation for the arrival of the wetting front; precision slightly decreased with the extension of the infiltration flow as preferential flow paths due to the wettability of the inner surface of the plexiglass column became more evident.

The sharpness of the wetting front sensibly decreased with the extension of the subsurface flow.

Fig. 22 – Column tests: soil moisture sensors positioning

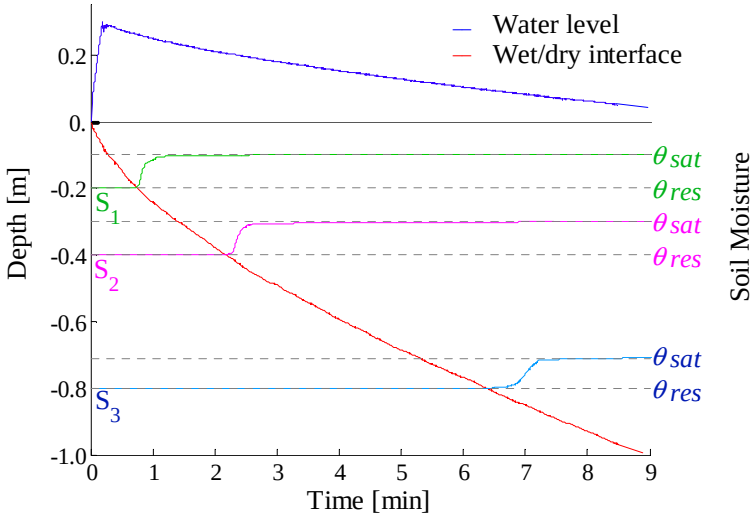

Fig. 23 – Column tests, detected time series of water level, wet/dry interface position, water content at three points.

2.4.4 Implementation of the numerical strategies

The data sampled during the lab activities allowed the implementation of two, different numerical strategies, i.e. (A) inverse parameter estimation techniques for both wetting and drying phases and (B) direct fitting of the main drying curve based on sampled data.
A complete numerical modeling of the wetting phase was achieved using the software Hydrus. The geometric domain obviously reproduced the real experimental set-up.
Previously defined sand parameters were used (specifically, saturated hydraulic conductivity, saturated water content, residual water content). A catalog of average parameters for 12 soil textural classes of the USDA textural triangle (Carsel and Parrish, 1988) and hierarchical pedotransfer functions as derived by Schaap et al. (2001) in their Rosetta program yielded to an initial estimate of the unknown parameters α, n for the complete description of the Van Genuchten model of SWRC.
A free drainage condition was the bottom boundary condition; no-flow boundaries represented the side walls of the plexiglass column. Experimental time series of water level provided the upper boundary condition, i.e. the variable hydraulic head above the sand column.
A spatially uniform residual water content value supplied the initial condition for numerical modeling.
Transient values of the position of the wet/dry interface and recorded water content values at three points of the infiltration domain provided the calibration data for the implementation of inverse parameter estimation strategies.
The computational mesh and a lower boundary threshold value of the computational time step were defined based on numerical analysis of the Peclet-Courant conditions.
HYDRUS software packages implement Marquardt-Levenberg's local optimization gradient method (Marquardt, 1963; Šimůnek and Hopmans, 2002) for inverse parameter estimation of soil hydraulic parameters from measured transient flow data. The Marquardt-Levenberg method is a local optimization gradient method that requires initial estimates of the unknown parameters to be optimized. Since the method can then be very sensitive to the initial values of the parameters, it is generally recommended to repeat the optimization

problem with different initial estimates of the optimized parameters (Šimůnek and Hopmans, 2002). The computational efficiency of Marquardt-Levenberg's local optimization gradient method was demonstrated by many authors (e.g. Wildenschild et al., 2001; Vrugt et al., 2008; Wöhling et al., 2008). Additionally, the Marquardt-Levenberg method provides confidence intervals for, and correlations between, the optimized parameters, thus facilitating immediate insight into the optimization problem.

Hydrus software packages incorporates hysteresis by using the empirical model introduced by Scott et al. (1983), as successively modifyed by Kool and Parker (1987) to account for air entrapment and by Vogel et al. (1996) to consider hysteresis in the hydraulic conductivity function. Since the implementation of this model requires the knowledge of both main wetting and main drying curves, the numerical modeling and parameters' assessment of one phase at a time avoided the problem of the hysteretic behavior.

The accurate modeling of the main wetting phase required the modification of the source code of the Hydrus package, kindly released by Šimůnek. The original Hydrus package does not allow mass accumulation at the upper boundary of the domain and any water excess is instantaneously removed (Šimůnek et al., 1999). Our modified version of the Hydrus package allowed water storage at the upper boundary of the computational domain according to the principle of mass conservation. Introducing as upper boundary condition the sampled data of water level time series, we aimed to point out a set of parameters values yielding to an accurate reproduction of the experimental evidence of water movement in the soil and a constant zero overland flow.

Direct fitting of the main drying curve was based on the measure of soil moisture values at three points of the vertical column at the end of the drainage phase. As previously detailed, during the drainage phase negative pressure values increase at all height and times, until an equilibrium condition, at which pressure is equal to elevation, is achieved. The least square fitting method thus allowed the assessment of Van Genuchten parameters based on the three known points of soil moisture-pressure head values.

Referring to our literature review, the hysteresis models proposed (i) by Parlange (1976) and modified by Baddroch (2001) and (ii) Feng

and Fredlund (1999) and improved by Pham (2004) were applied for the assessment of the main wetting curve starting from the main drying branch.

2.4.5 Results

2.4.5.1 Critical issues

Grain size distributions of sand samples collected from different containers or from different levels of the same container didn't overlap and resulted in different wetting and drying behaviors. Fig. 24 shows grain size distributions of four samples used for column tests; Fig. 25 represents the consequent time series of water depth and wet/dry interface position. The coarsest sample was used in Test 2 and yielded to the fastest lowering of both water depth level and wetting interface position.

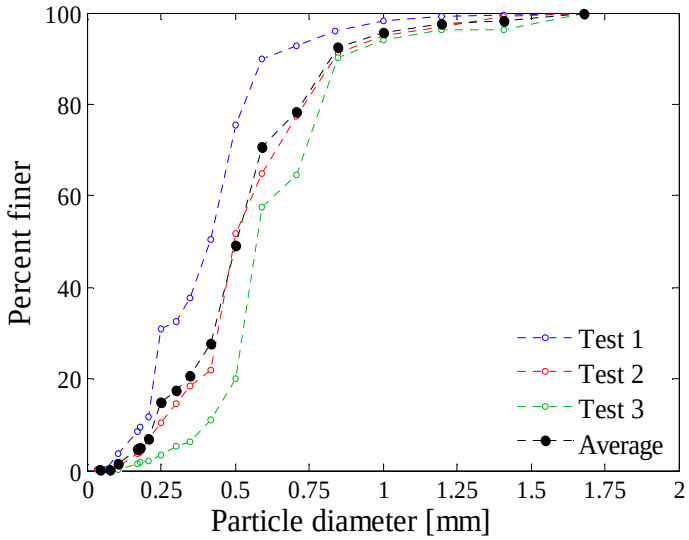

Fig. 24 – Grain size distribution of four samples used for column tests

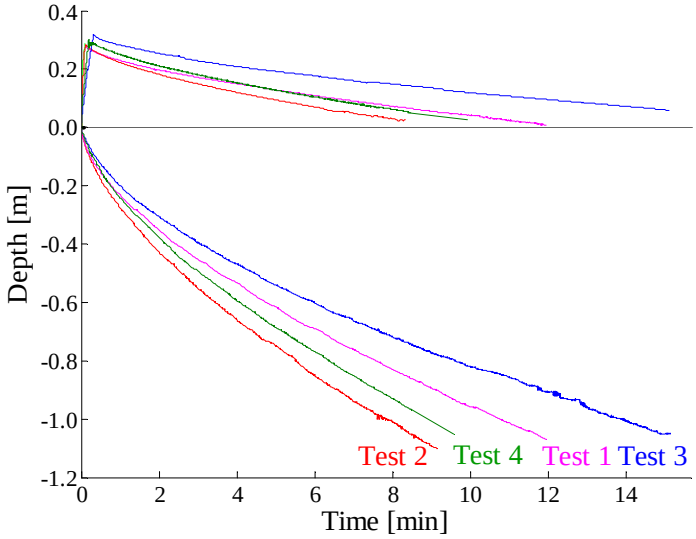

Fig. 25 – Detected values of water level and wet/dry interface position for four column tests

Tracing the containers specifically used for each experimental trial in the flume was not possible, furthermore, depending on practical issues, more than one container could have been used at a time. As a consequence, averaged, representative values of Van Genuchten parameters were required to overcome local grain size heterogeneities resulting in slightly different wetting behaviors.

2.4.5.2 Main drying curve

B1) Application of the drainage theory

Soil moisture values were retrieved at three points of the sand domain at the end of the gravity drainage phase. Based on previous numerical and experimental studies on gravity drainage (e.g. Liakopoulos, 1964; Whisler & Watson, 1968; Kastanek, 1971) , the pressure head of these points equals their elevation above the sand media/atmosphere interface. Additionally to the default starting point (saturated water content at zero pressure head), three points were then used for the numerical fitting of Van Genuchten parameters.

Fig. 26 shows the data collected during Test 2 and the consequent main drying behavio.

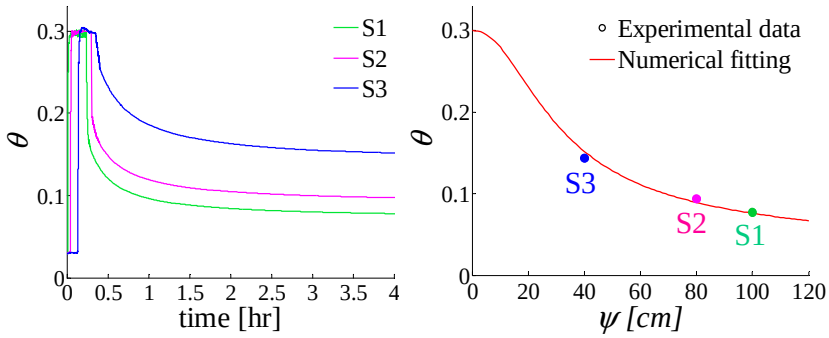

Fig. 26 a) Test2, soil moisture data; b) Test 2: computed main drying curve

Tabel 6 allows a direct comparison between the values of Van Genuchten parameters computed for Test 2, Test 3, Test 4.

Tabel 6 – Values of Van Genuchten parameters of the main drying phase, fitting of sampled data

	Van Genucthen parameters	
	α	n
Test 2	0.043	2.20
Test 3	0.040	2.10
Test 4	0.031	2.38

2.4.5.3 Main wetting curve

A) Inverse parameter estimation

Inverse parameter estimation techniques used soil moisture time series measured at three points of the sand domain during three experimental trials.
Fig. 27 compares computed and measured soil moisture values for Test 2.

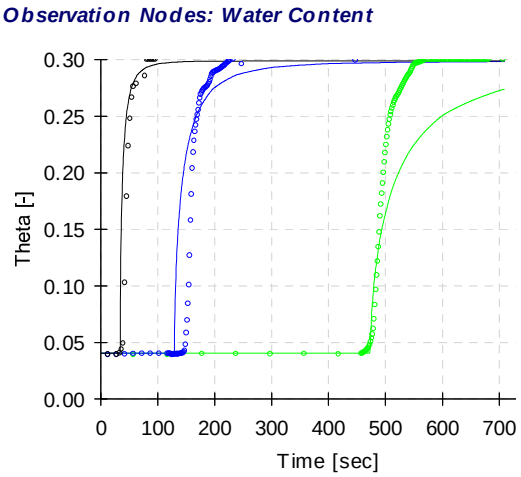

Fig. 27 - Test 2, wetting phase, measured (o) and computed (-) soil moisture values

Tabel 7 allows a direct comparison between the values of Van Genuchten parameters computed for Test 2, Test 3, Test 4.

Tabel 7 - Values of Van Genuchten parameters of the main wetting phase, inverse parameter estimation

	Van Genucthen parameters	
	α	n
Test 2	0.083	2.91
Test 3	0.075	2.96
Test 4	0.071	2.80

B2) Application of hysteresis models based on the analysis of the drainage phase

The hysteresis model of Parlange (1976) as modified by Baddrock (2001) as well as the model of Feng and Fredlund (1999) as improved by Pham (2004) were used for the assessment of the main wetting branch starting from the computation of the main drying branch.

Fig. 28 shows the main branches of the soil water retention curve computed using the data retrieved from Test 2. In particular, the main drying curve was based on the data sampled at the end of the drainage phase; the main wetting curve was based on the hysteresis models of Parlange (1976) and Feng and Fredlund (1999).

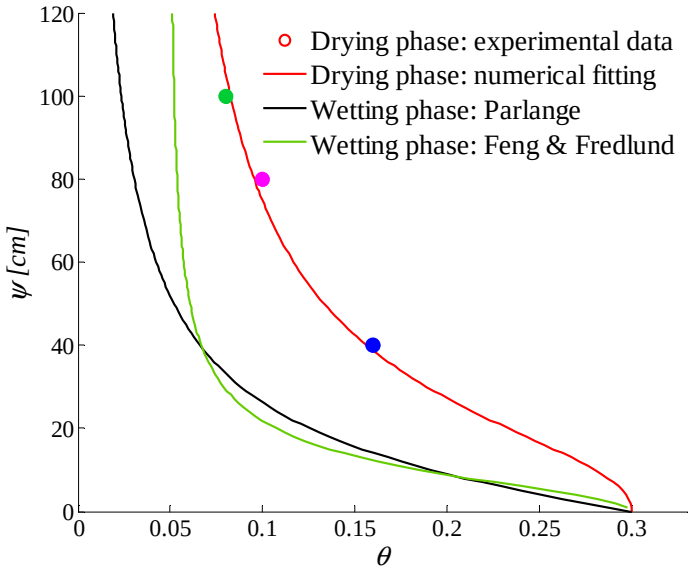

Fig. 28 – Test 2, soil water retention curve, main drying and main wetting branches

The main wetting branches computed using the hysteresis models selected, were fitted using the Van Genuchten model of the soil water retention curve in order to allow a direct comparison of the results (see, for example Fig. 29).
Tabel 8 and Fig. 31 allow a direct comparison between the main wetting branches of Van Genuchten model computed for Test2, Test3, and Test4 respectively using (A) the Marquandt Levenberg's inversion parameter estimation protocol; (B2) the hysteresis model of Parlange (1976) and of Feng and Fredlund (1999).

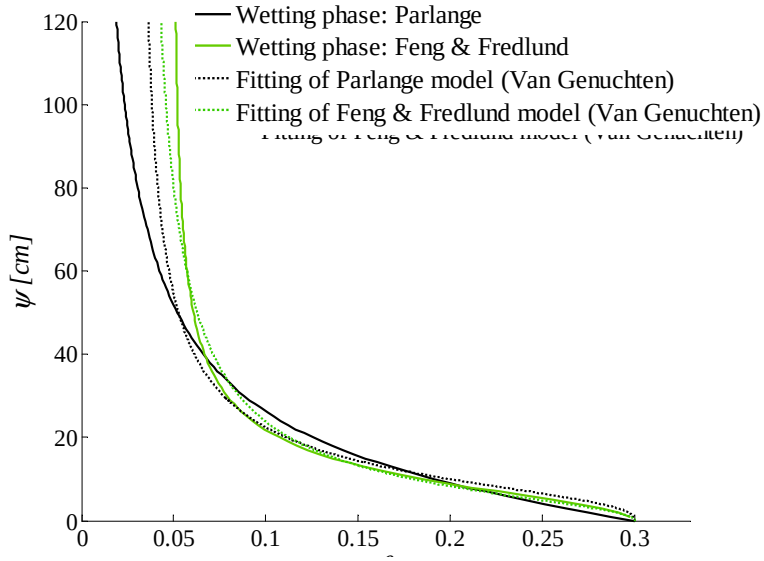

Fig. 29 – Test 2, main wetting branches based on the hysteresis models of Parlange (1976) and Feng and Fredlund (1999) (lines), and fitted behaviors based on the model of Van Genucthen (1980) (dots)

Tabel 8 –Main wetting branch of the SWRC, assessment of Van Genuchten parameters

	Van Genuchten parameters					
	Inverse parameters estimation		Hysteresis model of Parlange		Hysteresis model of Feng and Fredlund	
	α	n	α	n	α	n
Test 2	0.078	2.91	0.107	2.48	0.145	2.06
Test 3	0.051	3.30	0.125	2.66	0.181	1.96
Test 4	0.071	2.80	0.091	2.34	0.130	2.41

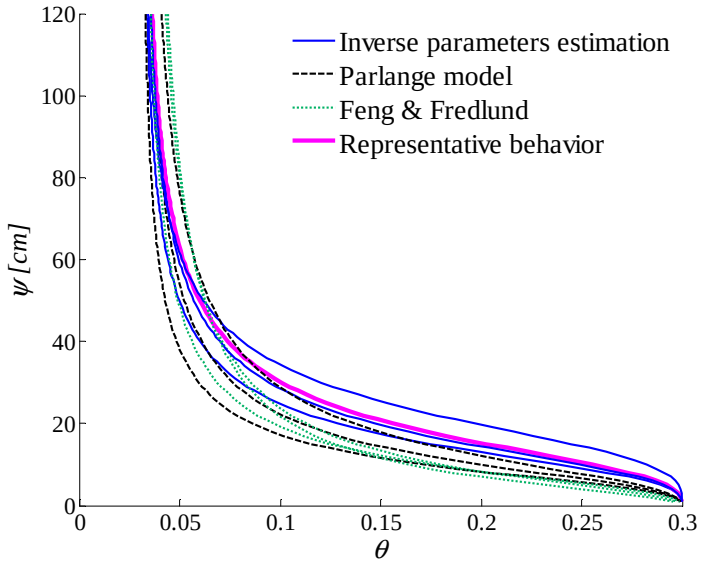

Fig. 30 – Main wetting phase, comparisons of results

The results matched adequately; stating the sensibly larger series of experimental data available, greater relevance was given to the results retrieved by inverse modeling techniques.
An averaged, representative behavior was assumed to overcome local grain size heterogeneities resulting in slightly different wetting behaviors (see Fig. 30).

2.5 Numerical model

In order to achieve a deep understanding of the physical process we first wrote an original Matlab code to solve Richards equation based on the "mass conservative" method proposed by *Celia et al.* (1990).
We then used a commercial software, Hydrus 2D (Šimůnek et al., 1999).
A zero-slope rectangular, 0.20 deep, 3.0m long computational domain reproduced the experimental set-up.
A uniform soil layer was used; Van Genuchten model was selected for the description of the main wetting branch of soil water retention curve. Tabel 9 lists the empirical values of the parameters used in the numerical model.

Tabel 9 – Parameters used in the numerical model

θ_s	θ_r	α	n	$k_s[m/s]$
0.03	0.03	0.08	2.80	$1.050 \cdot 10^{-4}$

Lateral and bottom boundaries were impervious (i.e. a “no flow” condition was assumed); measured time series of the hydraulic head values were imposed as upper boundary conditions.
The original version of the Hydrus packages allows only four, distinct time series of hydraulic head values. A second modification of the source code, kindly released by the author, J. Šimůnek, was required in order to allow the imposition of a time series of hydraulic head values at any point of the upper boundary of the computational domain. The computational mesh and a lower boundary threshold value of the computational time step were defined based on numerical analysis of the Peclet-Courant conditions. In particular, a lower threshold value of 10^{-4} sec was adopted, and an anisotropic spatial discretization 0.01 and 0.005m wide in the horizontal and vertical directions respectively was used.
Experimental time series of the wet/dry interface position were used to check the numerical results.

As shown, for example, by Fig. 31 (a,b) , they reasonably matched with the numerical lower boundary of the dry sand (corresponding to the residual water content value).

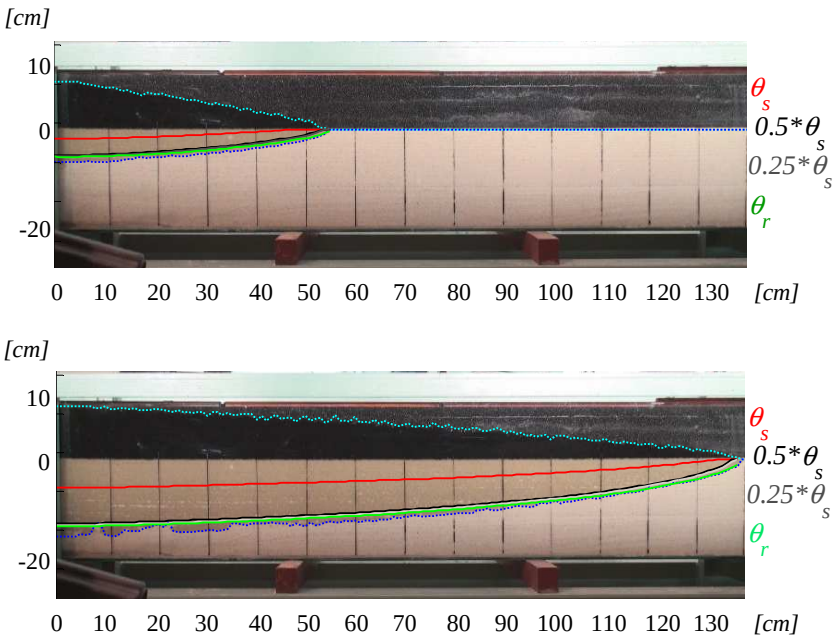

Fig. 31 – Detected and modeled wet/dry interfaces in the porous mattres and in the sand

The relative importance of horizontal and vertical water flows in the subsurface domain was evaluated by the implementation of a simplified numerical model developed in Matlab environment. The computational domain was discretized as a sequence of adjoining but independent 0.02cm wide, 0.20 deep sand columns. Hydraulic head time series detected at any 0.02cm distant position of the flume domain were used as upper boundary conditions for the numerical solution of the infiltration model proposed by Green & Ampt (1911). As widely explained in par. 1.2.6, the Green & Ampt model assumes a piston flow yielding to an abrupt change in water content switching from the residual value to the saturated value. Iso-saturation profiles computed by this simplified model and the more sophisticated two-

dimensional solution of Richards equation agreed. Fig. 32 shows the depth of the saturation profile as a function of time computed with both the simplified 1D (pink dots) and the complete 2D (blu line) numerical models for a cross section 4cm far from the inlet. The residual water content profile computed with the complete 2D numerical model (green line) and the wet/dry interface experimentally detected (black circles) complete the figure.

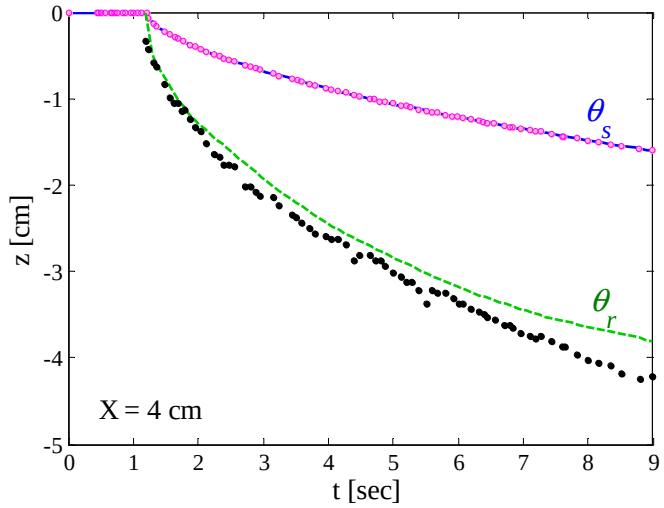

Fig. 32 – Depth of the saturation profile computed with the simplified 1D (pink dots) and the complete 2D (blu line) numerical models

Our results pointed out the higher importance of the vertical flow over the horizontal flow in the subsurface domain. In fact, the vertical component of the velocity vectors computed by Hydrus 2D was generally sensibly bigger than the horizontal component. Sharp horizontal soil moisture gradients near the wet/dry interface supported a local slight relevance of the horizontal component.

2.6 Conclusions

A series of lab experiments was performed in the *Hydraulics Laboratory "G.Bidone"* of Polytechnic University of Turin in order to study the routing of waves on a permeable boundary. Adopting a gradual analysis approach, the complex problem was decoupled to allow a deep insight in the physical modeling of the infiltration phenomenon. Experimental depth hydrographs were used as upper boundary conditions in an appropriate numerical model of the infiltration process.

A first outcome was the definition of a simple experimental set-up for the analysis of the routing of waves on rough, permeable boundaries. Many combinations of different reticulated foam textures (surface flow domain), sand textures (subsurface flow domain), and flow regimes were tested. Air-trapping, finger flows, preferential flow issues were detected; appropriate modeling conditions were pointed out.

A second outcome of this propaedeutic phase was a study on numerical solutions of Richards equation. In particular, the source code of the widely used commercial software Hydrus 2D was modified to fit experimental conditions: (i) a mass balance criterion was imposed at the upper boundary o f the computational domain thus allowing the modeling of both storage and depletion phases; (2) different hydraulic head time series could be imposed at any point of the upper boundary. This modified version turned out to be useful whenever the modeling of the infiltration process connected to the propagation of an externally computed or measured surge wave is required (see Chapter 3)

A third important outcome of this phase was the definition of a simple, time and money saving protocol to assess the parameters of the main branches of the soil water retention curve. The implementation of the protocol herein proposed involves column tests to measure both the wetting and the drainage phases of a soil sample. Data were sampled by a video-camera and a number of soil moisture sensors (three proved to be an adequate number) connected to a datalogger. The analysis of the equilibrium condition at the end of the drainage phase allowed the numerical fitting of the main drying

branch of the soil moisture retention curve. Literature analysis of the hysteretic behavior of the soil moisture characteristic curve provided reliable methodologies to assess the main wetting branch from the main drying branch (see, in particular, Parlange (1976) as modified by Baddroch (2001) and Feng and Fredlung (1999) as improved by Pham (2004)).

Inverse parameters estimation techniques (such as the Marquandt-Levenberg method implemented in any Hydrus package) provided an alternative for the assessment of the main wetting curve from the data measured during the imbibition phase.

The last outcome concerned the higher importance of vertical flows over horizontal flows in the subsurface domain.

Chapter 3

Overland flow and infiltration in near horizontal plots: numerical modeling

3.1 Introduction

Urban development, roadways, and associated infrastructure have significant negative effects on aquatic systems (e.g. Booth and Jackson, 1997).

An increase of impervious surfaces in a watershed generally results in an increase of stormwater runoff volumes, peak flows, flood frequency, and flood wave celerity. Furthermore soil storage available for base flows decreases (Wang et al., 2001; Davis 2003).

These hydrologic changes, termed *hydromodification*, result in widening and increased instability of stream channels, increased sediment loads, erosion and degradation of both fish habitat and riparian life cycle (e.g. Booth and Jackson, 1997; Bledsoe and Watson 2001; MacRae 1992; Annear et al. 2004; Asleson 2009).

In addition to sediments, urban runoff often contains a wide variety of pollutants including nutrients, oxygen-demanding substances, pathogens, road salts, petroleum hydrocarbons, heavy metals (e.g. USEPA, 2005; Hatt et al., 2004; Leopold, 1968; Meyer et al., 2005). These pollutants cause a further degradation of aquatic habitats.

Alterations to stream ecology have been noted in areas that are as low as a few percent impervious, and once the impervious fraction reaches 10–30%, major declines are found in habitat and water quality indicators (e.g. Wang et al. 2001).

Low impact development (LID) is an environmental philosophy that focuses on controlling urban stormwater runoff. The goal is to manage site design and construction so that the hydrology and water quality of a developed site approximates that of the initial undeveloped land. The LID approach acts to minimize grading, disconnect impervious areas, preserve the existing landscape and topography, increase flow lengths, and lengthen the concentration time for stormwater runoff.

Stormwater treatment technologies currently available are stormwater wetlands, sedimentation ponds, sand filters, infiltration systems and, more recently, biofiltration systems (e.g. Davis, 2005; Wong, 2006).

In particular, biofiltration systems (also called biofilters, bioretention systems or rain gardens) are vegetated on-site infiltration-based techniques that are gaining increased attention thanks to their ability in reducing outfall stormwater runoff volume while improving water quality. Additionally, their low cost, design flexibility, small footprint, and aesthetic value are encouraging a wide diffusion (e.g. Winogradoff, 2002; ARC, 2003; Melbourne Water, 2005)

Biofiltration systems are based on two actors: stormwater runoff is directed into the facility and filtered through dense vegetation and, subsequently, through soil filter media. Biofilters' soil and vegetation properties enhance pollutant removal efficiency and increase their span life compared to traditional sand or gravel filters (Davis et al.,2001; Read et al., 2008). Treatment is achieved via a number of processes including sedimentation, fine filtration, sorption, and biological uptake.

Structurally, bioretention facilities consist of small ponds characterized by a porous layer approximately 0.4–1.0m deep and composed of a sand/soil/organic matter mixture. This layer is sometimes covered with a thin (2.5–8 cm) layer of hardwood mulch. Various grasses, shrubs, and small trees are planted to (i) promote evapotranspiration; (ii) maintain soil porosity; (iii) encourage biological activity; and (iv) promote uptake of pollutants.

Water is poured in the biofiltration trench, a surge wave travels through vegetation while infiltrating in the permeable soil until it reaches the downstream wall, then a storage phase begins. Water can pond on the surface, typically up to 50 cm, a weir diverts excess water away from the site. Ponding water drains through the system and partly evapotranspires; drainage should complete in 4–6 h in order to prevent long-standing water (Davis, 2003).
Outflowing water is collected by under-drains at the base of the filter media and reused or discharged to receiving waters.
Although their performance highly depends on site-specific design characteristics, biofiltration systems are acknowledged as a promising technology for restoring both predevelopment hydrology and water quality.
In particular, several field studies reported in literature (e.g. Davis et al., 2008; Hatt et al., 2009; Li et al., 2009) highlighted the contribute of biofiltration systems in enhancing hydrologic storage and preserving both aquatic and riparian ecosystems of stream channels.
These systems reduce (1) volume, (2) peak discharge, and (3) celerity of stormwater runoff by providing detention storage and promoting retention through infiltration and evapotranspiration.
The water balance equation (Eq. 27) allows to point out the relative importance of the different processes involved:

$$V_{IN} = \mathrm{ET} + V_{OUT} + \mathrm{EXF} + \Delta S + \mathrm{bypass} \qquad \text{Eq. 27}$$

where:

- V_{IN} is the inflow volume;
- ET the evapotranspiration volume;
- V_{OUT} the outflow volume from the underdrain;
- EXF the exfiltration volume to groundwater;
- ΔS the change in soil storage.

Optimal reduction rates have been proposed in order to approach the hydrologic behavior of an undeveloped land (Davis, 2008).
Biofilters have also been shown to be effective in the treatment of suspended sediments, heavy metals, nutrients, and pathogens (e.g., Davis et al., 2001; Zinger et al., 2007; Chandrasena et. al, 2012). For instance, in Australia biofilters are expected to achieve annual pollutant removal efficiency of 80% for total suspended solids (TSS),

90% for heavy metals, 45% for both total nitrogen (TN) and total phosphorus (TP) (Victorian Stormwater Committee, 1999).

Although practical experience exists in constructing and operating biofiltration systems, they are still often looked at as a "black box" which positively affects quantity and quality of stormwater runoff. Their design is consequently mainly based on rules of thumb derived from input-output analysis of field or experimental data.

Many empirical surveys focused on the hydrologic performances of biofilters and pointed out site-specific design advice. A few examples are here listed.

The higher performances generally observed for small events suggested that large media volume to drainage area ratios could be advisable (e.g. Holman-Dodds et al., 2003; Brander et al., 2004; Williams and Wise, 2006; Sansalone and Teng, 2004-2005; Barber et al, 2003; Davis et al., 2008; Li et al., 2009). More specific outcomes had a site-specific validity. For instance, a field survey completed by Le Coustumer et al. (2007) on 30 biofilters installed in Melbourne (Australia) pointed out that a biofilter area sized at 2.5% of its impervious catchment area is able to treat around 88% of mean annual inflows. Based on a study on a wide range of watersheds in California (USA) Palhengy et al. (2012) concluded that facilities receiving runoff from 100% impervious surfaces should have specific areas ranging from 12 to 25%. Deepening the filter media is suggested as a valuable solution to increase filter volume while enhancing evapotraspiration in highly urbanized areas (Li et al., 2009).

The use of appropriate media is an important factor in achieving reliable hydraulic functioning of the biofilters. A slow drainage is generally detrimental to performances (e.g. Davis, 2008; Barber et al.,2003; Sansalone and Teng, 2004,2005; Brander et al., 2004). For small events a 30% decrease in peak reduction and peak delay performances was seen for as little as 1% increase in prestorm water content. On the contrary, for large storms a weak relationship was found between soil moisture antecedent conditions and hydrologic performances (Barber et al., 2003). Nevertheless, on one hand the filter media should drain quickly, on the other hand it must allow enough detention time for evapotranspiration and pollutants removal (Hatt et. al, 2009; Li et al., 2009). A balance between filtered water

volume vis-à-vis residence time is an important design consideration. Recommendations for the value of saturated hydraulic conductivity vary from one country to another. For example, specific guidelines require a minimum value of 12.5 mm/h in New Zealand and in the USA (ARC, 2003; Claytor and Schueler, 1996; Winogradoff, 2002); between 36 and 360 mm/h in Austria (ONORM B2501-1, 2000); between 50 and 200 mm/h in Australia (Melbourne Water, 2005). Many authors detected a temporal decrease in infiltration capacity (e.g. Bouwer, 2002; Achleitner et al., 2006; Le Coustumer et al., 2007-2009; Asleson, 2009). In order to ensure appropriate hydrologic performances, high values of the saturated hydraulic conductivity (k_s>250 mm/h) were then recommended; the implementation of a safety factor ranging from 2 (New Jersey Department of Environmental Protection, 2004) to 3-4 (Le Coustumer et al., 2012) was suggested. Besides meeting hydraulic requirements, an appropriate soil matrix should have physical and chemical properties to enhance pollutants removal.

Vegetation type and density affects evapotranspiration intensity, soil moisture and, generally, the maintenance of appropriate hydraulic conductivity values. Although the exact mechanisms by which vegetation affects hydraulic conductivity of biofiltration media remains an important knowledge gap (Le Coustumer et al., 2012), many authors (e.g. Quinton, 1996; Archer et al., 2002; Le Coustumer et al., 2012) encouraged the selection of plant species with thick roots. Soil type (physical and chemical properties), climate conditions (e.g. temperature span, dry and wet spells length), water quality characteristics provide boundary conditions for the selection of an appropriate, site-specific vegetation type.

Specularly, many empirical surveys focused on the performances of biofilters in removing stormwater pollutants and pointed out site-specific design advice.

A laboratory study on biofiltration columns' ability to remove total suspended solids, total fosforus and total nitrogen from stormwater was completed by Lintern et al. (2011) and highlighted four impacting factors, i.e. soil moisture, vegetation type, filter media nutrient content, media depth.

Of particular interest, a general positive correlation between soil moisture and pollutant removal performances was detected; this result

was confirmed by Zinger et al. (2007) for nitrogen and by Chandrasena et al. (2012) for pathogens.

Although many field surveys on hydrologic and pollutant removal performances of biofiltration systems allowed important empirical assertions, significant questions about the physical, chemical, biological processes involved and the relative impact of design parameters still remain (Davis, 2008; Le Coustumer, 2012).

Attempts to fill this knowledge gap mainly concentrated on the processes leading to the removal of stormwater pollutants. The multi-component reactive transport module CW2D (Langergraber, 2001; Langergraber and Simùnek, 2005) is probably the most widely known outcome of this research effort. The module CW2D was incorporated in Hydrus 2D (Langergraber and Simùnek, 2005) and it models transport and reactions processes of the main constituents of wastewater and stormwater. Since it was developed for the modeling of constructed wetlands, an "atmospheric" upper boundary condition is required. The potential fluid flux across this interface is controlled by external conditions (precipitation, evaporation) and by the (transient) moisture conditions in the soil. Soil surface boundary conditions may change from prescribed flux to prescribed head type conditions (and vice-versa). When the infiltration capacity of the soil is exceeded a prescribed, constant head condition is applied. An expedient was proposed by Dittmer et al. (2005) in order to model the temporal variations of the storage volume according to mass balance conditions. The supernatant water level (storage volume) was modeled by a virtual layer with a pore volume of 100% and a residual water content of 0%. On the top of the virtual layer an atmospheric boundary condition was applied. This approach was implemented, for instance, by Henricks et al. (2007, 2009) to assess the performances of biofiltration facilities for organic matter and ammonium reduction. Nevertheless, it has been shown that a good match of simulation results with CW2D can only be achieved once the hydraulic behavior of the system has been modeled successfully (Langergraber, 2003; Henricks et al., 2007).

The hydraulic behavior of the system not only controls impacts on hydromodification but also plays a primary role for pollutant removal by controlling water and pollutants residence time, oxygen renewal, soil moisture content, vegetation and micro-organisms health

conditions (Carlton et al., 2001; Hatt et al. 2006; Zinger et al., 2007; Ross et al., 2011; Lintern et al., 2011; Chandrasena et al., 2012).
Accurate modeling of water surface and subsurface flows is thus essential for (i) a reliable analysis of the behavior of a biofiltration trench, and (ii) the definition of appropriate design advice to maximize both hydrologic and pollutant removal performances.
In particular, a complete modeling involves three phases: advance, storage and depletion.
The methods so far used for the hydraulic modeling of biofilters were originally developed for constructed wetland applications and focus on the storage and depletion phases while neglecting the advance phase. In fact, in biofiltration trenches the unsteady state functioning and the consequent hydraulic head variations during the advance phase play a primary role in infiltration processes (e.g. Beach et al., 2005; Ross et al., 2011).
Four modeling strategies were identified (She and Pang, 2010):

- curve methods relying upon empirical data curves to simulate outflow;
- physical models mainly based on the solution of Richards' equation;
- analytical models that hypothesizes a combinations of linear storage reservoirs (with separate storages for the ponding zone and the filter media zone);
- water-balance models that hypothesizes a set of storages with flows between them restricted by laws (such as Darcy's Law).

Water balance models are probably the most commonly implemented (e.g. Konyha et al., 1995; Heasom et al., 2006; Palhegy et al., 2012; Lintern et al., 2012).
Physical models are generally based on the numerical solution of Richards equations. In addition to the well-known Hydrus 2D package (Šimunek, 1998), it is worth quoting the numerical solution of Richards equation proposed by Dussaillant (2004) for the modeling of a biofilter. Both of them cannot model the advance phase in a horizontal trench.
Ross et al. (2011) compared the results of five water balance methods with experimental data and pointed out sensible inaccuracies, i.e. large differences were detected between computed and measured

outflow hydrographs. According to the authors difficulties in modeling could arise from (i) spatial distribution and variation of preferential flow paths; (ii) misinterpretations of the soil moisture patterns of the biofiltration trench.
In this study we aimed at the development of a complete numerical modeling of advance, storage and depletion phases observed in a biofiltration trench.
Such a model could

(a) increase the system understanding;

(b) document hydrologic performances;

(c) provide a valuable prognostic tool to suggest optimal design and maintenance procedures for both quantitative and qualitative treatment of stormwater runoff according to the site specific conditions

Based on the previous studies, the most influent design parameters are:

1) filter media volume, as the product of surface area and depth;
2) soil type;
3) vegetation type.

The lining of the sides is considered a good practice when polluted water is conveyed to the biofiltration facility.
Shape and slope of the surface area should promote spatially uniform conditions, i.e. the inflow should quickly wet the whole surface of the filter media and the hydraulic head during the storage phase should be uniform. A rectangular, horizontal domain coaxial with the main stream direction of a punctual inflow source is a simple, yet effective solution (e.g. Worman et al., 2005)

3.1 Case study: the biofiltration trench installed at Monash university (Melbourne, Australia)

The biofiltration basin installed at Monash University (Clayton campus, Victoria, Australia) in 2006 is part of a two-stage treatment train draining runoff from a 100% impervious multi-storey carpark. Runoff coming from a 4500 m^2 impervious catchment area is firstly conveyed to two sedimentation tanks having a total volume of 18 m^3; the overflow discharge is then directed to a 4.5 m^3 parallelepiped tank hydraulically connected to a rectangular, 4.5m wide, 10m long, 0.7m deep biofiltration basin. A sketch of the treatment train is shown in Fig. 33.

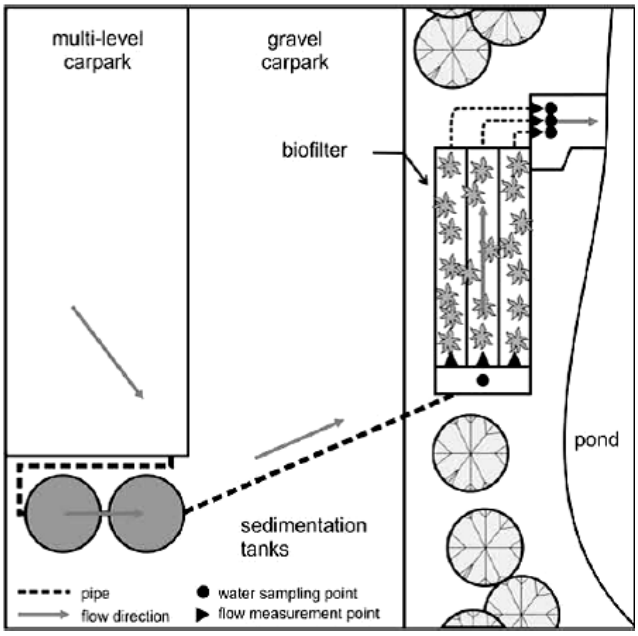

Fig. 33 – Sketch of the two-stage treatment train draining runoff from a 100% impervious multi-storey carpark

Australian guidelines require to size biofiltration facilities in order to treat at least 90% of the mean annual flow (Wong, 2006). A field survey completed by Le Coustumer et al. (2007) on 30 biofilters installed in Melbourne pointed out that a biofilter sized at 2.5% of its impervious catchment area is able to treat around 88% of mean annual inflows. The area of the biofiltration basin installed at Monash University is undersized according to current guidelines being only 1% of the total catchment area.

The biofiltration basin was divided into three separate cells by concrete barriers; each cell is 1.5 m wide, 10 m long and 0.7 m deep. The bottom and sides of the biofiltration system were sealed to prevent exfiltration of polluted water to the surrounding soil. Three triangular weirs introduce water into each cell, a surge wave travels on the permeable soil until it reaches the downstream impervious wall, then a storage phase begins. Three overflow weirs, 8.5m far from the inlet, allow water to pond to 0.41 m. Excess water is removed by the overflow weirs, storage water filters into a soil layer 0.50m thick, until it reaches a gravel drainage layer 0.20m thick. A sand layer overlaps the gravel layer in order to prevent any loss of filter media. Perforated 100 mm diameter PVC pipes were located in the drainage layer of each cell to collect the treated water. Outflow is discharged by three triangular weirs to a nearby detention pond and used for irrigation purposes.

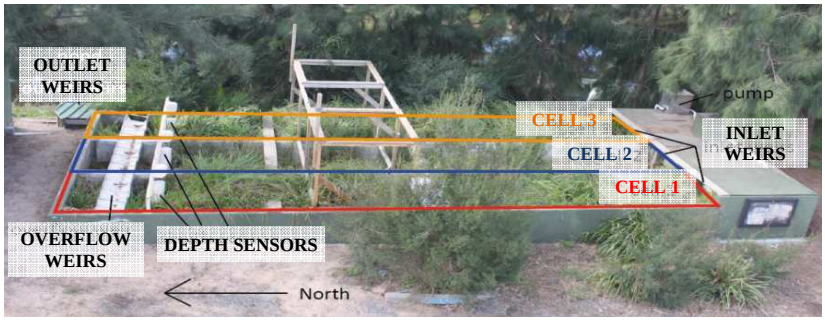

Fig. 34 – Picture of the biofiltration trench

The middle cell (i.e. Cell 2) was reconfigured in 2008 in order to build a submerged zone. The presence of a submerged zone was found to positively affect nitrogen (Zinger et al, 2007) and overall

pathogens removal (Chandrasena et al., 2012), nevertheless it showed no influence on total suspended solids and metals removal (Zinger et al., 2007), while it might be counterproductive for phosphorus removal.

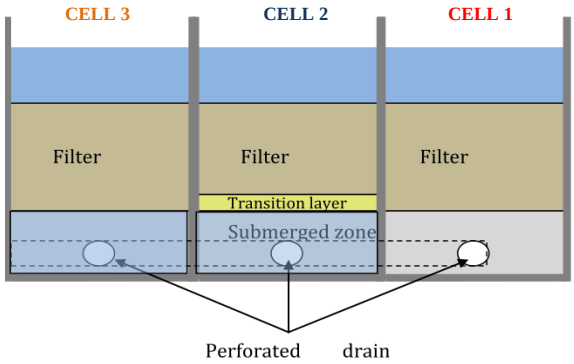

Fig. 35 – Sketch of the vertical cross section of the biofiltration trench

Filter media and drainage layers influence the efficiency of the biofilter by (i)maintaining healthy plant growth; (ii)controlling hydraulic conductivity; (iii)preventing leaching of pollutants.
Australian Standards recommend sandy loam as the base material for the filter media; a percentage lower than 3% of silt+clay is recommended to ensure soil structure and provide adsorption capacity, while maintaining flexibility in the larger particle size range. Furthermore filter media must not leach nutrients (e.g. phosphorus leaches must be lower than 100 mg/kg) and it must not inhibit plant growth (Electric Conductivity and pH must be within an appropriate range for healthy plant growth).
In order to investigate the pollutant removal performances of different combinations of filter media and vegetation type, each cell contains a different filter media:

- Cell 1 is made of sandy loam;
- Cell 2 has 80% sandy loam, 10% vermiculite, 10% perlite, by volume;
- Cell 3 has 80% sandy loam, 10% compost, 10% hardwood mulch, by volume.

Bioretention systems rely strongly on vegetation and its symbiotic relationships with bacteria and fungi for stormwater pollutant removal (e.g. FAWB, 2008). Each cell contains a dense growth of native sedges and rushes, in particular

- *Carex appressa, Carex tereticaulis, Lomandra longifolia, Isolepis nodosa, Caleocephalus lacteus, Juncus flavidis* were planted in Cell 1 and Cell 3;
- *Carex appressa, Malaleuca ericifolia* were planted in Cell 2.

All the selected species tolerate both droughts and occasional inundations and proved to have an overall effect on nutrient and pollutants removal. In particular, *Carex appressa* provided the highest performances in terms of nutrient removal thanks to its rapid root spreading, and the presence of symbiotic fungi around the root rhizosphere (Bratieres et al., 2008). *Maleleuca* species proved to be effective for the maintenance of soil hydraulic conductivity (Le Coustumer et al., 2007).

Flows and water quality were monitored starting from December 2006 to assess both hydrological and pollutant removal performances. Nine ultrasonic depth sensors (Siemens Miltronics) with a temporal resolution of 1 minute were used to assess flow rates through the three triangular input weirs, the three triangular output weirs and the three trapezoidal overflow weirs. Depth data were collected by a datalogger. Depth-discharge relationships were accurately calibrated and regularly checked for each input and overflow weir. The calibration procedure involved pumping water from the nearby pond at a number of flow rates, and recording the flow rate calculated by the monitoring equipment (Siemens Milltronics sensor and datalogger) as well as the flow rate calculated by measuring the volume of water passing over a weir for a given flow rate and time. A calibration curve was generated, linking logged and measured (actual) average flow rates. The uncertainty in the flow measurements at this site is well below the 10% (Fletcher and Deletic, 2007) that is below the standard threshold stormwater monitoring practice.

Autosamplers (Sigma 900) collected flow-weighted water quality samples (e.g. total suspended solids, total phosphorus, total nitrogen) at the inlet and from the outlet of each of the three cells during storm events.

Fig. 36 – Depth sensors for the detection of the outflow discharge

Five soil-moisture sensors were installed in Cell 1 (Tabel 10). As previously explained (par. 2.4.3.3), one common technique to assess soil moisture is to measure the dielectric constant, that is, the capacitive and conductive parts of a soil's electrical response. The dielectric constant was measured by commercially available probes, designed to be buried and left in-situ. Volumetric water content was derived implementing specific experimental calibration curves (Zinger et al., 2007). Data were sampled each minute and collected by a datalogger adopting a temporal resolution is 15 minutes. It is worth noting that each data represents the soil moisture content value averaged over 15 minutes.

Tabel 10 – Position of the five soil moisture sensors installed in Cell 1

	Distance from the inlet [m]	Depth from soil surface [m]
A	2	0.30
B1	5	0.03
B2	5	0.15
B3	5	0.30
C	8	0.30

3.2 Hydrologic performances

Research to date has generally focused on the pollutant removal performance of biofilters, with less attention given to their hydrologic performance (Hatt et al 2009; Li et al 2009).
Many studies have documented the important role of bioretention facilities in restoring the predevelopment hydrology of a drainage area (Davis et al. 2001, 2003; Barber et al., 2003; Sansalone and Teng 2004, 2005; Dietz and Clausen 2005, 2006; Hunt et al. 2006, 2008; Davis 2007, 2008). However, quantifying the hydrologic benefits of bioretention facilities in field situations is complicated by design variation and rainfall characteristic variability (Li et al., 2009).
McCuen (2003) recommended three metrics for describing the hydrologic performances of a bioretention facility, specifically, 1) hydrologic storage compensation; 2) stream channel preservation; 3) travel time maintenance.
Using these metrics as a guide, three quantitative parameters were proposed by Davis (2008):

- the effluent/influent volume ratio f_V (Eq. 28):

$$f_V = \frac{V_{OUT}}{V_{IN}} \qquad \text{Eq. 28}$$

  where V_{IN} is the inflow volume to the biofiltration trench and V_{OUT} is the corresponding volume of outflow.
  It was noted that outflows may continue at very low flow rates for many hours and, sometimes, even for many days. Because of the practical challenge of measuring low flows for extended times, an outflow volume was defined after 24h of flow ($V_{OUT} = V_{OUT,24}$) .

- the peak flow rate ratio of effluent to influent R_{peak} (Eq. 29):

$$R_{peak} = \frac{Q_{peak,OUT}}{Q_{peak,IN}} \qquad \text{Eq. 29}$$

- the peak discharge time span ratio of effluent to influent R_{delay} (Eq. 30):

$$f_V = \frac{time(Q_{peak,OUT})}{time(Q_{peak,IN})} \quad \text{Eq. 30}$$

Providing a buffer capacity for runoff surges with opportunity for infiltration, a successful bioretention facility simulate the predevelopment hydrology of a drainage area reducing f_V and R_{peak}, while correspondingly increasing R_{delay}.
Increased infiltration enhances water storage and base flows; the corresponding runoff volume reduction has important implications for management of urban waterways, where increased flows are a key stressor (Paul and Meyer, 2001). Peak flow decrease reduces erosion, scour, and sediment transport in the receiving stream. By delaying the peak, the hydrologic response through the bioretention facility more closely mimics that of undeveloped land, where natural meandering, infiltration, and vegetation slow the flow.
According to the widely used rational method to determine peak discharge from drainage basin runoff, the runoff coefficient of an undeveloped land is 0.3, while its value in case of a highly impervious area is 0.9. A target volume ratio f_V of 0.33 for infiltration trenches was then established.
The same argument applied for peak flow rate ratio R_{peak} and the same target value (0.33) was proposed (Davis et al., 2008).
A simple expression for sheet flow time of concentration, *Tc*, was given by Davis and McCuen (2005) (Eq. 31):

$$T_C = \frac{0.938}{i^{0.4}}\left(\frac{nL}{\sqrt{S}}\right)^{0.6} \quad \text{Eq. 31}$$

where *n* is the Manning's roughness coefficient; *L* the flow length; *i* the rainfall intensity; and *S* the drainage area slope. The time of concentration *Tc* of a paved drainage area (n=0.02) was compared to that of a light underbrush forest (n=0.4), the latter was assumed to be representative of undeveloped land. With the other parameters of Eq. 31 remaining unchanged, the time of concentration ratio for undeveloped to developed land is approximately equal to 0.4/0.02,

i.e. roughly 6. The latter value was set as the LID target for the bioretention delay ratio (Davis et al., 2008).
Based on these parameters, comparison among the performances provided by the biofiltration facility installed at Monash University and literature values are presented in Tabel 11.
Our analysis as well as literature studies dealt with many complex runoff events, with several peaks resulting from increases and lulls in rainfall intensity. Small effluent flows thus continued from the bioretention cells for long time, occasionally overlapping the next inflow runoff event. This made quantifying the hydrologic impact of the bioretention facilities more complex.
Referring to the biofiltration facility installed at Monash University, results from previous and this studies are presented. Generally, an inflow event was defined as the period during which flows exceeded the detection limit of the instrumentation (0.01 l/s). Lewis et al. (2008) and Hatt et al. (2009) analyzed the data collected from December 2006 to December 2007. In this first study, the proportion of the inflow volume that passed through each cell could not be calculated because the concrete barriers built to define the three cells did not extended above the ground level. Therefore, the volumes from the three outlets were summed to assess the global performances of the facility.
In September 2008 the concrete barriers were extended up to 0.50m above the ground level to coherently divide the detention basin.
In this study we analyzed the data collected from September 2010 to April 2012 and we were able to assess the performances of each cell. Cell 3 was obstructed by plants roots, fragments were detected in the outflow after many inflow events and overflow was highly frequent. Due to unlucky design and management choices Cell 3 could not be regarded as representative; consequently we focused on the analysis of the hydrologic performances of Cell 1 and Cell 2.
A few literature studies providing a complete analysis of the hydrologic performances of bioretention cells were selected for the purpose of comparison.
In particular, Davis (2008) analyzed the data of 49 runoff events to point out the performances of two bioretention cells constructed in the University of Maryland (USA) in Fall 2002/Spring 2003 to capture and treat stormwater runoff from an asphalt surface parking

lot. They had a surface to drainage ratio over 2%. The media in each cell consisted of an engineered soil mix of 50% (by volume) sand, 30% topsoil, and 20% compost, with a clay content of less than 10%. The total media depth in each cell was 0.9m and 1.2m. Each cell was covered by 0.08 m of mulch and planted with shrubs and herbs. Both cells were lined to minimize migration of water into or out of the system.

Li et al. (2009) evaluated the performances of six bioretention cells two to seven years-old, located in North Carolina (4) and in Mariland (2) (USA), and treating heavily impervious watersheds (asphalt parking lots, rooftops). They had a specific area ranging from 2% to 6%. Ponding depths ranged from 0.10 to 0.34 m while media depths ranged from 0.50 to 1.20 m. Soil textures were similar among the six cells (sandy loam; sandy clay loam; loamy sand). Only one cell was lined to prevent exfiltration.

Tabel 11 – Hydrologic performances of many biofiltration facilities: literature review and original data. μ is the mean value of the parameter; P_{AC} is the expected probability of achieving the target.

Parameter and metric target value					
f_V **<0.33**		R_{peak} **<0.33**		R_{delay} **>=6**	
P_{AC} %)	μ	P_{AC} (%)	μ	P_{AC} (%)	μ
Davis (2008)					
55-62	0.18-0.23	30-42	0.40-0.48	31-38	2-2.7
Li et al. (2009)					
15-82	0.01-0.6	70-99	0.01-0.14	25-80	3-200
Monash University, lumped system, Dec.2006-Dec.2007 (Lewis et al., 2008; Hatt et al., 2009)					
5	0.67	80	0.2	-	-
Monash University , Cell1, Sept. 2010-Apr. 2012					
1.5	0.77	60	0.3	37	4.5
Monash University , Cell2, Sept. 2010-Apr. 2012					
2	0.73	59	0.3	40	5.2

Both Davis (2008) and Li et al. (2009) registered small runoff events that did not produce outflow; they were able to evaluate an average rainfall intensity (0.052 cm/h and 0.003-0.8cm/h respectively) that can be completely managed by the bioretention cell. Bioretention cells generally exhibited higher hydrologic performances for small rain events while performance were poor under more extreme precipitation events during which the filter media was saturated and evapotranspiration almost stopped. Yet, for large events, the flow volume was frequently spread beyond 24h at a low output flow, so hydrologic storage compensation capability of the bioretention cells could be overestimated (i.e. *fv*24 may result unrealistically small).
The biofiltration trench installed at Monash University showed poor hydrologic performances, especially in terms of hydrologic storage conservation.
A detailed evaluation is here presented. The results of the previous studies (Lewis et al., 2008; Hatt et al., 2009) were compared with our original analysis. In particular, Fig. 37-38-39 show the cumulative frequency of the three hydrologic parameters (f_V, R_{peak} , R_{delay}) based on the data collected in Cell 1 from September 2010 to April 2012.

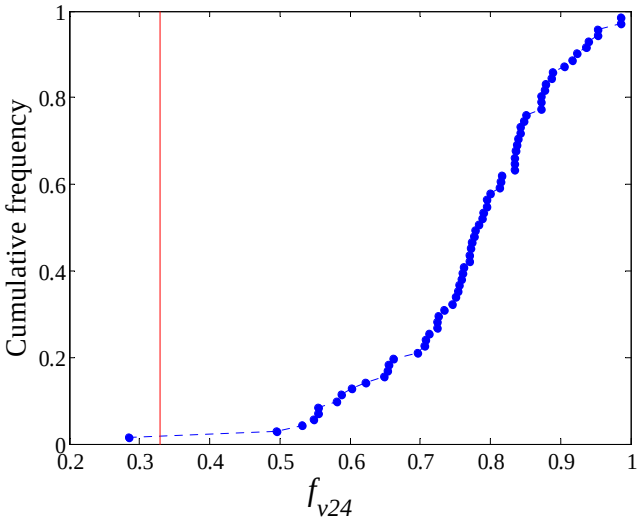

Fig. 37 – Cumulative frequency of effluent/influent volume ratio computed for Cell 1 of the biofiltration trench of Monash University, Sept.2010-April 2012. The red line shows the target value.

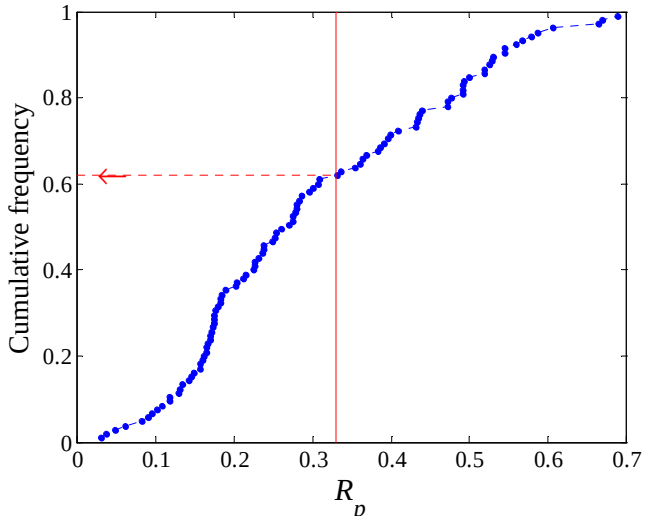

Fig. 38 – Cumulative frequency of inflow/outflow peak discharge ratio computed for Cell 1 of the biofiltration trench of Monash University, Sept.2010-April 2012. The red line shows the target value.

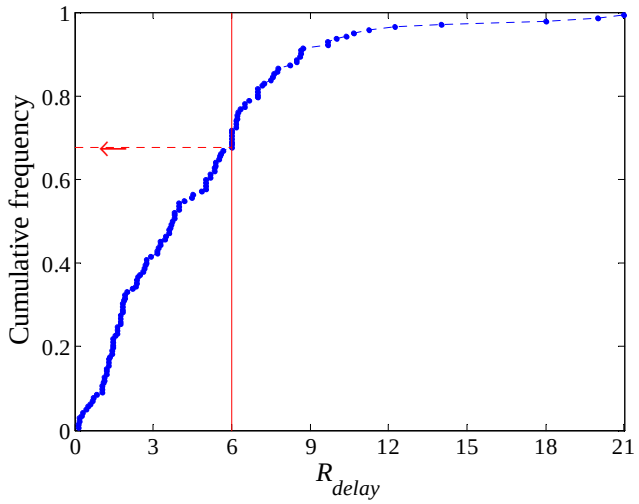

Fig. 39 – Cumulative frequency of inflow/outflow peak delay ratio computed for Cell 1 of the biofiltration trench of Monash University, Sept.2010-April 2012. The red line shows the target value.

During the first monitoring period (December 2006 – December 2007), Lewis et al. (2008) and Hatt et al. (2009) analyzed 51 storm events. The flow bypass weir was engaged on 19 occasions, i.e. a percentage equal to 37% of monitored events overflowed. As the bypass weir had not been rated, these events were excluded from hydrologic analysis.

During the second monitoring period (September 2010-April 2012) we detected 141 storm events, the overflow weir was engaged 11 times in Cell1 and 15 times in Cell 2, i.e. an overall percentage equal to 10% of monitored events overflowed.

Since hydrologic regime variations were excluded, the temporal decrease in the rate of overflowing events was likely due to sensible changes in infiltrability conditions. In particular, bad management choices led to a sensible decrease of infiltration capacity up to October 2006, a recovery phase lasted until April 2007 (more details on this issue are provided in par. 3.3.2). Furthermore, preferential flow paths developed with time increasing the overall ability of the infiltration trench to convey water downwards (more details on this issue are provided in par. 3.7)

The target value for effluent/influent volume ratio was rarely achieved, the performances in terms of storage conservation decreased with time. On average, a percentage equal to 33% of the inflow volume was retained by the biofilter during the first monitoring period; this value decreased to 25% during the second monitoring period. Only very small storm events were completely intercepted during the first monitoring period, while all the inflow events produced outflow in the second monitoring period.

Better performances for incoming peak flow reduction were observed, a deterioration with time was again detected. The mean peak inflow reduction rate was 80% in the first monitoring period; 70% in the second monitoring period.

Peak delays values were not provided for the first monitoring period; in the second period the outflow peak discharge released by the biofiltration trench was generally faster compared to a pre-development condition and the target value was achieved on average for 38% of the observed events.

An attempt was made to relate volume losses to the storm event size and intensity (rainfall intensity averaged across the event, event

duration, inflow volume) and seasonal influences (date, antecedent dry weather period). Following the approach proposed by Hatt et al. (2009), the relationships between losses, flow reductions and the five predictor variables were assessed using multiple linear regression. The distribution of the datasets were checked for normality using Kolmogorov– Smirnov tests (significance accepted at $p>0.1$) prior to using hierarchical regression analysis to determine the proportion of variance explained by each variable. Hatt et al. (2009) highlighted that the five predictor variables jointly explained about 75% of the total variance in losses, however inflow volume alone explained 68% of the variance in volumetric losses. Not surprisingly, the proportional loss decreases non-linearly with increases in inflow volume. Although it might be expected that evapotranspiration would be higher in warmer months (e.g. Hunt, 2003), the influence of inflow volume was overwhelming. These results were roughly confirmed by our analysis; antecedent soil moisture conditions (available exclusively for Cell 1) seemed to affect storage conservation.

The diagnostic studies reported in literature and briefly quoted in par.3.1, allowed to partly explain the poor hydrologic performances provided by the facility installed at Monash University. For instance, the low value of its specific area (or volume) was highlighted as an important negative feature.

The simple data analysis here performed described the overall behavior of the infiltration trench but did not provide any remarkable correlation.

A complete hydraulic model could provide a deeper understanding and a valuable prognostic tool to point out the optimal design solutions according to the site specific conditions.

In particular, we implemented, calibrated and validated a complete hydraulic model of one cell of the biofilter installed at Monash University, Clayton Campus. Being the only one equipped with soil moisture sensors, Cell 1 was selected. As detailed in par.3.7 this numerical analysis suggested a valuable hypothesis for the detected temporal decrease of hydrologic performances (volume storage, peak reduction, peak delay) accompanied by a lower number of overflow events: preferential flow paths likely developed with time leading to a reduction in the buffering capacity of the infiltration trench.

3.3 Hydraulic parameters of the filter media

Filter media of Cell 1 was sandy loam. A detailed study on its hydraulic parameters was required to model the functioning of the infiltration trench. A study on saturated water content , residual water content, saturated hydraulic conductivity, soil water retention curve was completed based on (i) previous field campaigns and (ii) original field data analysis. Details are presented in the following paragraphs.
For the purpose of comparison Tabel 12 lists the values of the main hydraulic parameters proposed by Carsel & Parish (1988).

Tabel 12 – Sandy Loam, values of the main hydraulic parameters proposed by Carsel & Parrish (1988)

	θ_r	θ_s	k_S [mm/h]	α [cm^{-1}]	n
Mean	0.065	0.41	44.2	0.075	1.89
Standard deviation	0.017	0.09	56.3	0.037	0.41

3.3.1 Saturated and residual water contents

Saturated water content value was assessed by field tests; residual water content was based on (a) numerical analysis of the soil water retention curve (see par.3.4) and (b) literature values (Carsel & Parrish, 1980). The values are listed in Tabel 13.

Tabel 13 – Saturated and residual water content of the filter media of Cell 1

θ_r	θ_s
0.09	0.43

3.3.2 Saturated hydraulic conductivity

Recommendations for saturated hydraulic conductivity of soil media used in infiltration trenches vary from one country to another (par.3.1). Current Australian guidelines suggest values between 50 and 200 mm/h (Melbourne Water, 2005).

The design value of the infiltration trench installed at Monash University was 180 mm/h.
Saturated hydraulic conductivity was measured in eight field campaigns completed between February 2006 and April 2010. A constant flowrate was pumped from the nearby pond into the upstream basin until overflow was detected in order to ensure the achievement of a stable constant head. The value of saturated hydraulic conductivity was then calculated using Darcy's law (details on this topic can be found in par. 1.2.5 and in par. 2.3.4)
The results, shown in Fig. 40, were compiled by Lewis et al. (2008) and by Radion and O'Gallagher (2010).

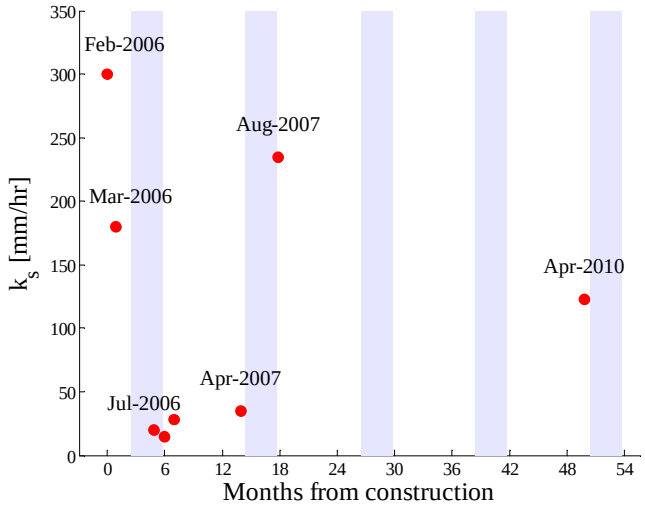

Fig. 40 – Saturated hydraulic conductivity values measured by field tests

Compaction of soil under hydraulic loading and initial growth of plants roots decreased the initial, undisturbed, high saturated hydraulic conductivity (300 mm/h) until a value approaching the target design (a value of 180 mm/hr was detected when the infiltration trench was one month old) . This foregone effect was followed by a sensible, totally unexpected decrease and an extremely low value of 15 mm/hr was detected in August 2006. In fact, a hothouse was erected over the biofilter in order to enhance vegetation growth over winter (from June to September 2006) and it had the

unforeseen effect of stimulating the growth of a thick moss layer over the surface of the soil. Both the hothouse roof and the moss were removed in October 2006. A recover of hydraulic conductivity was detected as plants continued to mature and their root systems penetrated the filter media (Lewis et al., 2008); in September 2007 the saturated hydraulic conductivity of the system was greater than 200 mm/hr.

The tests performed in April 2010, when the biofilter was four years old, pointed out a marked decrease until 123 mm/hour.

Field and laboratory studies on the features of infiltration systems reported in literature highlighted a similar decrease of hydraulic capacity with time. Lindsey et al. (1992) and Le Coustumer et al. (2009) reported that a percentage respectively equal to 62% and 40% of infiltration systems was either not functioning as designed, or anyway unable to meet current design guidelines with respect to hydraulic conductivity, after a few years of operation. Le Coustumer et al. (2009) undertook a review of 37 biofilters aged between 6 months to 7 years located in Melbourne, Sydney and Brisbane (Australia) and found that a large number had measured hydraulic conductivity around 25-50% of their initial value.

Based on a lab survey on 18 non-vegetated filter columns made of sandy loam and sandy loam variations, Hatt et al. (2007) concluded that all filter media types exhibited a significant reduction of hydraulic capacity with time. They argued that, unlike sand filters, soil filters experience a high level of compaction. Furthermore, a sensible influence of moisture content was highlighted. Clay particles and organic matter swelled during wet periods reducing the porosity of the filter media and shrinked as water content decreased during dry periods thus increasing porosity.

According to Asleson (2009), soil properties such as porosity and, consequently, hydraulic conductivity can change over time due to compaction, loss of soil structure, and/or clogging.

Soil compaction reduces infiltration rates by reducing the pore space available for water transmission. Post-construction soil compaction only occurs when heavy machinery is used for maintenance or redevelopment of the site.

The loss of soil structure may be due to loss of vegetation, chemical reactions, and compaction.

Lindsey et al. (1992), Bouwer (2002), Le Coustumer et al. (2009), and Schueler et al. (1992) showed that clogging is an issue of primary importance.

In general terms, clogging is the outcome of a combination of mechanical, biological and chemical processes (Langergraber et al.,2003). Sediment deposition is considered to be the principal cause of clogging (Bouwer, 2002); it can occur at the surface of the system or deeply (interstitial clogging) (Langergraber et al. 2003; Winter et Goetz, 2003). Single ring infiltration test and deep ring infiltration test performed by Le Coustumer et al. (2009) on 37 biofilters around Australia highlighted that the hydraulic conductivity of the system is controlled primarily by the top layer.

Le Coustumer et al. (2012) performed a laboratory study to investigate the main parameters affecting surface clogging. In particular, 75 large columns were used in order to understand the influence of design parameters, such as (a) biofilter size (and, consequently, the loading rate), (b) pollutant concentration, (c) soil type, and (d) vegetation species. Hydraulic conductivity decreased on average by a factor of 3.6 after 72 weeks of service; the rate of reduction decreased over time, appearing to reach an asymptote value after 45 weeks. This temporal trend confirmed the results of a field survey performed by Le Coustumer (2009). In case clogging does occur, it occurs within the very first few years, consequently age is not a significant predictor of the hydraulic capacity of a system.

The loading rate depends on the hydrologic regime of the area and it increases with decreasing specific area of the system (i.e. the ratio between infiltration trench and treated basin area). The bigger the loading rate, the more the system is prone to clogging.

Sediment concentration showed a weaker impact.

Referring to the soil type, the addition of compost, vermiculite or perlite to the traditional sandy loam increased the initial hydraulic conductivity and slightly helped to slow the decrease in conductivity over time. Nevertheless, the poor nutrient removal performance for filter media containing compost should also be considered (Braitières et al., 2008).

Maintenance of hydraulic conductivity by vegetation was shown only for *Maleleuca* species, i.e. plants with thick roots, while columns planted with thin-rooted species such as *Carex appressa, Dianella,*

Microleana, Leucophyta do not performed significantly differently to those with no vegetation. This result was coherent with previous studies. An experimental based conceptual model proposed by Quinton (1996) implied that fine roots do not necessarily increase hydraulic conductivity. Results of experimental tests performed by Morgan et. al (1995) even suggested a decrease of hydraulic conductivity when roots form a thick matting in the soil surface.

Archer et al. (2002) detailed the different effects of fine and coarse roots. Long and thin roots have a rapid turnover and form large amounts of fine organic matter, which over time will facilitate soil aggregation and reduces hydraulic conductivity. Coarse roots have a slower turnover rate, they increase hydraulic conductivity through the creation of macropores.

Stating that clogging primarily occurs on the surface, Elkins (1986) and Archer et al. (2000, 2002) questioned the impact of thick roots dieback on biofilter hydraulic capacity.

Nevertheless, interaction and competition between plant species should be taken into account. Despite these insights, the exact mechanisms by which vegetation affects hydraulic conductivity of biofiltration media remain an important knowledge gap (Le Coustumer et al., 2012).

Given the widely acknowledged difficulty in maintaining hydraulic conductivity in biofiltration media, many authors (e.g. Achleitner et al., 2006; Le Coustumer et al., 2009) underlined the importance of its initial value. A statistical analysis completed by Achleitner et al. (2006) pointed out two main different behaviors. Systems with a high initial hydraulic conductivity (k_s=50mm/h) decrease substantially over time; however, final hydraulic conductivities are still relatively high (k_s=130 mm/h), and likely to be adequate. Systems with low initial hydraulic conductivity (k_s=25mm/h) show a negligible decrease over time: the small relative difference in particle size between the filter media and the influent sediment cushion the impact of any build-up of sediment at the surface has proportionally less impact.

The selection of an appropriate media is thus an important factor for achieving a reliable hydraulic functioning of the biofilter. The use of conservative values of the saturated hydraulic conductivity is advisable; many guidelines proposed a safety factor ranging from 2

(New Jersey Department of Environmental Protection, 2004) to 3-4 (Le Coustumer et al., 2012).
Secondly, stating that the interaction between hydraulic conductivity, filter area and hydraulic load is critical to maintain treatment performances, oversizing of biofilter area is suggested to "buffer" against unintended reduction in infiltration capacity (Le Coustumer et al, 2009-2012).
Thirdly, vegetation should be selected based on (i) its pollutant removal performances and (ii) its ability to enhance hydraulic conductivity throughout the creation of macropores.
Based on this literature review, Cell 1 of the infiltration trench installed at Monash University is likely prone to clogging: (a) it is undersized, and (b) its vegetation lacks of thick rooted plants such as *Maleleuca*.
As a first attempt, the last measured value of the saturated hydraulic conductivity was introduced in the numerical model.

3.3.3 Soil Water Retention Curve

Van Genuchten model was selected for the description of the soil water retention curve of the filter media.
During the first phase of our study on coupled surface-subsurface flows, we applied two, different reliable protocols for the assessment of the main wetting branch of the soil water retention curve of a porous media. In particular, (A) experimental time series of soil moisture values sampled during the wetting of a vertical column provided the calibration data for the implementation of inverse parameters estimation techniques embedded in numerical models of the subsurface flow; (B) soil moisture values measured at the end of the drainage phase allowed the computation of the main drying branch of the soil water retention curve, literature studies focusing on hysteresis between recursive wetting and drying phases provided reliable methods for the assessment of the main wetting curve starting from the main drying curve. These protocols are detailed in par 2.4.2.
The hydraulic behavior of an infiltration trench strongly depends on its global, site-specific, time dependent field conditions, i.e. mainly (i) soil structure and compaction level; (ii) vegetation type and density; (iii) existence and development of a clogging layer; (iv)

presence and features of macropores, preferential paths, cracks. Furthermore, (v) hysteresis effect are important in repeated wetting and drying phases.

The assessment strategy (B) based on the theory of the drainage phase was parsimonious and effective; it allowed the description of the behavior of the infiltration trench as a global system while taking into account its hysteretic behavior.

Theoretical and experimental studies on vertical gravity drainage (e.g. Liakopoulos, 1964; Whisler & Watson, 1968; Kastanek, 1971) showed negative pressure values increasing at all height and times, until an equilibrium condition, at which the pressure is equal to the elevation, is achieved.

Measures of soil moisture content values could straightly yield to the reconstruction of a drying branch of the soil water retention curve. Braddock et al. (2001) introduced the Van Genuchten (1980) model into the Parlange (1976) hysteresis model. They obtained a first order ordinary differential equation whose solution leads to a pair of formulae for the wetting and drying scanning curves. Adopting the Van Genuchten model for the main drying curve, the main wetting curve $\theta_{w,main}$ is given by Eq. 32.

$$\theta_{w,main}(\psi) = -\theta_s \alpha\psi + \theta_s[1 + (\alpha\psi)^n]^{1/n} \qquad \text{Eq. 32}$$

Eq. 33 and Eq. 34 describe the general forms for the p^{th} wetting and drying cycles:

$$\theta_{w,p}(\psi) = \theta_{w,main} + \left(\psi - \psi_{d,p-1}\right) C\left(\psi_{w,p}\right) + \sum_{k=1}^{p-1} \left(\psi_{d,k} - \psi_{d,k-1}\right) C\left(\psi_{w,p}\right) \qquad \text{Eq. 33}$$

$$\theta_{d,p}(\psi) = \theta_{w,main} + \left(\psi - \psi_{d,p}\right) C(\psi) + \sum_{k=1}^{p-1} \left(\psi_{d,k} - \psi_{d,k-1}\right) C\left(\psi_{w,p}\right) \qquad \text{Eq. 34}$$

In which the specific capacity *C(ψ)* is given by Eq. 35:

$$C(\psi) = -\frac{d}{d\Psi}\left[\theta_{w,main}(\psi)\right] = \theta_s(1 + (\alpha\psi)^n)^{1/n}\alpha^n\psi^{n-1} - \alpha\theta_s \qquad \text{Eq. 35}$$

$\theta_{w,p}(\psi)$ is the p^{th} wetting curve starting at $\psi_{w,p}$ and ending at $\psi_{d,p}$, that is the curve is defined for $\psi_{w,p} \geq \psi \geq \psi_{d,p}$. The switch points are denoted by $\psi_{w,p}$, which is the switch on the *p-1* drying curve, and denotes the ending of the *p-1*th drying phase, and the start of the p^{th} wetting phase.

Asymptotic soil moisture values were extrapolated after each inflow event from field data series sampled at five points of the filter domain (see par. 3.2)

Soil moisture measures of the drainage phases following inflow events which led to the complete saturation of the filter media (i.e. all the moisture sensors detected, approximately, the saturated water content, $\theta_s = 0.43$) were used to assess the main drying branch of the soil water retention curve. This aim was achieved by simple numerical fitting of Van Genuchten parameters based on 5 averaged measured points in the soil moisture-pressure head domain.

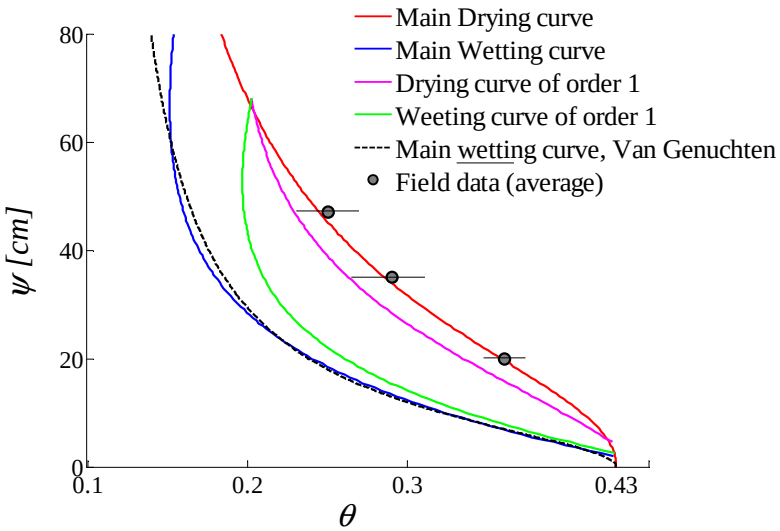

Fig. 41 – Soil water retention curves computed for the filter media of Cell 1

The Parlange (1976) hysteresis model modified by Braddock (2001) yielded to the definition of the main wetting curve and of the subsequent scanning curves; in particular Fig. 41 shows the main branches and the scanning curves of first order computed for the filter media of Cell 1 of the infiltration trench installed at Monash University.
Numerical fitting pointed out the values of Van Genuchten parameters describing the main wetting curve. A large number of events led to the complete saturation of the filter media; inflow events were often observed before the complete drying of the filter media. Wetting scanning curves detached from the main drying curve, the switch point $\Psi_{w,p}$ was retrieved from the measured antecedent soil moisture value of the filter media. As previously explained, the ending point $\Psi_{d,p}$ was often 0. Focusing on the range of soil moisture values detected (i.e. 0.19-0.43), wetting scanning curves of different order almost overlapped. Representative values of Van Genuchten parameters are listed in Tabel 14.

Tabel 14 – Wetting phases, representative values of Van Genuchten parameters

	α	n
Mean value	0.118	1.93
Standard deviation	0.04	0.33

3.4 Numerical model

Our complete numerical model was based on the external iterative coupling strategy for surface-subsurface flow calculations proposed by Bautista et al. (2010) (details are presented in 1.3.2)
The computational domain and the boundary conditions simulated the biofiltration trench installed at Monash University (Clayton, Victoria, Australia). The largest calibration and validation data set available was related to Cell 1. Measured values of inflow hydrographs were the input data; measured time series of (a) ponding depth values close to overflow weir, (b) soil moisture values at five points of the filter media, (c) outflow hydrographs were used for calibration and validation purposes.
The protocol implemented is here briefly detailed.
The zero-inertia solution of WinSRFR numerical model (Strelkoff et al., 1990) was used to model the routing of an inflow hydrograph on a permeable soil. Several inflow events were analyzed individually; recorded data provided input flow data with an accuracy of 0.01 l/s and a temporal resolution of 1 minute. Based on the data provided by *Melbourne Regional Office, Bureau of Meteorology, National Climate Centre, Australian Government*, direct rainfall input was negligible compared to runoff surge waves. Rain impact on soil moisture was taken into account throughout the definition of adequate initial conditions based on field data.
The computational domain was a rectangular, 10 m long and 1.5m wide, horizontal basin with impervious lateral boundaries 0.50m high. Manning's empirical formula was used to synthetically represent surface roughness effects on wave routing. A literature analysis on vegetation type and density pointed out 0.15 $sm^{-1/3}$ as a reasonable value for the Manning's coefficient. The filter media was uniform and 0.50 m deep. Infiltration was taken into account using the empirical formula proposed by Kostiakov.
The computed temporal series of surface flow depths at a number of selected nodes were then introduced as upper boundary conditions into the Hydrus package for subsurface flow modeling (Šimůnek et al., 1999). In particular, we used our edited version of the original source code, kindly released by Prof. Šimůnek. Our originally

modified version ensured the mass balance condition at the interface between the surface and subsurface domains and allowed the extension of the external coupling strategy proposed by Bautista et al. (2010) to the storage and depletion phases.
The Hydrus domain was a 0.5m deep, one-dimensional column of uniform soil; a seepage face was used as bottom boundary condition to allow gravitational flow from the filter media to the drainage layer; a 0.02m spatially uniform computational mesh and a minimum computational time step of 0.01s satisfied both Peclet and Courant conditions for numerical stability.
A critical analysis of soil moisture field data provided every fifteen minutes for five points of the filter media yielded to the definition of the initial conditions required for the numerical solution of the infiltration problem. Firstly, we analyzed the data sampled in the same soil column (i.e. three vertically aligned points 5m far from the inlet, named B1, B2, and B3), we checked and extrapolated a downward increasing soil moisture profile typical of the drainage phenomenon. Secondly we compared the field data sampled at the same soil depth (i.e. three points horizontally aligned at a depth of 0.30m, and 2, 5, and 8m far from the inlet, respectively named A, B3, C) with the purpose of a spatial extrapolation of the vertical soil moisture profile previously detected. Generally, based on (a) the time elapsed from the previous inflow event and (b) field soil moisture data, the hypothesis of an ongoing, although negligible or not even detected, drainage flow was reasonable. In case of complex runoff events, due to a succession of several rain showers, the whole bulk of the filter media could show homogeneous soil moisture values, often close to the saturation condition.
Filter media parameters were porosity (or saturated water content), residual water content, saturated hydraulic conductivity, soil water retention curve. Saturated water content value was assessed by field tests, residual water content was based on literature values (Carsel & Parrish, 1980). More efforts were required for an appropriate assessment of saturated hydraulic conductivity and soil water retention curve. The complete procedures are detailed in par. 3.3.3.
The Hydrus model was then run and the resulting soil moisture profiles yielded to cumulative infiltration depth time series and

consequently to physically based parameters values of the Kostiakov empirical infiltration equation for each calibration node.
Performance analysis proved that eleven one-meter equidistant nodes yielded to an adequate representation of the total domain while limiting computational time. In fact, sensitive analysis performed by Bautista et al. (2010) pointed out that surface flow hydrographs computed using single *vs* multiple calibration nodes are very similar.
The iterative coupling strategy was performed until convergence was achieved according to criterion proposed by Bautista et al. (2010).The complete iterative strategy showed fast convergence.
Field data of ponding depth values were then compared to the computed values in the corresponding cross section, i.e. 8.5m far from the inlet. In case of discrepancies, a critical analysis of the parameters used and the phenomena involved was performed.
Final surface depth hydrographs were then introduced as upper boundary conditions in the Hydrus 2D package in order to compute soil moisture spatial and temporal patterns, and the outflow hydrograph. In particular, we used our originally modified version of the Hydrus source code. Our version

1. ensured the mass balance condition at the interface between the surface and the subsurface domains during the storage and drainage phases;
2. allowed the introduction of a different hydraulic head time series for each upper boundary node.

The computational domain was a 10 m long, 0.5 m deep, horizontal rectangle of uniform soil having impervious sides and a seepage bottom face. The computational mesh and a lower boundary threshold value of the computational time step were defined based on numerical analysis of the Peclet-Courant conditions. In particular, a lower threshold value of 0.01 sec was adopted, and an anisotropic spatial discretization 0.04 and 0.005m wide in the horizontal and vertical directions respectively was used. A surface head hydrograph for any upper boundary node (i.e. 201 nodes) was computed by WinSRFR and then introduced into Hydrus2D. Soil parameters were obviously defined in the previous phase.

The analysis of storms causing multiple surges in the biofilter demanded a third editing intervention on the original source code. In particular, our modified version

3. allowed multiple switches of the upper boundary condition from hydraulic head to no-flow and viceversa.

Five observation nodes were located in correspondence with the soil moisture sensors, time series of computed soil moisture values were compared to measured data for calibration purposes. Similarly, cumulative outflow discharge from the bottom seepage face was compared to outflow measured hydrographs.
The numerical protocol here described was completely automated by the implementation of an original Matlab code which allowed to avoid cumbersome, repeated event-specific interactions with the graphical user interfaces provided by WinSRFR and Hydrus packages.
It was initially used for single-event based analysis in order to investigate the hydraulic behavior of the biofiltration trench installed at Monash University. In particular, the impact of design parameters such as geometry, soil type and vegetation cover was analyzed and peculiar hydraulic features were highlighted.
As further detailed in 3.10 the modeling of a complete hydrologic cycle is a short outcoming of this work. It will allow the modeling of inter-event periods highlighting (1) the impact of evapotranspiration on the hydrological performances of the facility; and (2) the temporal patterns of soil moisture. In particular, temporal patterns of soil moisture highly affects hydrologic and pollutant removal efficiency (see 3.1).

3.5 Analysis of "large" storm events

We called "large" inflow events all the events that showed an advance phase, a storage phase and, eventually, a depletion phase. "Small" inflow events were, obviously, all the events that showed an advance phase and a depletion phase, while the storage phase was missing.
Ponding depth values measured 8.5m far from the inlet were available for each "large" event. Since these data were highly useful for the calibration of the numerical modeling, our analysis started from many selected "large" inflow events. This strategy later proved to be useful for a deep insight in the hydraulic behavior of the infiltration facility. We demonstrated that "large" events and "small" events werer the outcome of both inflow hydrograph and initial conditions of the infiltration basin.

3.5.1 Event A: clogging of the filter media

Inflow event A was considered as representative in terms of volume and peak discharge values.
It started at 3:08 AM of 2011/05/14 and it lasted 86 min; its volume was 4.7 m^3 with a peak discharge of 5.47 l/s; storage and depletion phases lasted 319 minutes, the maximum ponding depth was 195 mm. Outflow started 15 minutes after the inflow and it lasted 600 minutes; its total volume was 4.17 m^3 with a peak discharge of 0.26 l/s.

Tabel 15 – Inflow event A

Inflow	Volume [m^3]	4.7
	Peak discharge [l/s]	5.47
	Length [min]	86
Ponding	Maximum depth [mm]	195
	Length [min]	319
Outflow	Volume [m^3]	4.17
	Peak discharge [l/s]	0.26
	Length [min]	600

Tabel 16 – Inflow event A

Hydrological parameters	f_{v24}	0.887
	R_{peak}	0.045
	R_{delay}	6.17

Numerical simulations using the parameters described in par.3.3 couldn't fit ponding depth, outflow, neither soil moisture time series sampled data. In particular, our numerical results showed (i) faster and smaller storage and depletion phases; (ii) a faster and higher outflow peak value.
A sensitivity analysis on the importance of the model's parameter highlighted the leading role of the saturated hydraulic conductivity value. Referring to the discussion on the clogging effect of the filter media (Le Coustumer et al., 2009, 2012; see 3.3.2), we hypothesized a sensible decrease in the saturated hydraulic conductivity value after the last experimental measure in April 2010.
Round mean square errors between computed and sampled values of ponding depth, outflow and soil moisture time series were minimal when the saturated hydraulic conductivity of the numerical model was only 0.35 times the measured value.

Fig. 42 compares computed and measured ponding depth, outflow, soil moisture time series.

A first result of this analysis was the assessment of the current value of the saturated hydraulic conductivity; the large decrease with respect to the value measured in April 2010 was attributed to the clogging of the filter media. According to Le Coustumer et al. (2009; 2012) this phenomena shows a quick, early development and, then, a negligible evolution. Following the last intervention on the biofiltration facility in 2008, a decrease in the saturated hydraulic conductivity value was experimentally pointed out (field campaign completed in September 2007, April 2010).
We assumed $k_s=43$ *mm/h* (i.e. $k_s=0.35*k_{s,measure2010}$) as the asymptotic value. Numerical analysis were performed to check this hypothesis.

The next step was the numerical modeling of the inflow event B previous to event A.

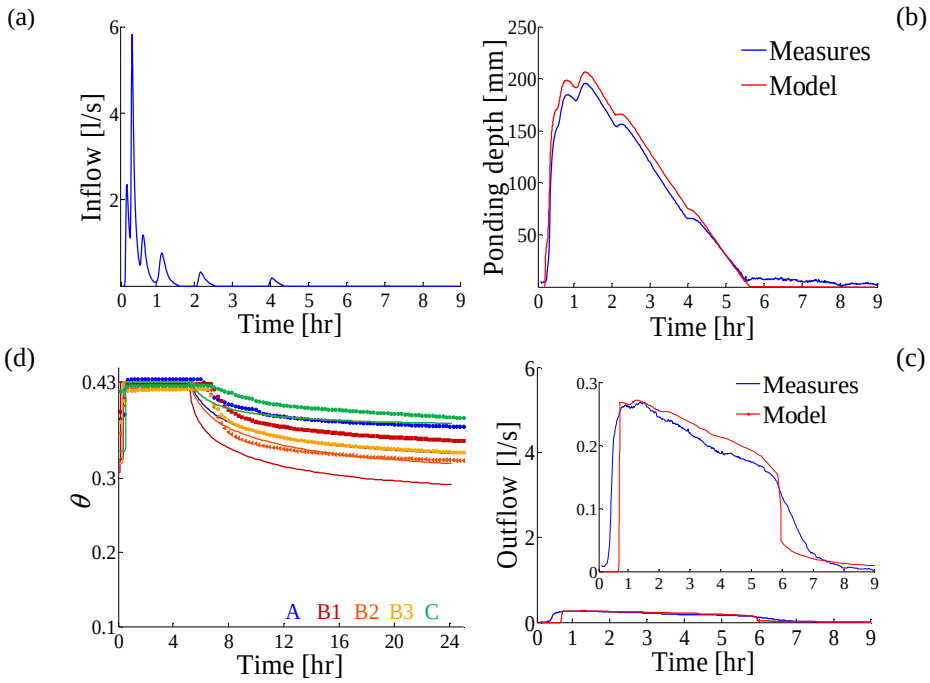

Fig. 42 – Event A: (a) Inflow hydrograph, measures; (b) Ponding depth time serie, measures and model; (c) Outflow hydrograph, measures and model; (d) Soil moisture time series, measures and model

3.5.2 Event B: anomalous functioning

Inflow event "B" started at 22:55 of 2011/02/13 and it lasted 38 min; its volume was 6.68 m^3 with a peak discharge of 8.36 l/s; storage and depletion phases lasted 47 minutes, the maximum ponding depth was 235 mm. Outflow started 8 minutes after the inflow and it lasted 118 minutes; its total volume was 6.5 m^3 with a peak discharge of 2.38 l/s (see Tabel 17).

Tabel 17 – Inflow event B

Inflow	Volume [m^3]	6.68
	Peak discharge [l/s]	8.36
	Length [min]	38
Ponding	Maximum depth [mm]	235
	Length [min]	47
Outflow	Volume [m^3]	6.5
	Peak discharge [l/s]	2.38
	Length [min]	118
Hydrological parameters	f_{v24}	0.97
	R_{peak}	0.2846
	R_{delay}	3.63

The numerical model, in which saturated conductivity value was updated to account for the clogging of the filter media (k_s*=43 mm/h*), couldn't fit ponding depth, outflow, neither soil moisture time series sampled data. With respect to measured data, our numerical results showed (i) highly slower and deeper storage and depletion phases; (ii) outflow started several minutes later and had a smaller peak discharge. A sensitivity analysis confirmed the saturated hydraulic conductivity value as the parameter leading the infiltration process. Sampled data could be fitted provided that the saturated conductivity value was threefold higher than the measured data, i.e. 8.6 times bigger than the clogged value: $k_{s,B}$*=369 mm/h*

Fig. 43 compares computed and measured ponding depth, outflow, soil moisture time series.

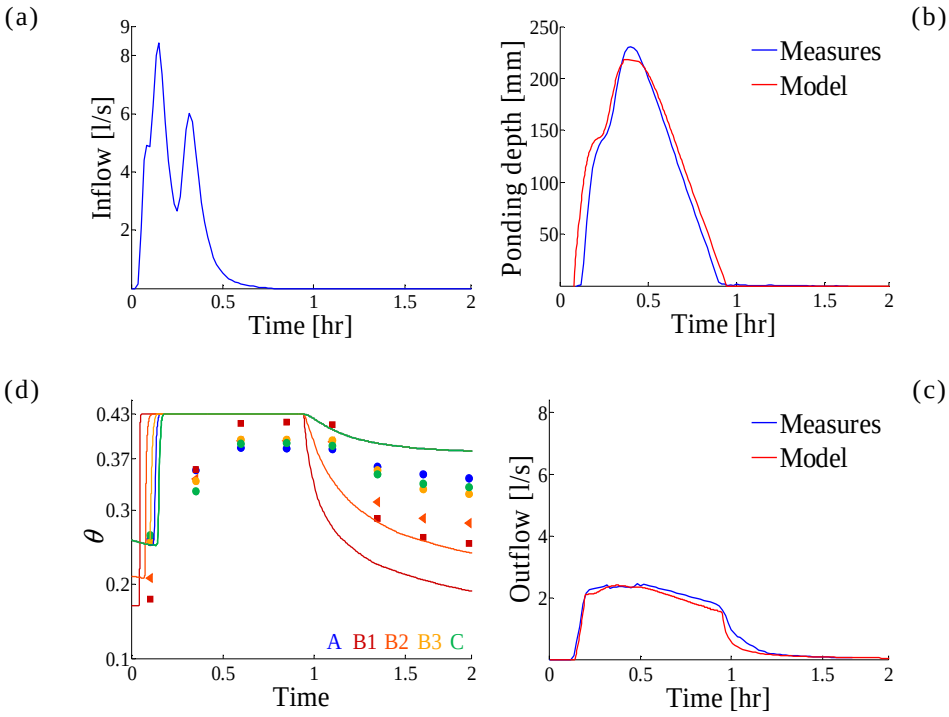

Fig. 43 – Event B: (a) Inflow hydrograph, measures; (b) Ponding depth time serie, measures and model; (c) Outflow hydrograph, measures and model; (d) Soil moisture time series, measures and model.

3.5.3 The value of saturated hydraulic conductivity as a bulk parameter

The totally unexpected result required further investigations on the functioning of the biofiltration trench.
A direct comparison (see Tabel 18) highlighted that a smaller event, i.e. inflow A, yielded to a much longer, although similar in depth, ponding phase than a bigger event, i.e. inflow B. Furthermore, the biofiltration trench performed much better for the inflow event A than for the inflow event B. The latter statement is even more interesting if we observe that the biofiltration trench was wetter, i.e. it had a smaller storage capability, before the inflow event A (Fig. 44). Saturated conditions were achieved during both the events.

Tabel 18 – Comparison between inflow event A and inflow event B

		A	B
Inflow	Volume [m^3]	4.7	6.68
	Peak discharge [l/s]	5.47	8.36
	Length [min]	86	38
Ponding	Maximum depth [mm]	195	235
	Length [min]	319	47
Outflow	Volume [m^3]	4.17	6.5
	Peak discharge [l/s]	0.26	2.38
	Length [min]	600	118
Hydrological parameters	f_{v24}	0.89	0.97
	R_{peak}	0.045	0.285
	R_{delay}	6.2	3.6

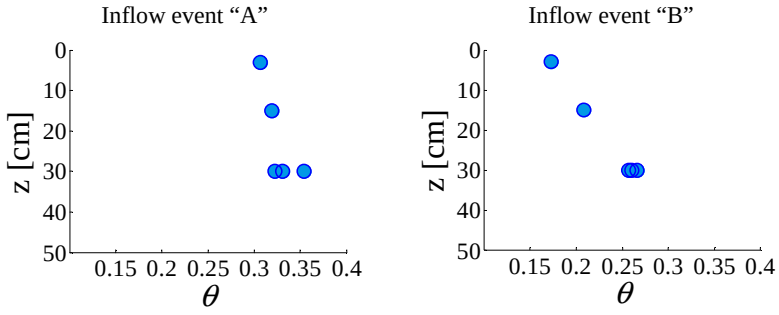

Fig. 44 – Soil moisture values detected before the events A and B

Fig. 45 overlaps the measured time series of ponding depth. Event A yielded to a much longer ponding phase characterized by a sensibly slower depletion phase.

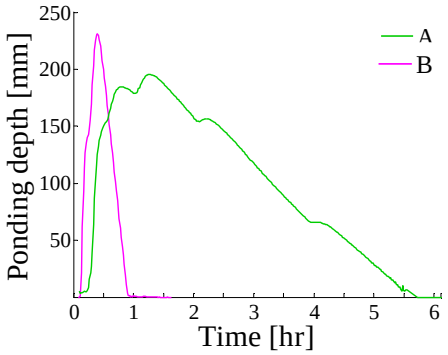

Fig. 45 – Events A and B: detected water levels

During the depletion phase inflow was zero and the filter media was saturated; Eq. 36a,b provide a simple mathematical expression for mass conservation condition:

$$\frac{dV_{storage}}{dt} = Q_{inflow}(t) - Q_{inf}(t) \qquad \text{Eq. 36a}$$

$$A\frac{dh}{dt} = -Q_{inf} \qquad \text{Eq. 36b}$$

where $V_{storage}$ is the volume of water stored above the ground level at time t; $Q_{inflow}(t)$ is the inflow discharge; $Q_{inf}(t)$ is the volume infiltrated per unit time; h is the ponding depth at time t; A is the surface area of the infiltration trench.

Darcy's law allows the computation of the infiltration flow yielding to Eq. 37:

$$A\frac{dh}{dt} = -k_s\frac{h+d}{d}A_\rho \qquad \text{Eq. 37}$$

where d is the depth of the filter media; A_ρ is the effective flow area of the soil media.

Solving this differential equation with respect to the ponding depth h we get Eq. 38.

$$h(t) = \left[\exp\left(-k_s \frac{A_\rho}{A}\frac{1}{d}t\right)\right](h_i + d) - d \qquad \text{Eq. 38}$$

where h_i is the value of the ponding depth at the beginning of the depletion phase.

A numerical analysis based on the parameters of this specific problem was performed. The maximum possible value of the hydraulic head was 0.41 m; the saturated conductivity value was allowed to span from the fifth part to five times the last field data. Here, the rigorous exponential decrease may adequately be represented by a linear behavior.

Based on field data of event A and B, Tabel 19 lists the average celerity of water level drop during the depletion phase $\overline{dh/dt}$. Coherently with the analysis here performed, these values are roughly proportional to the saturated hydraulic conductivity values $k_{s,L}$ imposed in the numerical model.

Tabel 19 –Events A and B: average field celerities of water level drop and imposed values of the saturated hydraulic conductivity

	$\overline{dh/dt}$ [mm/hr]	$k_{s.Large}$ [mm/hr]
Event A	56	43.08
Event B	497	369

The numerical modeling of many inflow events allowed the validation of the latter statement. In particular, based on the measured data, the celerity of water level drop during the depletion phase was computed for many inflow events.

A blind, simple variation of the saturated hydraulic conductivity value was imposed in the numerical model to roughly account for this effect. We thus adopted a lumped modeling approach.

In a lumped model all the parameters impacting the system response are spatially averaged together to create uniformity across the spatial domain (Johnson 1997; Shah 1996). Our lumped model considered the biofiltration trench as a unit, characterized by a relative small number of parameters and variables.

Numerical analysis pointed out the best fitting saturated hydraulic conductivity values .

Referring to each event, Tabel 20 lists the antecedent soil moisture content θ_0 ; inflow volume, length, and peak discharge; the average measured celerity of water level drop and the saturated hydraulic conductivity value $k_{s.L}$ correspondingly imposed in the numerical model. In particular, the initial condition θ_0 was the spatial-weighted mean of the soil moisture values detected by the sensors before the inflow event.

Tabel 20 – Numerical analysis of many "large" inflow events.

	Inflow event features, field data						Model
id	Date	θ_0 [-]	Volume [m^3]	Length [min]	Peak [l/s]	$\overline{dh/dt}$ [mm/h]	$k_{s.Large}$ [mm/h]
A	2011/05/14 03:08	0.305	4.7	86	5.47	56	43.08
B	2011/02/13 h22:55	0.234	6.68	38	8.36	497	369
C	2010/10/30 h23:58	0.295	9.5	282	2.84	85.5	86.4
D	2010/12/06 h12:47	0.236	5.12	43	8.60	429	394
E	2011/02/10 h20:30	0.234	5.24	28	15.56	462	369
F	2011/03/24 h16:29	0.263	9.08	52	12.96	486	344
G	2011/04/12 h20:02	0.297	7.2	91	5.76	104.4	74
H	2011/04/13 h15:15	0.293	2.92	42	4.88	94.2	99
I	2011/05/11 h16:39	0.364	12.55	187	12.10	82.2	59
L	2011/05/12 h15:45	0.305	3.07	32	6.62	83.4	74
M	2011/06/07 h22:40	0.329	6.14	348	1.16	55.81	49
N	2011/06/21 h02:50	0.274	12.61	143	11.60	186.6	166
O	2011/07/17 h23:12	0.273	11.53	89	6.15	337.8	209
P	2012/01/12 h08:56	0.305	1.83	19	7.14	73.8	74
Q	2012/01/08 h02:59	0.301	2.95	38	4.54	139.2	123
R	2012/03/11 h14:55	0.247	12.05	73	14.89	512	469

Fig. 46 compares measured and computed outflow volumes highlighting the good performances of the numerical model. The root means square error is 0.67 m^3; the average ration between measured and model values is 0.96.

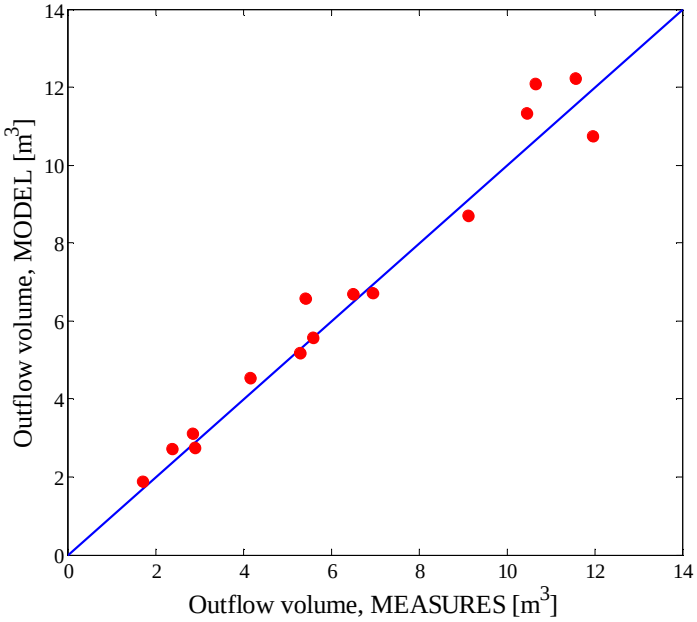

Fig. 46 – "Large" inflow events, modeled and measured outflow volumes

The saturated hydraulic conductivity value was so far simply regarded as a bulk parameter of the numerical model, its value was arbitrarily changed to fit measured data.
An appropriate, physically based investigation on the functioning of the biofiltration trench started with a insight on the depletion phase.
The celerity of water level drop ranged from 50 to 520 mm/h. Based on our numerical analysis, the saturated hydraulic conductivity value pointed out by the last field campaign (i.e. April 2010) roughly corresponded to a water level drop celerity of 150 mm/h. As shown in Fig. 47, about 60% of the measured values were lower, the remaining 40% were obviously bigger.

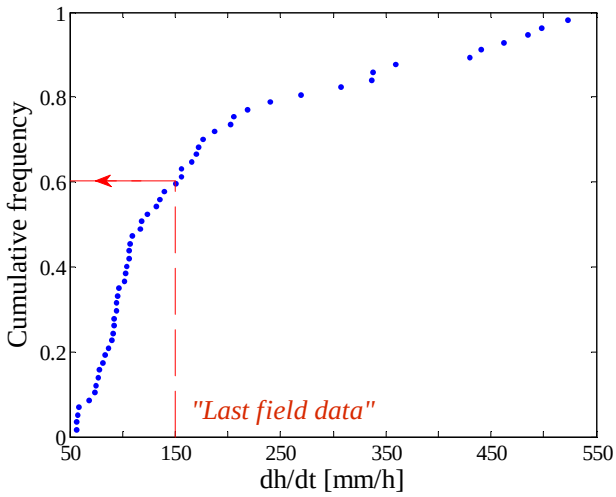

Fig. 47 – Measured average celerity of water level drop during the depletion phase: cumulative frequency

A simple look at the temporal distribution of the values, represented in Fig. 48 denied evident seasonal effects or the impact of any unpredictable, not detected vegetation change.

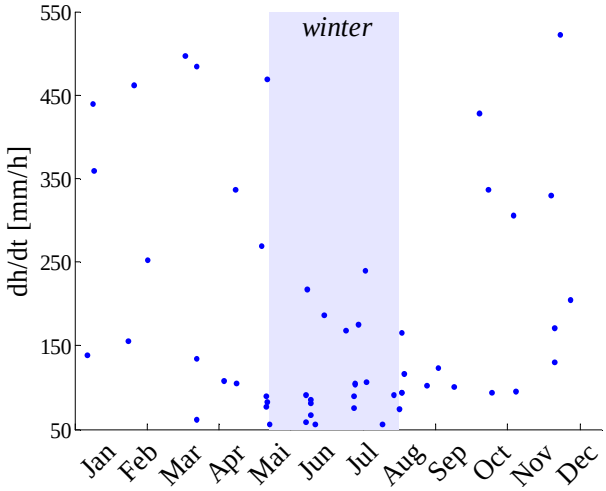

Fig. 48 - Measured average celerity of water level drop during the depletion phase, temporal distribution

An attempt was made to relate the celerity of the failing head to the initial conditions of the biofiltration trench (i.e. (1) the average soil moisture value), and the features of the inflow event (i.e. (2) volume, (2) length, and (3) average intensity of the inflow hydrograph). The relationship between the celerity of the water level drop and the four predictor variables were assessed using multiple regression. The distribution of the datasets were checked for normality using Kolmogorov– Smirnov tests (significance accepted at $p>0.1$) prior to using hierarchical regression analysis to determine the proportion of variance explained by each variable. The four predictor variables jointly explained about 86% of the total variance in the celerity of the failing head, however average initial soil moisture alone explained 57.5% of the total variance.

It is absolutely worth noting that the correlation between the initial soil moisture value of the biofiltration trench and the celerity of water level drop during the storage phase deeply contradicted the traditional theory of infiltration flows in unsaturated media. As previously briefly explained (par.1.2.3), the hydraulic conductivity value generally increases with soil moisture. According to our data, the wetter the filter media, the slower the depletion phase. In our lumped model we blindly reduced the saturated hydraulic conductivity value in order to fit measured time series of ponding depth, outflow discharge, soil moisture data.

Fig. 49 to Fig. 54 and Tabel 21 show four, representative examples of the impact of the initial moisture content of the filter media on the behavior of the biofiltration trench.

Total volume V [L^3] and average intensity $\bar{Q}$ [L^3/T] (the latter defined as the ratio between volume and length of the inflow hydrograph, Eq. 39) were used to describe the inflow event.

$$\overline{Q_{IN}} = \frac{V_{IN}}{time_{IN}} \qquad \text{Eq. 39}$$

The average moisture content of the filter media had the same, low value (θ_0=0.236) before both inflow events E and D, a quick decrease of the ponding depth was observed, poor hydrological performances were pointed out; the same, high saturated hydraulic conductivity value had to be imposed in our lumped numerical model.

The average moisture content of the filter media had the same, high value (θ_0=0.304) before both inflow events L and P, a slow decrease of the ponding depth was observed, improved hydrological performances were pointed out; the same, low saturated hydraulic conductivity value had to be imposed in our lumped numerical model.

Tabel 21 – Analysis of inflow events with highly different antecedent soil moisture conditions

	θ_o	Inflow event		Storage and depletion phases			MODEL	Hydrological performances		
		V [m^3]	$\bar{Q}$ [l/s]	h_{max} [mm]	Length [min]	$\overline{dh/dt}$ [mm/hr]	$k_{s.Large}$ [mm/hr]	f_v	R_{peak}	R_{delay}
E	0.236	5.24	3.12	207	38	462	369	0.99	0.14	7
D	0.236	5.12	1.98	114	35	432	369	0.99	0.27	2.33
L	0.305	3.07	1.60	146	125	84	74	0.92	0.06	6.25
P	0.305	1.83	1.61	73	71	75	74	0.92	0.04	8.67

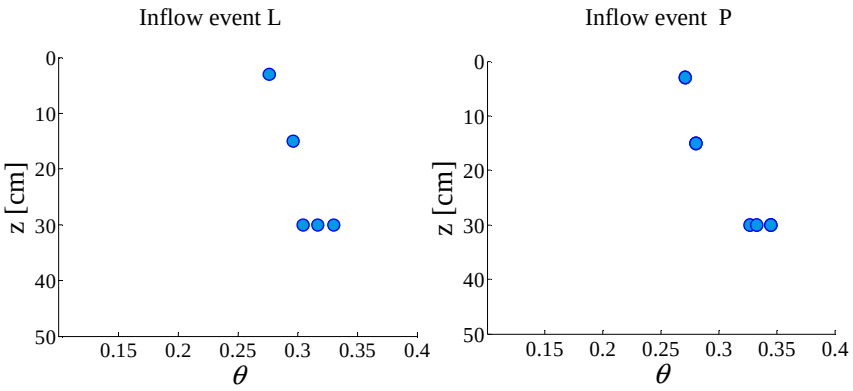

Fig. 49 – Events L and P, antecedent soil moisture conditions

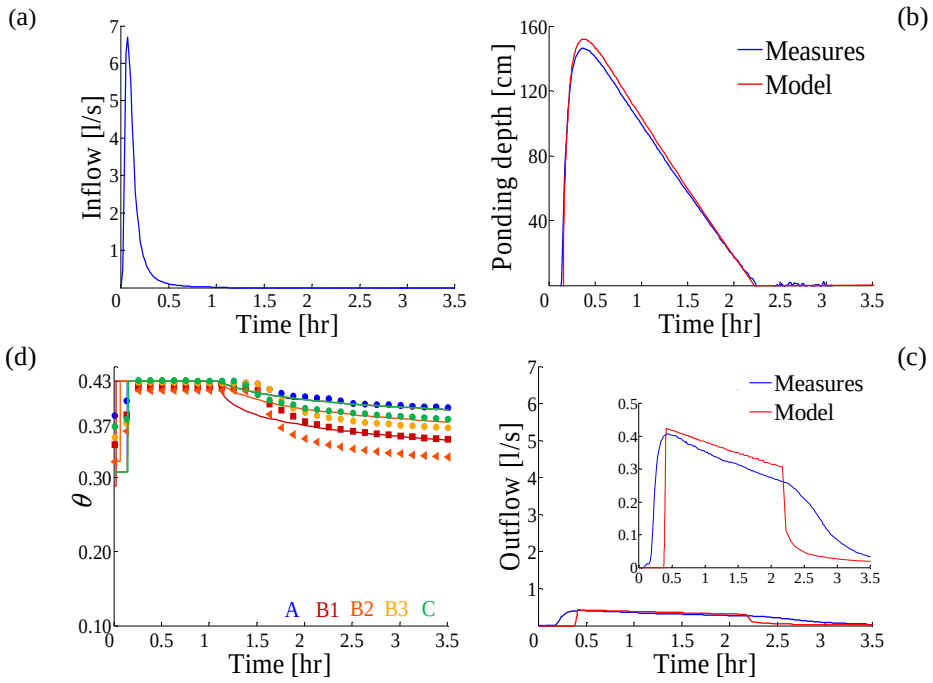

Fig. 50 – Event L : (a) measured inflow hydrograph; (b) measured and modeled ponding depth values; (c) measured and modeled outflow hydrograph; (d) measured (symbols) and modeled (lines) soil moisture values

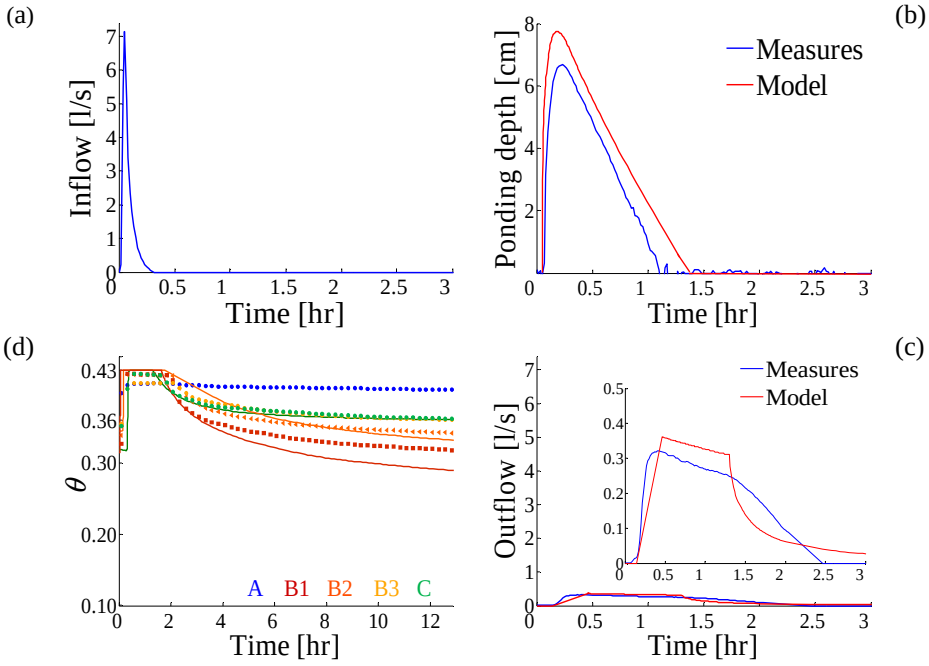

Fig. 51– Event P : (a) measured inflow hydrograph; (b) measured and modeled ponding depth values; (c) measured and modeled outflow hydrograph; (d) measured (symbols) and modeled (lines) soil moisture values

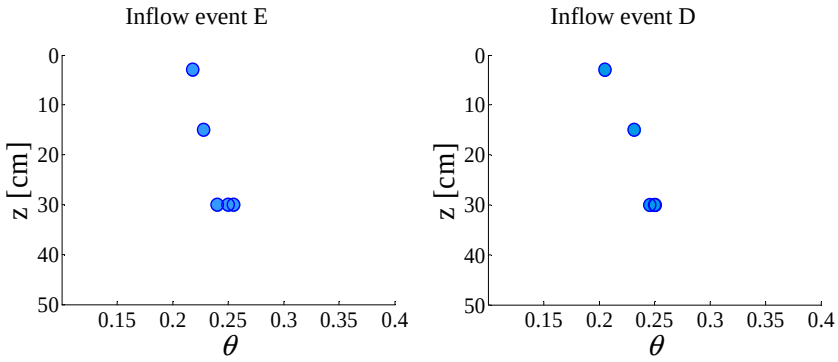

Fig. 52 – Events E and D, antecedent soil moisture conditions

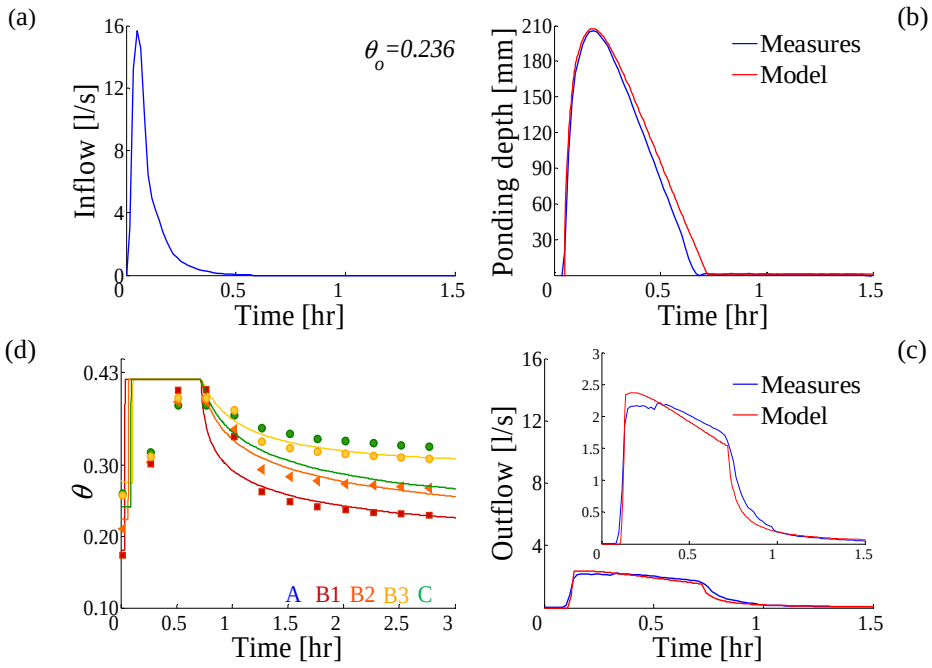

Fig. 53 – Event E : (a) measured inflow hydrograph; (b) measured and modeled ponding depth values; (c) measured and modeled outflow hydrograph; (d) measured (symbols) and modeled (lines) soil moisture values

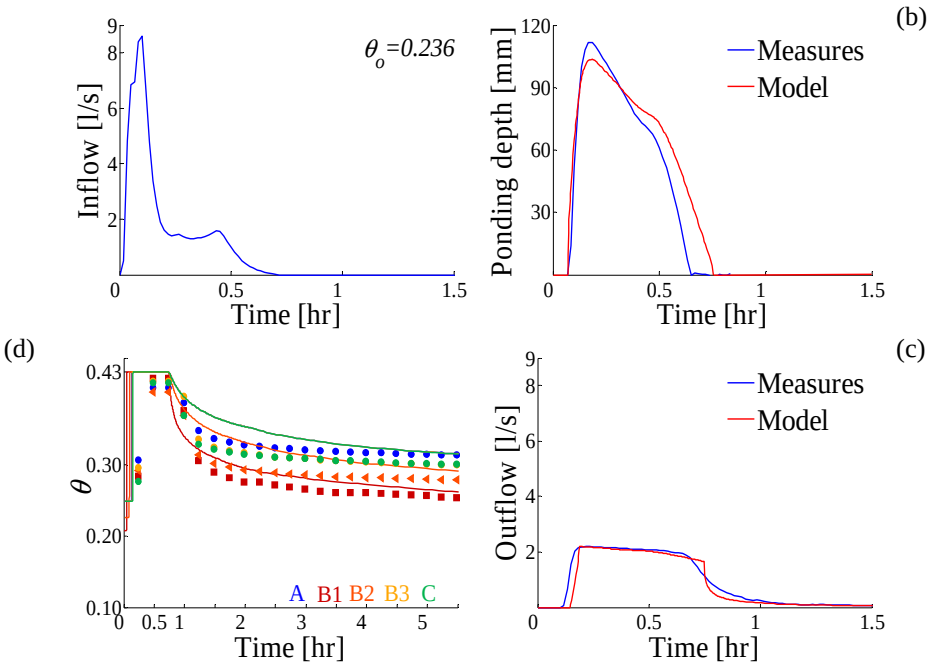

Fig. 54 – Event D: (a) measured inflow hydrograph; (b) measured and modeled ponding depth values; (c) measured and modeled outflow hydrograph; (d) measured (symbols) and modeled (lines) soil moisture values

Nevertheless, changes in the initial moisture content of the biofilter media couldn't completely explain the wide variability of the behavior of the biofiltration trench. As a consequence of specific features of the inflow events, (i) the same initial conditions could lead to different behaviors; (ii) different initial moisture content could result in similar behaviors; (iii) exception to the general inverse relationship moisture content-celerity of water level drop could be observed.

Meaningful examples of the three conditions listed are here presented, their data are listed in Tabel 22; Fig.55 to Fig. 60 show the inflow hydrograph and compare outflow and soil moisture measured and modeled data.

Notwithstanding the moisture content of the filter media was the same (0.27) before both the inflow events N and O, the depletion phase of the latter was sensibly quicker and, consequently, the saturated hydraulic conductivity value required in the lumped numerical model was bigger.

The filter media was drier before the inflow event G than before the inflow events L and Q, nevertheless its depletion phase was as slow as L's and even slower than Q's.

Conversely, although the filter media was wetter before the inflow event I, the depletion phase following the inflow event M was slower.

Tabel 22 - Analysis of inflow events and antecedent soil moisture conditions impact on the behavior of the biofiltration trench

	θ_o	Inflow event		Storage and depletion phases			MODEL	Hydrological performances		
		V [m^3]	$\bar{Q}$ [l/s]	h_{max} [mm]	Length [min]	$\overline{dh/dt}$ [mm/hr	$k_{s,Large}$ [mm/h]	f_v	R_{peak}	$R_{dela\ y}$
G	0.297	7.20	1.32	387	254	104	74	0.97	0.09	11.3
L	0.305	3.07	1.50	146	125	83	74	0.92	0.14	6.3
Q	0.301	2.95	1.29	121	70	139	123	0.98	0.24	1.8
N	0.273	12.61	1.47	389	170	187	166	0.92	0.13	2.7
O	0.273	11.53	2.16	378	131	338	209	0.99	0.17	4.5
I	0.361	12.55	1.12	385	561	89	59	0.85	0.08	1.9
M	0.329	6.14	0.29	123	402	56	49	0.88	0.06	7

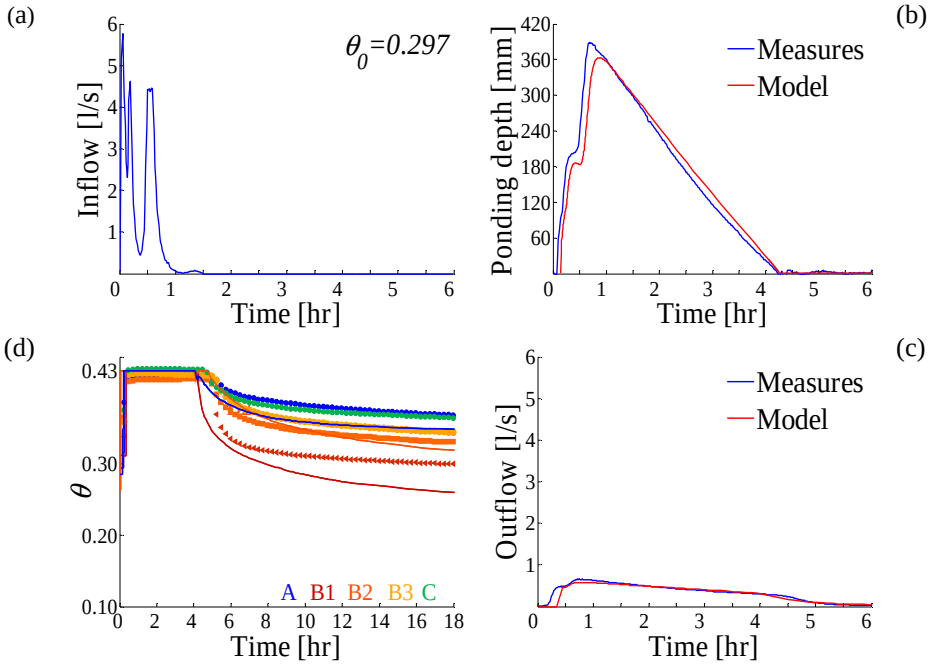

Fig. 55 – Event G: (a) measured inflow hydrograph; (b) ponding depth values; (c) outflow hydrograph; (d) measured (symbols) and modeled (lines) soil moisture values

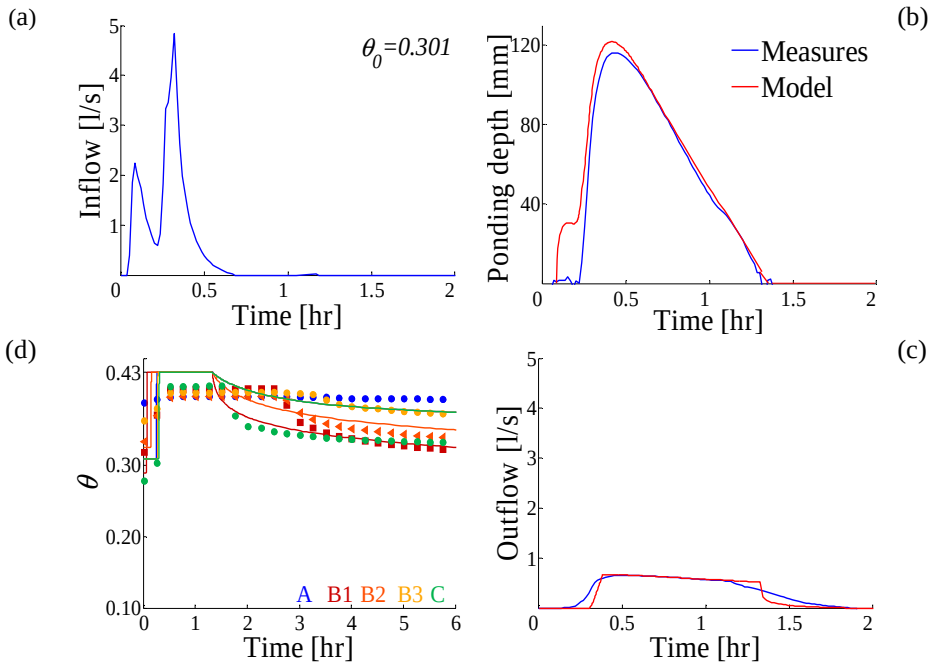

Fig. 56 – Event Q: (a) measured inflow hydrograph; (b) ponding depth values; (c) outflow hydrograph; (d) measured (symbols) and modeled (lines) soil moisture values

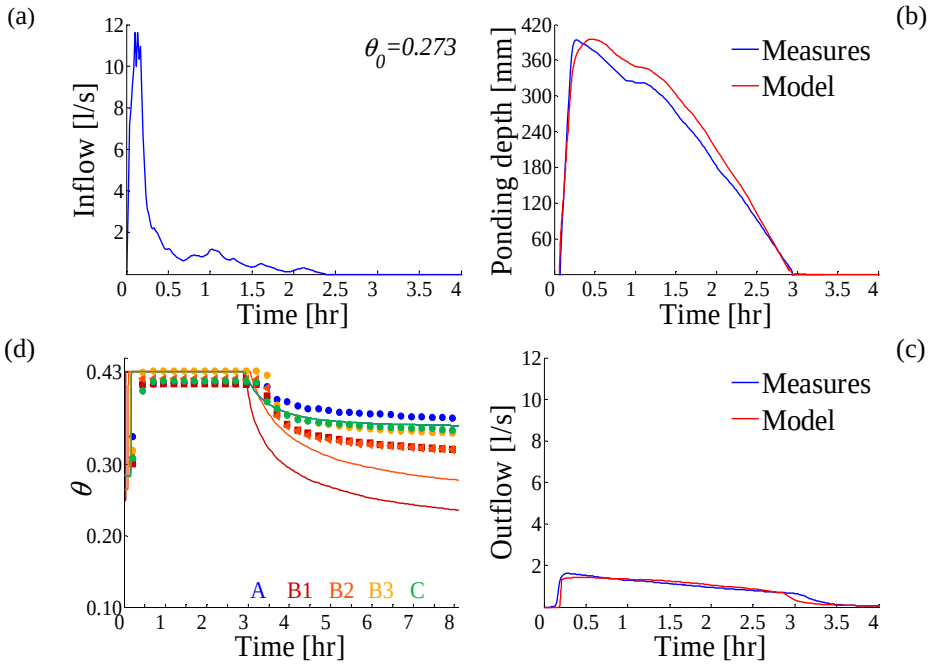

Fig. 57 – Event N: (a) measured inflow hydrograph; (b) ponding depth values; (c) outflow hydrograph; (d) measured (symbols) and modeled (lines) soil moisture values

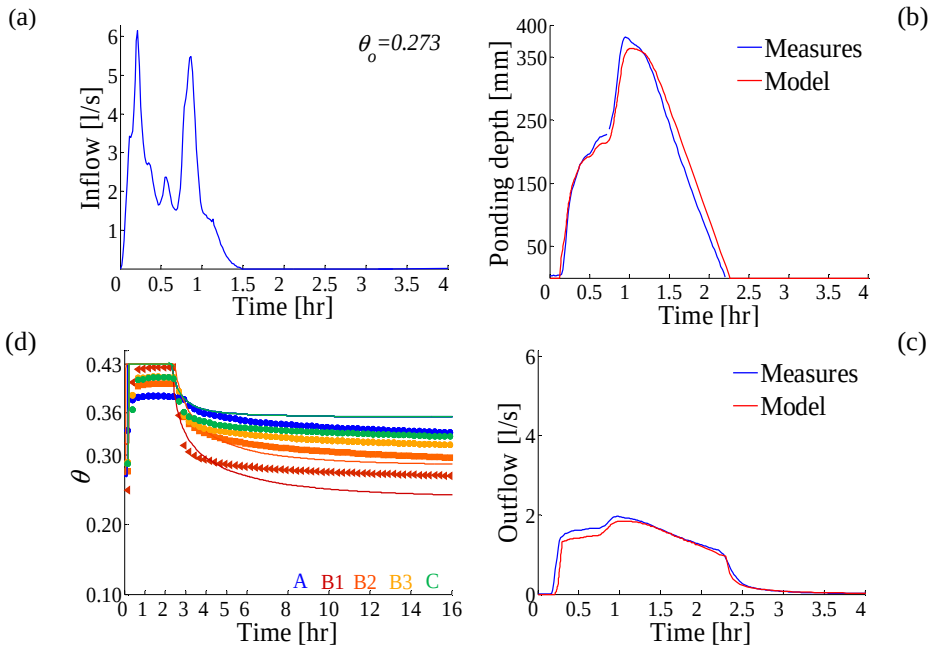

Fig. 58 – Event O: (a) measured inflow hydrograph; (b) ponding depth values; (c) outflow hydrograph; (d) measured (symbols) and modeled (lines) soil moisture values

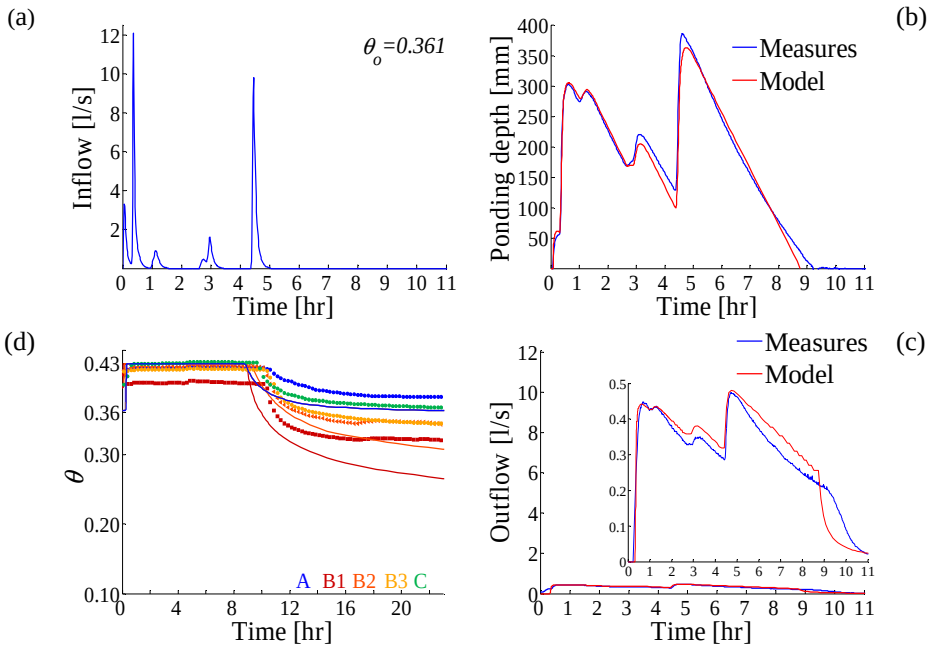

Fig. 59 – Event I: (a) measured inflow hydrograph; (b) ponding depth values; (c) outflow hydrograph; (d) measured (symbols) and modeled (lines) soil moisture values

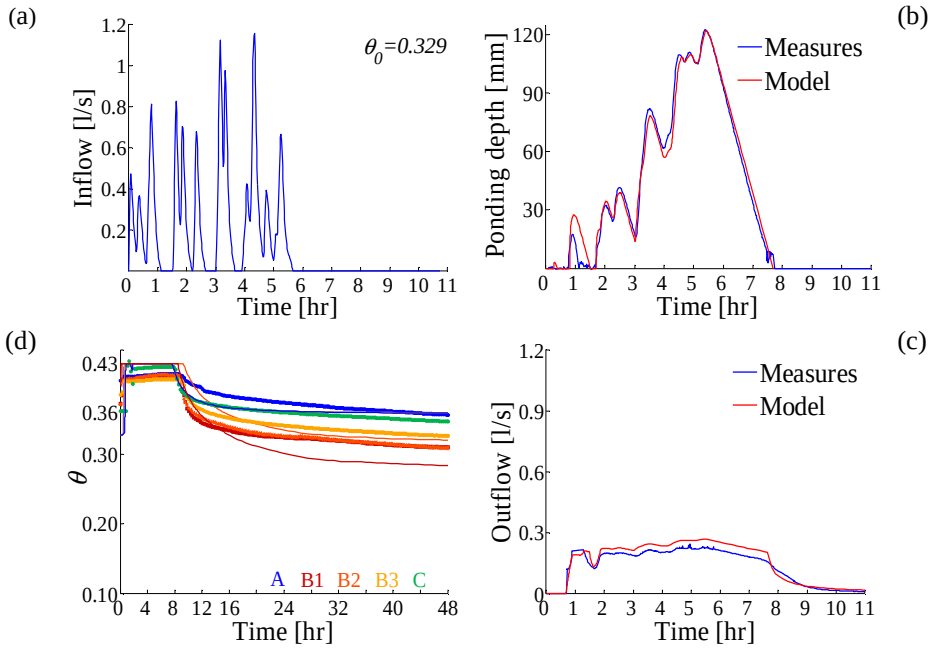

Fig. 60 – Event M : (a) measured inflow hydrograph; (b) ponding depth values; (c) outflow hydrograph; (d) measured (symbols) and modeled (lines) soil moisture values

The analysis of the measured data allowed a qualitative diagnosis: depending on specific features of the inflow hydrograph, the average soil moisture of the filter media increased during the event, and the celerity of water level drop decreased.
The behavior of the infiltration trench was thus a function of its

(1) initial conditions and
(2) event dependent alteration.

Although reasonable in terms of general meaning, the latter assertion was based on a diagnosis in contradiction with the general theory of the unsaturated flows.
In particular, a few possible correlations between the features of the inflow events and the behavior of the infiltration trench were highlighted:

(a) bigger volumes of the inflow events reasonably yielded to a greater increase in the moisture content of the filter media thus inducing longer depletion phases. Inflow event G indeed started from drier initial conditions but had a bigger inflow volume than inflow events L and Q. It is worth noting that the average intensity of the inflow discharge was similar for the three events.
(b) bigger values of the average intensity of the inflow event somehow allowed faster depletion phases. Starting from the same initial conditions, inflow events N and O poured similar volumes in the infiltration trench, nevertheless a smaller inflow intensity was accompanied by a slower decrease of the failing head. Despite the higher values of both initial water content and inflow volume, the more intense inflow event I showed a faster depletion phase than the inflow event M.

Prior to investigate the existence of a physically based explanation for these empirical diagnosis, a further confirm was provided by the numerical analysis of the “small” inflow events, i.e. the inflow events lacking of the storage and depletion phases.

3.6 Numerical analysis of “small” events

We called “small” inflow events all the events that showed an advance phase and a depletion phase, while the storage phase was missing. Furthermore, the advance phase wasn’t generally able to reach the downstream end of the biofiltration trench and no data were detected neither by the water depth sensor nor by the soil moisture sensor located 8m far from the inlet.
The numerical modeling of these events was thus a little bit more challenging. A constant, zero water depth value in the last 2m of the biofiltration trench was imposed for the calibration of the external iterative coupling strategy.
Referring to our previous numerical analysis on “big” inflow events, the lacking of a storage phase suggested the antecedent soil moisture content of the filter media as the only parameter leading the behavior of the infiltration trench.
This hypothesis was verified by the numerical modeling of several “small” storm events. Adopting a lumped model approach, the bulk value of the saturated hydraulic conductivity was recursively changed in order to fit the measured values of outflow and soil moisture.
Tabel 23 lists the main features of the “small” events modeled as well as the bulk value of the saturated hydraulic conductivity which minimized round mean square errors between measured and modeled outflow and soil moisture time series.
Fig. 61 to Fig. 64 prove the good performances of the lumped numerical modeling strategy.
Fig. 65 compares measured and computed outflow volumes. The root means square error is 0.175 m^3; the average ration between measured and model values is 0.92.

Tabel 23 –Numerical analysis of many “small” inflow events

	Date	θ_0	Inflow event		Hydrological performances			$k_{s,Small}$
			V [m^3]	$\bar{Q}$ [l/s]	f_v	R_{peak}	R_{delay}	[mm/hr]
a	2010/10/16 h07:51	0.305	0.52	0.30	1.05	0.22	5.0	148
b	2010/11/19 h05:34	0.308	0.42	0.22	1.08	0.23	4.8	135
c	2011/01/11 h12:35	0.198	0.74	0.54	0.71	0.33	6.0	394
d	2011/01/24 h06:04	0.213	3.65	0.87	0.93	0.39	3.8	369
e	2011/03/09 h17:56	0.220	3.58	0.77	0.96	0.58	3.2	369
f	2011/05/17 h04:36	0.266	5.12	0.36	0.86	0.44	1.1	209
g	2011/07/17 h23:12	0.337	1.57	0.27	1.20	0.65	1.5	86
h	2012/01/30 h14:10	0.239	0.20	0.14	0.48	0.21	2.2	246

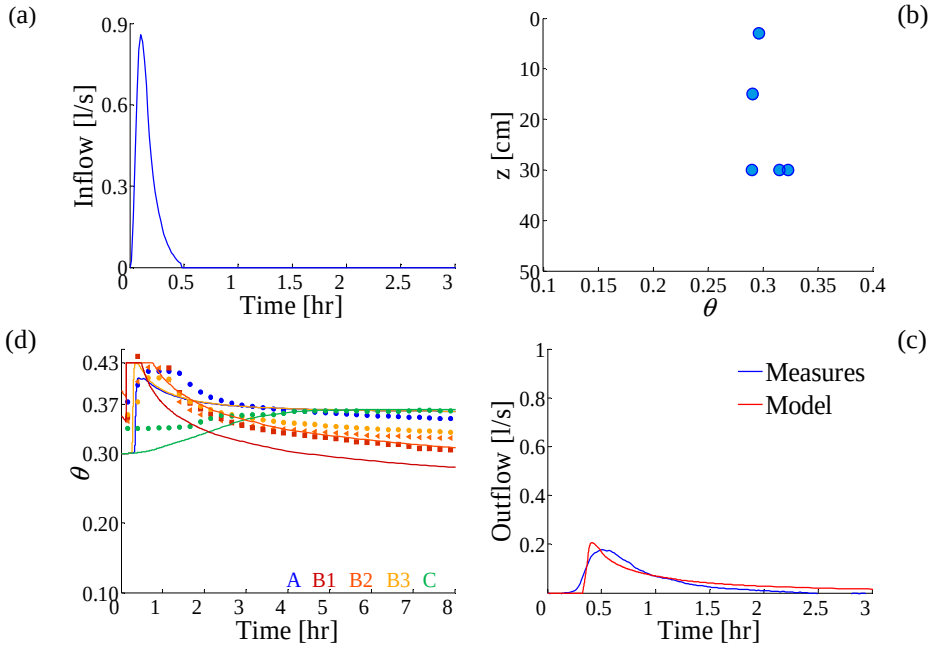

Fig. 61 – Event "a": (a) Inflow hydrograph, measures; (b) antecedent soil moisture content; (c) Outflow hydrograph, measures and model; (d) Soil moisture time series, measures and model

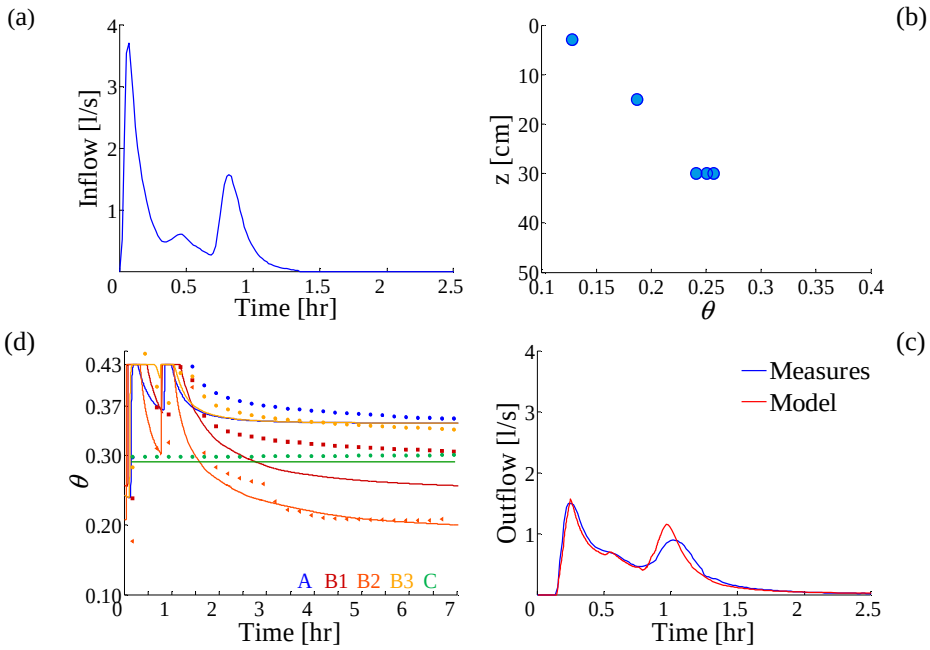

Fig. 62 – Event "d": (a) Inflow hydrograph, measures; (b) antecedent soil moisture content; (c) Outflow hydrograph, measures and model; (d) Soil moisture time series, measures and model

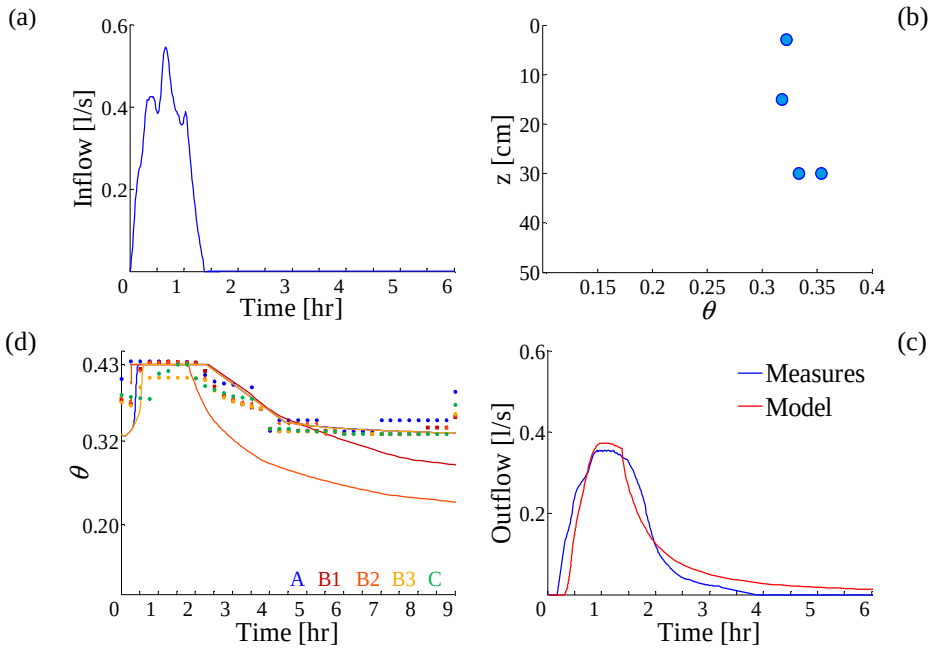

Fig. 63 – Event "g": (a) Inflow hydrograph, measures; (b) antecedent soil moisture content; (c) Outflow hydrograph, measures and model; (d) Soil moisture time series, measures and model

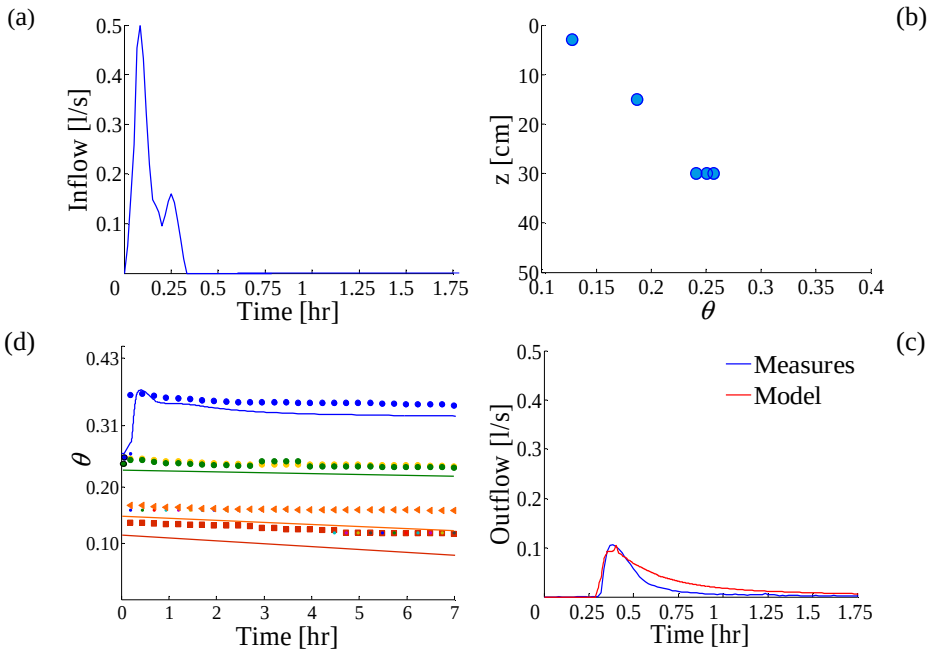

Fig. 64 – Event "h": (a) Inflow hydrograph, measures; (b) antecedent soil moisture content; (c) Outflow hydrograph, measures and model; (d) Soil moisture time series, measures and model

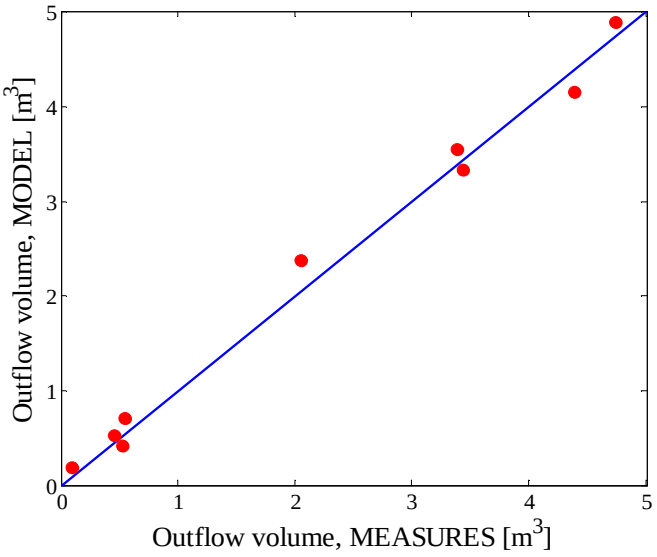

Fig. 65 – "Small" events, volume of the outflow hydrograph, results of the numerical model and measured data

Numerical analysis pointed out a best fitting mathematical representation of the correlation between antecedent soil moisture conditions $\bar{\theta}_0$ and the optimal value of the saturated hydraulic conductivity $k_{s,Small}$ based on the results of our numerical model (Eq. 40, RMSE=24 mm/hr ; Fig. 66)

$$k_{s,Small} = 917 \cdot \exp\left(-20.5 \cdot \bar{\theta}_0{}^2\right) \qquad \text{Eq. 40}$$

It is worth noting that the value of the saturated hydraulic conductivity $k_{s,Small}$ implemented in our numerical model had to adequately represent the behavior of the infiltration trench during the whole inflow event taking into account the obvious gradual increase of soil moisture content. Nevertheless, according to our analysis, it could be efficiently expressed a function of the antecedent soil moisture conditions. For this reason, in the next paragraphs we replaced $k_{s,Small}$ with $k_{s,0}$.

The empirical expression suggested (Eq. 40) is intrinsically limited by the extreme values of moisture content. In particular, referring to the lowest average initial value of the soil moisture content detected

during the monitoring period (September 2010-April 2012) and the saturated water content we got:

$$\begin{aligned} \overline{\theta}_{0,min} &= 0.198 \rightarrow \quad k_{s,0} = 410\, mm/hr \\ \bar{\theta}_{0,sat} &= 0.430 \rightarrow \quad k_{s,0} = 21\, mm/hr \end{aligned} \qquad \text{Eq. 41}$$

The highest value of the antecedent soil moisture content detected in the monitoring period (September 2010-April 2012) was 0.37; it leads to $k_{s,NS} = 43\, mm/hr$. These statements are coherent with our numerical results.

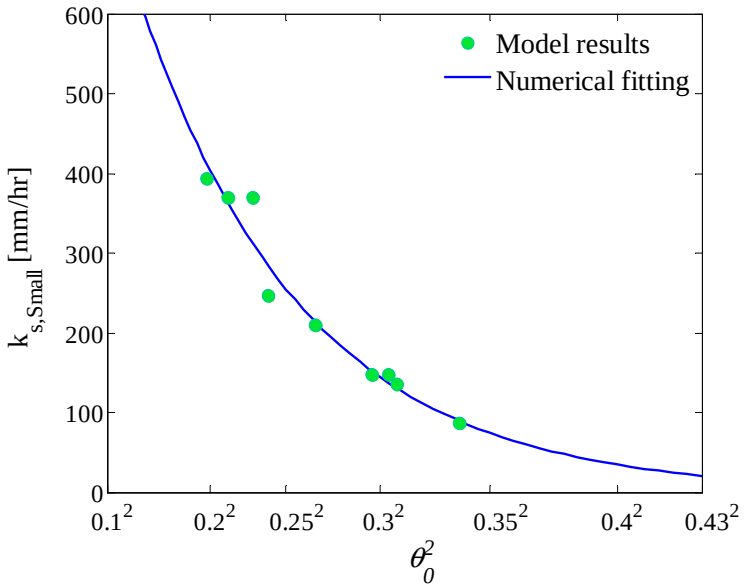

Fig. 66 – "Small" events, bulk value of the saturated hydraulic conductivity as a function of the antecedent soil moisture content

Nevertheless, the numerical evidences showed so far needed a physically based explanation.
A literature review yielded to the hypothesis of soil water repellency (or hydrophobicity). The next paragrpaph describes this phenomenon with reference to its effects on infiltration and unsaturated flows.

3.7 Soil water repellency

Soil water repellency (or hydrophobicity) reduces the affinity of soils to water such that they resist wetting for periods ranging from a few seconds to hours, days or weeks (e.g. King, 1981; Doerr and Thomas, 2000). Soil water repellency has been reported for varying soils, land uses, and climatic conditions (Dekker et al.,1998; Blackwell, 2000; DeBano, 2000; Dekker and Ritsema, 2000; Doerr et al., 2000; Keizer et al., 2005; Moral Garcia et al., 2005). Water repellent soils are difficult to manage and pose negative effects on agricultural productivity and environmental sustainability (Debano, 1969; Letey, 1969; Bond, 1969; van't Woudt, 1969; Jamison, 1969; Holzhey, 1969; Letey et al., 1975; Ritsema et al., 1993).
The affinity or repellency between water and solid surfaces depends on the prevailing of adhesion or cohesion effects. A hydrophilic surface allows water to spread over it in a continuous film whereas water on a hydrophobic surface 'balls up' into individual droplets (Adam, 1963) (Fig. 67).

Fig. 67 – Water drop on a hydrophobic soil (Dekker & Ritsema, 2000)

Surface free energy quantifies the disruption of intermolecular bonds that occurs when a surface is created. All principal soil minerals have a much higher surface free energy than water and are therefore hydrophilic (Tschapek, 1984), whereas soft organic solids, such as waxes or organic polymers, can exhibit lower surface free energy values and are thus hydrophobic (Zisman, 1964).
Soil water repellency has been proven to be the rule rather than the exception in most field soils (Wallis et al., 1991,1992; Steenhuis et al., 1996; Dekker, 1998). According to the review compiled by

Dekker et el. (2005), water repellent soils have been found and studied in at least 21 States of America, in Canada, in Mexico, in Equador, in Chile, in Peru, in Venezuela, in Brazil, in Egypt, in Mali, in Congo, in South Africa, in Israel, in Spain, in Portugal, in Germany, in United Kingdom, in Denmark, in Sweden, in Finland, in Poland, in Slovakia, in France, in Greece, in Italy (Giovannini and Lucchesi, 1983, 1997), in Turkey, in Russia, in Nepal, in India, in Japan, in New Zealand, in Australia.
Referring to Australia, the southern region has the largest area of water repellent soils of any country in the world. About 2 Mha in Western Australia, 2 Mha in South Australia and 1 Mha in Victoria are known to be affected and a further large area has the potential to be repellent (Blackwell, 1993; Moore and Blackwell, 1998).
Numerous techniques have been developed to determine the water repellency of soil. The most physically meaningful method is a direct measurement of soil-water drop contact angle (Woche et al. 2005). Stating its practical issues, alternative strategies were developed. The most common method is probably the water drop penetration time test, which is based on the time required by a drop of water to infiltrate into soil (Dekker et al. 1998).

3.7.1 Origin

Soil water repellency has been observed for a huge range of soil textures and clay content (up to 40%) values (Crockford et al., 1991; Chan, 1992; Dekker and Ritsema, 1996) and it is generally believed to be caused by long-chained hydrophobic organic compounds (Doerr et al., 2000; Franco et al., 2000; Dekker et al., 2001; Morley et al., 2005; Xiong et al., 2005). The identification of the specific compounds causing water repellency has been a focus of soil research in the last decades (e.g. Franco et al., 1994; Hudson et al., 1994; McIntosh and Horne, 1994). In general terms, the compounds identified from water-repellent soils can be divided into two main groups, i.e. the aliphatic hydrocarbons, and the polar substances of amphiphilic structure (McIntosh and Horne, 1994). These hydrophobic compounds all derive from living or decomposing plants, plant root exudates, decomposing soil organic matter, fungal residues, resins, waxes, aromatic oils, and soil microorganisms

(McGhie and Posner, 1981; Mallik and Rahman, 1985; Bisdom et al., 1993; Dekker and Ritsema, 1994; Doerr et al., 1998; DeBano, 2000; Doerr et al., 2000; McKissock et al., 2000; Mainwaring et al. 2004; Hallet et al, 2006,2007).

Plants most commonly associated with water repellency are trees with a considerable amount of resins, waxes or aromatic oils such as pines and eucalyptus, Australian varieties of the latter are said to produce the most severe repellency patterns observed in the world (Doerr et al., 2000; Coelho et al., 2005; Keizer et al., 2005a; Leighton-Boyce et al., 2005). Water repellency has also been found under shrubs ranging from temperate heathland (Mallik and Rahman, 1985) or mediterranean shrubland (Giovannini et al., 1987) , to semi-desert chaparral (DeBano, 1991). Finally, soil under grassland can also resist wetting (Karnok et al., 1993; York, 1993; Crockford et al., 1991; Ritsema et al., 1994; McIntosh and Horne, 1994; Carter et al., 1994)

Generally speaking, a small amount of hydrophobic compounds is necessary to cause water repellency (Wallis et al., 1990; Berglund and Persson, 1996; McKissocketal., 1998; Teramura, 1980 ; Jungerius and de Jong, 1989; DeBano, 1991; Wallis et al., 1993).

Referring to a range of Australian soils, McKissock et al. (1998) concluded that it is impossible to use any of the individual soil or vegetation characteristics on their own to accurately predict the occurrence or the degree of water repellency.

Nevertheless, the leading role of organic compounds must be taken into account when planning low impact strategies for the treatment of sewage waters (e.g. wetlands).

Apart from the biological factors listed above, fire has been observed to induce hydrophobicity (DeBano and Krammes 1966 , DeBano et al. 1970 and Savage 1974).

3.7.2 Hydrological consequences: focus on preferential flow pathways

According to the reviews reported in literature (DeBano, 1981; White and Wells, 1982; Wallis and Horne, 1992; Doerr et al., 2000; Blackwell, 2000), soil water repellency may result in contrasting hydrological impacts.

Field observations have indicated that the rates of infiltration into repellent soils are very irregular. Water infiltration in initially dry, water repellent soils is retarded compared to infiltration in wet soils (e.g. Wallis et al., 1991), causing water to be retained in the top layer at first. With prolonged rainfall, minor perturbations in an originally planar infiltrating wetting front may grow to form preferential flow paths, often called "fingers" (Fig. 68).

(a)  (b)

Fig. 68 – Preferential flow paths in water repellent soils (a) field image, http://www.splu.nl/waterrepellency ; (b) laboratory image, Doerr et al.(2000)

Preferential flow is the concentrated vertical movement of water via discrete pathways through the soil matrix resulting in an uneven distribution of soil moisture. Water (and solutes) may move to far greater depths, and much faster, than would be predicted with the Richards equation using area-averaged moisture contents and pressure heads (Beven, 1991).

Although preferential flow may originate for a variety of reasons such as cracks and macropores, textural discontinuities and unstable wetting fronts due to soil layering or air entrapment (Ritsema et al., 1993); several researchers (e.g. Raats, 1973; Philip, 1975; Parlange et Hill, 1976; Glass et al., 1989; Wang et al., 1998) noted that fingered by-passing flow is more likely to occur in repellent soils rather than in wettable soils.

Wang et al. (1998, 2000) carried out laboratory infiltration experiments to quantify the effects of soil water-repellency on wetting front instability and infiltration rate. They proved the

reliability of two alternative criteria for predicting the onset of wetting front instability, i.e.:

a) the velocity criterion (Parlange et Hill, 1976) (Eq. 42):

$$i < k_S \qquad \text{Eq. 42}$$

where i is the infiltration rate and k_S is the saturated hydraulic conductivity

b) the pressure criterion (Raats, 1973; Philip, 1975) (Eq. 43):

$$\mathrm{H} = h_0 - h_{we} - h_{af} < 0 \qquad \text{Eq. 43}$$

Where H is the net matrix pressure head difference across the wetted layer, h_0 the surface pressure head, h_{we} the water-entry pressure of the porous medium, i.e. the critical soil water potential at which water starts to displace air in the porous medium; h_{af} the gauge air pressure below the wetting front.

Wetting front instability can thus be induced by the individual or combined effects of three factors:

(i) a decrease in surface pressure head h_0, for instance during redistribution of water following infiltration (see par. 2.2);

(ii) an increase in water-entry value h_{we} due to, for instance, the presence of a fine-over-coarse layering in the direction of flow, the occurrence of macropores ($h_{we} \sim 0$);

(iii) an increase in soil air pressure below the wetting front (see par. 2.2).

The same experimental studies proved that water repellent soils have positive water-entry value ($h_{we} > 0$), condition (b) is consequently often verified and preferential instable flow occurs.

Field soils are heterogeneous and layered.

The topsoil is often macroporous or sometimes water repellent.

The soil air can easily be entrapped during high-intensity rainfalls or ponded surface irrigation events. The soil surface is otherwise under non-ponding infiltration or drainage conditions resulting in negative water heads at the soil surface.

All these natural conditions tend to induce unstable flow. Hence, fingering is more likely a common phenomenon rather than the exceptions in the field.

Furthermore, hydrophobicity can be particularly effective at preventing or hindering downward water movement, directing it into structural (e.g. root channels and rodent burrows) or textural preferential flow paths or creating an unstable irregular wetting front (Kung, 1990; Ritsema and Dekker, 1994).
Fingered flow pathways tend to persist once they have formed. Repeated wetting and drying of these pathways over a protracted period of time will probably lead to the leaching of hydrophobic substances from the pores along the fingered flow pathways. This leaching can make the fingered flow pathways more wettable than the surrounding hydrophobic media. In the long term, originally instability-driven fingers might become heterogeneity-driven fingers (Ritsema et al., 1993; Ritsema and Dekker, 1995). Field studies showed that preferential flow is exacerbated by soil water hysteresis between wetting and drying phases (Ritsema et al., 1998).
Referring to the listed impacts of soil water repellency, many studies (e.g. Scott, 1992; Moore and Blackwell, 1998; Doerr et al., 2000; Leighton-Boyce et al., 2005; Twaites et al, 2006) suggested that the release of hydrophobic substances in the soil may be used by plants to suppress the germination of competing vegetation, and to increase water conservation by channeling water deep into the soil profile along preferential flow pathways, thereby reducing evaporation.

3.7.3 Moisture effect on infiltration patterns in water reppelent soils

Water repellency is usually a transient soil property; many authors reported an inverse relationship between soil water content and soil water repellency (e.g. Gilmour 1968; DeBano, 1971; King, 1981; ; Wallis et al., 1990; Witter et al., 1991; Carter et al., 1994; Dekker and Ritsema, 1994; Dekker et al., 1998; Doerr et al., 2000; Coelho et al., 2005; Keizer et al., 2005; Leighton-Boyce et al., 2005).
A volume of soil remain hydrophobic until the organic layer covering its surface undergoes molecular conformational changes during its contact with water (Ma'shum and Farmer, 1985; Wallis et al., 1990; Richardson and Hole, 1978; Barrett and Slaymaker, 1989; Tschapek, 1984; Ma’shum and Farmer, 1985; Dekker and Ritsema 1994; Soto et al. 1994; Doerr et al. 2000).

Dekker and Ritsema (1994) hypothesized the existence of a soil-specific "critical soil moisture threshold" dividing wettable and hydro-repellent conditions. In a later study, Dekker et al. (2001) replaced the concept of the transition threshold with a moisture 'transition zone' concept, within which both wettable and repellent soil conditions may occur, but only repellent and wettable conditions are possible respectively under and above the moisture boundaries of this zone.

Leighton-Boyce et al.(2005) observed a dichotomous distribution of water repellency concluding that the transition from water repellent to wettable conditions must be sudden. They argued that the transition zone observed by Dekker et al. (2001) could be a consequence of hysteretic soil water-repellency, with water repellency breaking down and re-establishing a different soil water contents.

Several field studies aimed at quantifying moisture content threshold values or transition zones as a function of both soil and vegetation features. For example, water repellency was found to be present for soil moisture contents up to 22% in sandy loams (Doerr and Thomas, 2000); up to 38% in a clayey peat (Dekker and Ritsema, 1996); up to 2% in coarse sands (Dekker and Ritsema, 1994).

A huge scatter of results is listed in literature pointing out the extreme importance of local conditions representing the outcome of specific, not reproducible combinations of several time and spatial varying soil and vegetation parameters (e.g. Leighton-Boyce et al. (2005); L.A. Thwaites (2006))

Bauters et al. (2000) completed a series of experiments to examine infiltration patterns in hydrophobic (and coarse) soils as a consequence of varying values of initial water content. As initial soil moisture content increased from the residual value up to the saturated value, three flow regimes were detected: unstable, intermediate and stable Richards' (Fig. 69). Unstable flow was observed at very low moisture content values and fingers did not widen. Stable Richards' flow was obtained closed to saturated conditions, the wetting front moved both sideways and downwards. In the intermediate range of moisture content values, the fingers changed gradually from unstable to stable Richards'. These results are consistent with Di Carlo et al.(1999) who studied the sideways expansion of fingers over an extended time period.

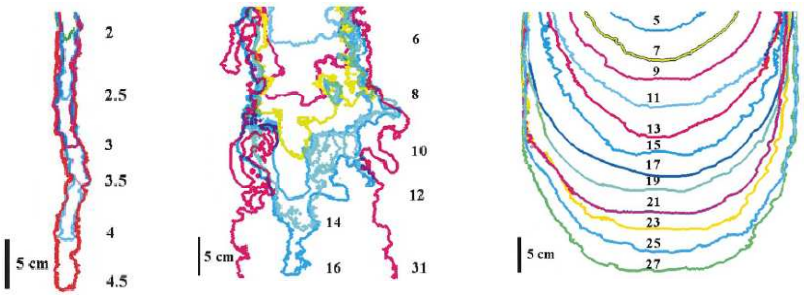

θ=0.01 Unstable | θ=0.03 Intermediate | θ=0.047 Stable Richards'

Fig. 69 – Three flow regimes observed with increasing soil moisture content (Bauters et al., 2000)

Bauters et al. (2000) calculated the unsaturated conductivity as a function of moisture content. During their experiments the wetting front velocity was approximately constant. The highest velocity corresponded to the smallest finger diameter; generally, the advance was much slower for the high water contents than for the low water contents. In particular, a sixfold velocity decrease from very low to saturated initial water contents was measured.
It is worth noting that this outcome is highly counterintuitive since classical Richards' type wetting front theory defines an increase in velocity with increasing water content.

3.7.4 Concluding remarks

Water repellent soils are highly prone to preferential flows (e.g. Wang et al., 2008). As a consequence, (i) soil may not wet completely with the passage of a wetting front, and (ii) water may be quickly channeled downwards by-passing the soil matrix. Consequently, water storage and residence times in the unsaturated zone could be sensibly reduced (Burch et al., 1989; Van Dam et al., 1996).
For instance, Walsh et al. 1995 considered that such by-pass routes explained why even large storms produced little overland flow for highly hydrophobic mature pine and eucalyptus forest soils in Portugal.

Furthermore, water repellency affects (iii) soil moisture dynamics, including evaporation patterns. A water-repellent surface layer with preferential flow routeways can lead to dry surface soil and higher soil moisture in the subsoil (e.g. Meeuwig, 1971; Burch et al., 1989; Imeson et al., 1992).
Specularly, soil water repellency is inversely affected by soil moisture content. A shift from preferential, unstable flow to matrix, stable flow and a related decrease of the water front celerity were detected as soil moisture content increased.
Three clues supported the hypothesis of soil water repellency of the filter media of the facility installed at Monash Univesity. In particular, in order of importance they are:

1. soil water repellency is a highly common issue in Victoria;
2. the leaves of the native species planted in the biofiltration trench have a thick wax layer;
3. our numerical analysis pointed out a faster percolation as soil moisture decreased.

Soil water repellency probably developed as plants grew. Preferential flow paths as a consequence of soil water repellency could coherently explain the temporal decrease of hydrologic performances (volume storage, peak reduction, peak delay) accompanied by a lower number of overflow events detected for the biofiltration system installed at Monash University (par.3.3). In many events finger flow by-passed the soil matrix thus sensibly reducing the buffering capacity of the system.
Soil moisture negatively affected soil water repellency leading to a shift from a finger flow regime to a matrix flow regime. Fast percolation through preferential pathways was observed for dry antecedent soil moisture conditions; slow matrix infiltration occurred for wet antecedent soil moisture conditions. Ponding depth values led the first, gravity driven flow regime; soil water retention characteristics led the latter. A transient flow regime operated for intermediate antecedent soil moisture conditions.

Management strategies. Physical, chemical and biological approaches exist to ameliorate soil water repellency, the most common are (a) plant adaptation; (b) soil or hydrophobic layer removal; (c) reduced soil drying; (d) claying (Blackwell, 2000).

3.8 Discussion on the implementation of a lumped model

The hypothesis of soil water hydrophobicity coherently explained the widely varied hydraulic behavior of the infiltration trench installed at Monash University. Although the clogging of the filter media was reasonably speculated, preferential flow paths induced by soil water repellency highly enhanced water downward movement.
Several mathematical formulations have been proposed to model and predict multidomain flow processes; most of them were developed to assess solute leaching. They mainly refer to three approaches (Gardenas et al., 2006):

a) the use of soil hydraulic properties artificially modified to account for accelerated flow (e.g. Vogel and Cislerova, 1988; Durner, 1994; Mohanty et al., 1997) ;

b) the dual-porosity approach (e.g. Šimůnek et al., 2003);

c) the dual-permeability formulation (e.g. Gerke and van Genuchten, 1993, 1996).

According to the first approach, the hydraulic functions evaluated for the soil matrix domain are simply multiplied by appropriate factors to describe the behavior of the preferential flow domain. These factors are based on the statistics of the fractional cross-sectional areas of the domains considered. Although this approach may be mathematically appropriate, the task of testing these functions is formidable in view of current experimental limitations (Mohanty et al., 1997). Some researchers (e.g., Anderson and Hopmans, 1994; Singh et al., 1991) attempted to quantify preferential pathways by direct measurement using computer tomography. On the other hand, Ela et al. (1992) suggested that knowledge of the number and size of preferential pathways is not enough to adequately model finger flow. Mohanty et al., 1997 suggested a simplified protocol based on the use of single continuous piecewise hydraulic functions retrieved from in situ and laboratory measurements. They assumed that water flow through the overall porous but rigid matrix could be described with Richards'

equation in conjunction with hybrid piecewise continuous hydraulic functions.

Dual-porosity models assume that water flow is restricted to the preferential flow domain and that the water in the matrix does not move at all. The Richards' equation with properly defined parameters is employed to describe flow in the preferential paths, while a mass balance equation describes moisture dynamics in the matrix.

Dual-permeability approaches assume that water flow can take place in both the preferential paths and the matrix. Some models invoke similar equations for flow in both regions (e.g. Gerke and Van Genucthen, 1993, 1996, applied the Richards equation to both pore regions), while others use different formulations (Larsbo and Jarvis, 2003). Approaches for calculating water flow in macropores range from the Green and Ampt or Philip infiltration models (Ahuja and Hebson, 1992; Chen and Wagenet, 1992), the kinematic wave equation (Germann, 1985; Germann and Beven, 1985; Jarvis, 1994), and the Richards equation (Gerke and van Genuchten, 1993a).

According to Gardenas et al. (2006) dual-permeability approach most accurately simulates preferential drainage flow. An attractive feature of the dual-permeability model is the ability to simulate both the peak flow resulting from macropore flow, and the base flow reflecting matrix characteristics. They have been increasingly used for analysis of preferential flow paths, both on the laboratory column scale (Gwo et al., 1995-1996; Allaire et al. 2002; Castiglione et al., 2003; Greco, 2002; Katterer et al., 2001) and on the plot or field scale (Jarvis et al., 1994; Andreu et al., 1994; Larsson and Jarvis, 1999; Kohler et al., 2001).

An new module, called DualPerm, has been recently included in the HYDRUS (2D/3D) software package (Version 2) (Šimůnek et al., 2012). It simulates two-dimensional variably-saturated water movement and solute transport in dual-permeability porous media (dual-porosity approaches were included in the previous versions of the software package). Based on the model proposed by Gerke and van Genuchten (1993), the dual-permeability formulation for water flow uses Richards equation. The mass transfer of water between the two domains is driven by the gradient of pressure heads. Numerical stability issues have been reported by the authors (Šimůnek et al., 2012)

Unluckily dual permeability models are based on a huge number of site-specific assumptions about the geometry and the hydraulic features of preferential pathways. They typically need soil hydraulic conductivity and soil water retention functions for each flow domain, including terms accounting for the interaction or exchange of water between the different domains.
For example, the dual-permeability model of Gerke and van Genuchten (1993), in its full complexity, needs 16 parameters to describe water flow. Additionally to the six soil hydraulic parameters required to describe the hydraulic properties of the fingers and the matrix region, estimates of structural parameter are needed to characterize the hydraulic conductivity of the finger–matrix interface when using the Mualem–van Genuchten model. Simplified approaches (e.g. the kinematic wave model can be used to describe flow in the fingers domain) or practical assumptions may slightly reduce the total number of parameters.
Many different protocols have been proposed to evaluate some of these parameters (Beven, 1991; Clothier et al., 1995; Jaynes et al.,1995, Kodešová, 2011). Nevertheless, they are expensive (e.g., Panguluri et al., 1994; Köhne et al., 2005) and they rarely provide enough information to fully calibrate multidomain flow models (Šimůnek et al, 2003). Most available techniques for measuring of hydraulic properties (conductivity and retention) can neither distinguish between the different flow domains and their relative contribution to flow (Luxmooree et al., 1990), nor be used to determine the between-domain exchange terms.
A need still remains to apply currently available modeling tools to natural systems (Evans et al., 2001).
Furthermore, Coppola et al. (2012) highlighted that dual-permeability models proposed in literature assume a rigid porous medium, that is a medium with stable preferential flow (for instance, fractures or burrows). This assumption badly fits the intrinsic transient behavior of preferential flow paths due to soil water repellency.

Aiming at a parsimonious, synthetic, yet effective model we hypothesized a simplified version of the first approach (a) based on the use of artificially modified soil hydraulic properties.

Referring to the protocol proposed by Mohanty et al., 1997, we replaced the real, deeply heterogeneous system with an equivalent media (e.g. Lin and Govindaraju, 1996) encompassing both

(a) the time-dependent preferential paths and
(b) the soil matrix

of the infiltration trench.
This equivalent media was expected to process the inflow hydrographs in the same way as the complex, highly varying real system. Computed outflow hydrographs and average soil moisture content time series had to fit measured data.
Although lumped approaches cannot represent the interactions between the flow domains, they may be beneficial for addressing large-scale in situ flow problems (e.g. Mohanty et al., 1997).
According to our analysis, the results of the coupled surface-subsurface numerical model were highly sensitive to the value of the saturated hydraulic conductivity. Partially neglecting its physical character, our trivial protocol imposed event-specific bulk values of the saturated hydraulic conductivity.
We then assumed that water flow in the equivalent media could be described with Richards' equation in conjunction with the fictitious value of the saturated hydraulic conductivity and the previously assessed hydraulic functions.
The bulk value of the saturated hydraulic conductivity had to be adequately changed to account for bidirectional recursive shifts from a preferential flow regime to a matrix flow regime through many transitional regimes. Soil moisture conditions deeply affected soil water repellency, preferential flow pathways and the flow regime. Antecedent water content of the filter media was a leading parameter. Nevertheless, a further challenge was the modeling of the effects of progressive wetting coupled with the features of the inflow event.
As shown in par.3.5 and in par. 3.6 this lumped model provided a reliable representation of the overall behavior of the infiltration trench thus validating the selected strategy.

3.9 From diagnosis to prognosis

The diagnostic approach was useful for a deep insight on the behavior of the infiltration trench as a function of its initial conditions and the features of the storm event. A complete, reliable numerical model was proposed; in particular, a lumped model was selected to parsimoniously represent ephemeral preferential flow pathways.
Shifting our attention from a diagnostic approach to a prognostic one, we aimed at the numerical definition of a semi-empirical, practical protocol to assess the parameters required by the numerical model for a good fitting of the sampled data of outflow and soil moisture time series.

3.9.1 Assessment of the soil water retention curve

Porosity and residual water content were assumed to be constant; the assessment of Van Genucthen parameters was based on the numerical fitting of the soil moisture data sampled at five points of the filter media domain immediately before the inflow event (details on this protocol can be found in par.3.3.3).

3.9.2 Assessment of the saturated hydraulic conductivity

Event-dependent switches from a preferential flow regime due to hydrorepellency to a matrix flow regime controlled the behavior of the infiltration trench. This complex physical phenomenon was synthetically represented forcing sensible numerical variations of the value of the saturated hydraulic conductivity, considered as a semi-quantitative, bulk parameter in a lumped model. Empirically detected correlations between the initial conditions of the filter media, the features of the inflow event, and the bulk value of the saturated hydraulic conductivity represented a valuable tool for a reliable, complete numerical modeling of the hydraulic behavior of the infiltration trench.

The initial conditions of the filter media, i.e. its average moisture content, completely described the behavior of the infiltration trench provided that a storage phase was missing (i.e. in case of "small" events, see par.3.6). When a storage phase was observed, the features of the inflow event, mainly its intensity and volume, played a not negligible role (i.e. in case of "large" events, see par.3.5).
A storage phase occurred when the average intensity of the inflow event exceeded the initial infiltration capacity of the system, i.e. its hydraulic capability of conveying downwards the inflow discharge. A discriminating parameter, named *Storage index*, was consequently defined (Eq. 44) :

$$Storage\ index(S.I.) = \frac{\overline{Q_{IN}}}{Q_{filter,0}} \begin{cases} > 1 & Existence\ of\ a\ storage\ phase \\ \leq 1 & NOT-existence\ of\ a\ storage\ phase \end{cases} \quad \text{Eq. 44}$$

where

- $\overline{Q_{IN}}$ is the average intensity of the inflow event computed as the ratio between the volume V_{IN} and the total length $time_{IN}$ of the inflow hydrograph (Eq. 39):
- $Q_{filter,0}$ is the initial infiltration capacity of the infiltration trench.

The infiltrability of the system was a function of

(a) the soil matrix and
(b) the existence, density, and hydraulic capability of the preferential flow paths.

The moisture content of the filter media exerts opposite effects: the drier the filter media, the smaller the hydraulic conductivity of the soil matrix, but the higher the occurrence of preferential flow paths that quickly channel downward the inflow discharge.
Despite infiltrability obviously changed with time, the establishment of a storage phase was adequately predicted using its initial value.
A global, representative index of the initial behavior of the system was induced from the numerical analysis of the "small" storm events; this index was a lumped value of the saturated hydraulic conductivity

$k_{s,0}$ (par. 3.6). In particular, our numerical analysis pointed out Eq. 40 for the assessment of the bulk value of the saturated hydraulic conductivity $k_{s,0}$ as a function of the initial average moisture content $\bar{\theta}_0$ of the infiltration media.
Introducing the surface area of the infiltration basin, we assessed the initial infiltration capacity of the system (Eq. 45).

$$Q_{filter,0} = k_{s,0} \cdot Area \qquad \text{Eq. 45}$$

Measured data proved the reliability of the *Storage index* (Eq. 44). "Large" and "small" inflow events were detected with a discrimination error of 7% (Fig. 70).

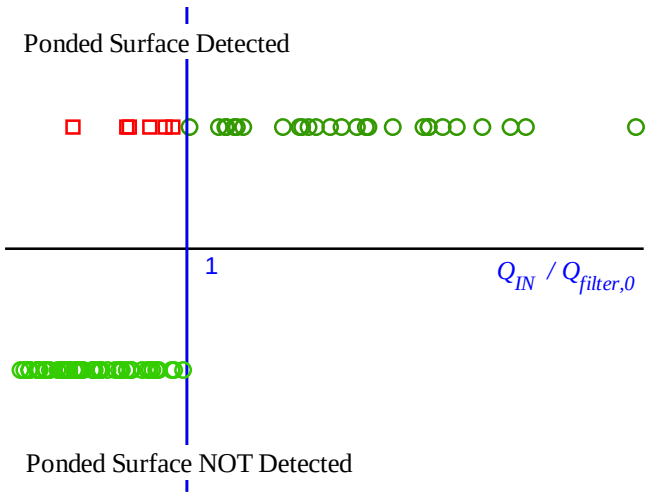

Fig. 70 – Measured and predicted occurrence of the storage phase for Cell 1 of the biofiltration facility installed at Monash University.

In case the *Storage index* (Eq. 44) was lower than 1, Eq.40 straightly provided the numerical value of the overall value of the saturated hydraulic conductivity $k_{s,0}$ (=$k_{s,small}$) to introduce in our lumped numerical model.

This protocol was implemented and validated.

Tabel 24 lists the main features of two representative events which showed a *Storage Index* lower than 1. The bulk value of the saturated

hydraulic conductivity was computed by Eq. 40 and introduced in the lumped numerical model. Fig. 71 and Fig. 72 (c and d) overlaps measured and modeled outflow and soil moisture values. Tabel 25 compares measured and modeled values of the outflow volume.

Tabel 24 –Events *i** and *l**, main features: validation of the protocol

	Date	V [m^3]	$\bar{Q}_{IN}$ [l/s]	$\bar{\theta}_0$	$k_{s,0}$ [mm/hr]	$Q_{filter,0}$ [l/s]	*S.I.*
*i**	10/16/2010 h 5:34	0.421	0.219	0.311	127	0.528	0.42
*l**	2011/01/11 h 12:35	0.733	0.531	0.242	276	1.152	0.46

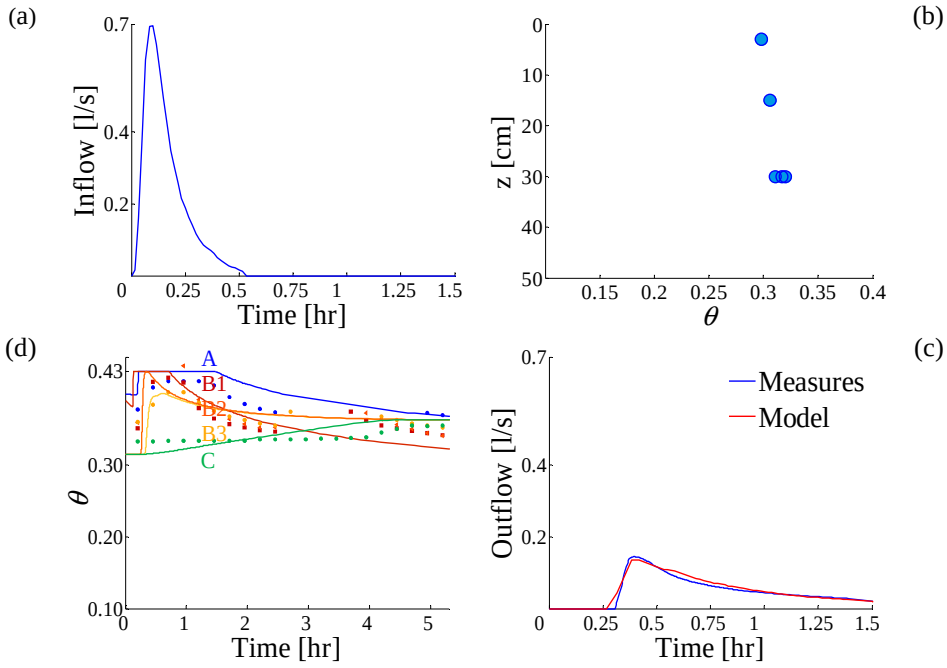

Fig. 71 – Event *i**: (a) Inflow hydrograph, measures; (b) antecedent soil moisture content; (c) Outflow hydrograph, measures and model; (d) Soil moisture time series, measures and model

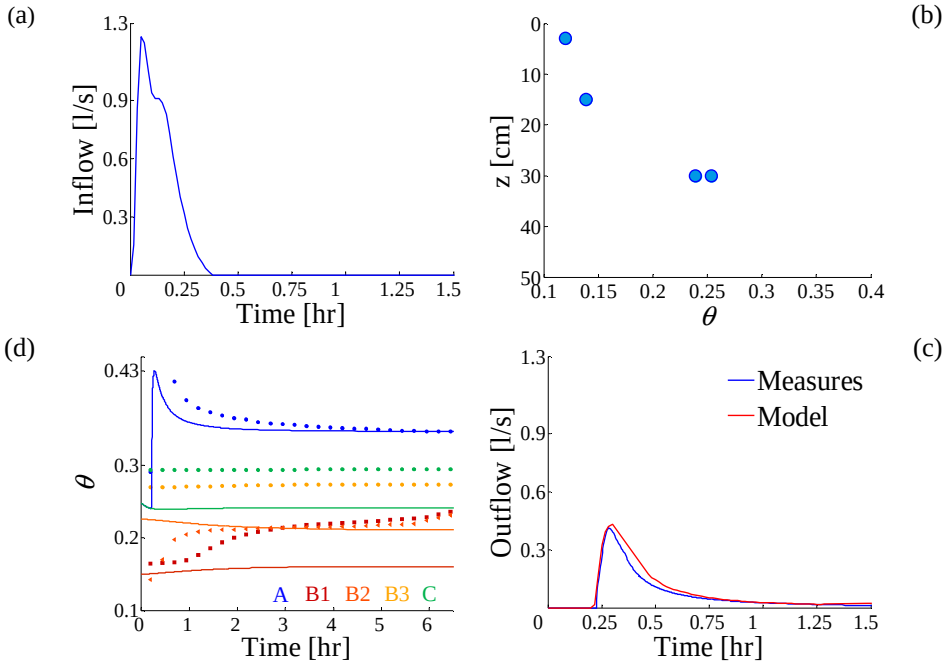

Fig. 72 – Event *l**: (a) Inflow hydrograph, measures; (b) antecedent soil moisture content; (c) Outflow hydrograph, measures and model; (d) Soil moisture time series, measures and model

Tabel 25 - Events *i** and *l** , results : validation of the protocol; *Fd*=field data; *Mod*=model results; *%Rel.err.*=(*Mod-Fd)/Fd*100*

	Outflow volume [m^3]		
	Fd	*Mod*	*%Rel.err.*
*i**	0.452	0.471	0.04
*l**	0.526	0.571	0.09

In case the *Storage index* (Eq. 44) was greater than 1, the overall value of the saturated hydraulic conductivity required by our lumped numerical model was the outcome of (i) the initial conditions of the filter media and (ii) the features of the inflow event (see par. 3.5).
According to our diagnostic analysis, peculiar features of the inflow event, i.e. volume V_{IN} and average intensity $\overline{Q_{IN}}$, could lead to a

lumped value of the saturated hydraulic conductivity either higher or lower than its initial state (see par. 3.5).
The higher the volume and, especially, the longer the event, the higher the increase in soil moisture and, consequently, the higher the reduction of soil water hydrophobicity. Matrix flow was thus enhanced and a decrease in the overall value of the saturated hydraulic conductivity was detected.
The more intense the inflow event, the faster the advance phase, the higher the initial ponding depth, the faster the depletion phase. High hydraulic head values on the soil surface exacerbated the gravity-driven flow through the preferential paths. As a result, an increase of the overall saturated hydraulic conductivity with respect to its soil moisture-driven value (Eq. 43) was detected.
Nevertheless, the overall behavior of the infiltration trench was more sensitive to the averaged intensity than to the total volume of the inflow event.
Keeping in mind these assertions, numerical analysis were performed to point out a mathematical expression for the overall saturated hydraulic conductivity value $k_{s,Large}$ required by our lumped model in case of "large" inflow events. Our efforts yielded to Eq. 46 (Fig. 73; R^2=0.8):

$$\frac{k_{s,Large}}{k_{s,0}} = 0.0326 \cdot \left(\frac{\overline{Q_{IN}}}{Q_{filter,0}} \cdot \frac{k_{s,0}}{k_{s,0}(\theta_{sat})} \right) + 0.1654 \qquad \text{Eq. 46}$$

where $k_{s,0}(\theta_{sat})$ was the representative value of the initial infiltrability at $\theta = \theta_{sat}$, computed by Eq. 43 and introduced here as a reference value.
Numerical efforts pointed out that introducing the inflow volume did not lead to a significative improvement in prognostic performances of Eq. 46.

Many "large" inflow events were modeled in order to validate the proposed protocol.

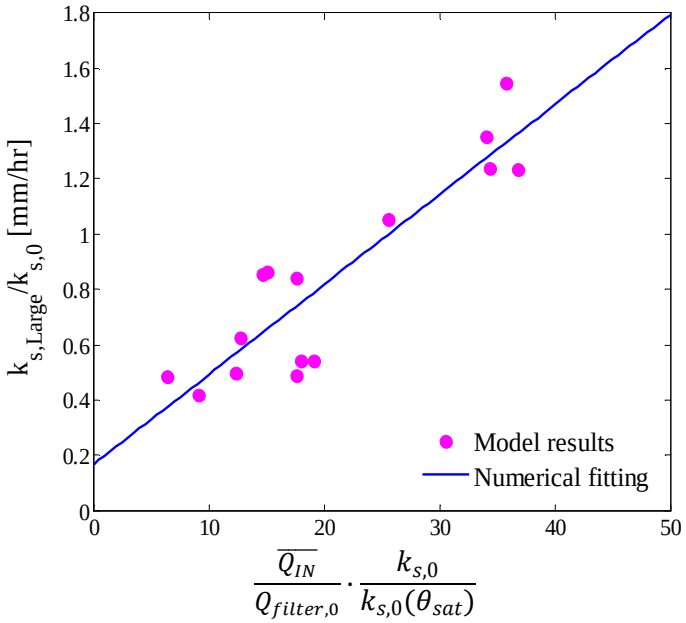

Fig. 73 - "Large" events, bulk value of the saturated hydraulic conductivity as a function of the antecedent soil moisture content

Tabel 26 lists the main features of two representative events *S** and *T** which showed a *Storage Index* greater than 1. The bulk value of the saturated hydraulic conductivity $k_{s,Large}$ was then computed by Eq. 46 Eq. 40 and introduced in the lumped numerical model.
Fig. 74 and Fig.75 (c and d) overlaps measured and modeled outflow and soil moisture values. Tabel 27 compares measured and modeled values of the outflow volume.

Tabel 26 –Events "*S**" and "*T**", main features: validation of the protocol

	Date	V [m^3]	$\bar{Q}_{IN}$ [l/s]	$\bar{\theta}_0$	$k_{s,0}$ [mm/hr]	$Q_{filter,0}$ [l/s]	*S.I.*	$k_{s,Large}$ [mm/hr]
*S**	2010/10/30 h 23:58	9.11	0.969	0.296	152	0.634	1.5	83
*T**	2011/03824 h16:29	9.31	3.465	0.256	239	0.997	3.5	364

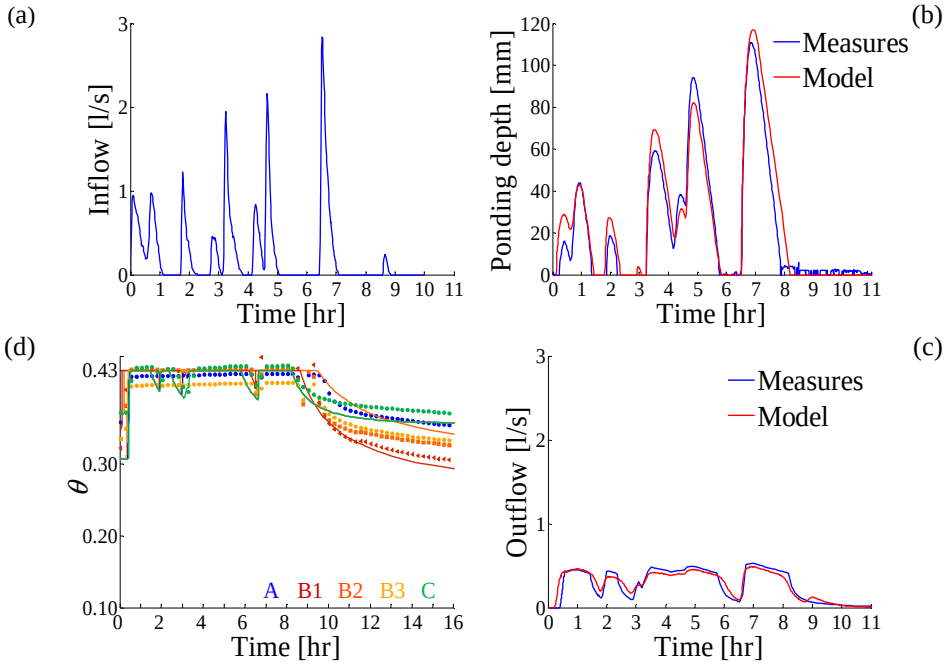

Fig. 74 – Event S*: (a) Inflow hydrograph, measures; (b) Ponding depth time serie, measures and model; (c) Outflow hydrograph, measures and model; (d) Soil moisture time series, measures and model

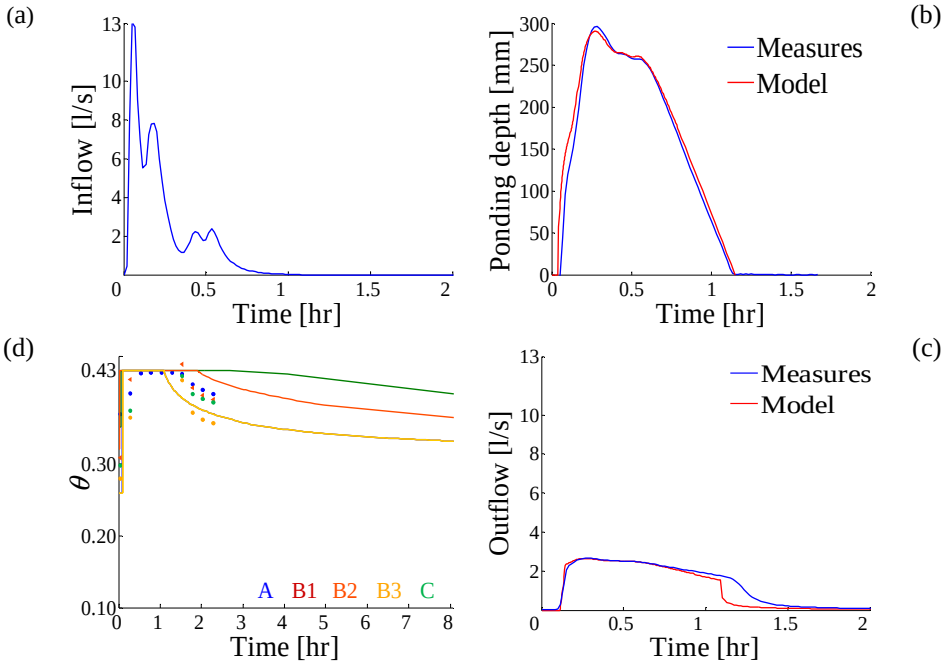

Fig. 75 – Event T*: (a) Inflow hydrograph, measures; (b) Ponding depth time serie, measures and model; (c) Outflow hydrograph, measures and model; (d) Soil moisture time series, measures and model

Tabel 27 - Events *S** and *T** , results : validation of the protocol; ; *Fd*=field data; *Mod*=model results; *%Rel.err.*=(*Mod-Fd)/Fd*100*

	Outflow volume [m^3]		
	Fd	*Mod*	*%Rel.err.*
S*	10.46	11.30	0.08
T*	9.27	7.91	-0.15

Focusing on the practical outcomes of the proposed protocol, a gross evaluation of the accuracy of the complete strategy was achieved by a further analysis of the inflow events for which Eq. 46 showed the largest negative either positive error.
The inflow event F was adequately modeled provided that a overall saturated hydraulic conductivity value equal to 344mm/hr was implemented in our lumped numerical model. The value of 296mm/hr, computed by Eq. 46 , underestimated peak discharge, volume and celerity of the outflow hydrograph.
The inflow event G was adequately modeled provided that an overall saturated hydraulic conductivity value equal to 74mm/hr was implemented in our lumped numerical model. The value of 112mm/hr, computed by Eq. 46, overestimated peak discharge, volume and celerity of the outflow hydrograph.
Absolute and relative errors are listed in Tabel 28.

Tabel 28 - Events F and G , results : validation of the protocol; *Fd*=field data; *Mod*=model results; *%Rel.err.*=(*Mod-Fd)/Fd*100*

	V_{OUT} [m^3]			$Q_{OUT,peak}$ [l/s]			time ($Q_{OUT,peak}$) [min]		
	Fd	*Mod*	*%Rel.err.*	*Fd*	*Mod*	*%Rel.err.*	*Fd*	*Mod*	*%Rel.err.*
F	9.11	8.98	-1.5	2.71	2.12	-22	17	20	18
G	6.98	7.11	1.9	0.65	0.86	32	45	34	-24

Errors in the assessment of the volume of the outflow hydrograph are hidden by the low storage capacity of the biofiltration trench.
Stating the rapid, parsimonious approach selected, overall errors were tolerable and the proposed protocol cost-effectively depicted the hydraulic behavior of the biofiltration facility installed at Monash University.

3.10 Conclusions and further developments

A study on overland and infiltration flows in near horizontal plots was based on the analysis of the hydraulic behavior of the biofiltration facility installed at Monash University (Clayton, Victoria, Australia).
Biofiltration facilities are best management practices for quantitative and qualitative management of stormwater runoff in urban, impervious areas. Basically, they are vegetated infiltration basins that provide a buffer capacity for runoff surges to mimick predevelopment hydrologic conditions of a drainage area while reducing pollutants concentration. Although some field experiences exist, biofilters are usually regarded as black-box systems. Empirical input-output analysis yielded to many, site-specific rules of thumb for design and management purposes. The hydraulic functioning of the system leads its hydrological performances and deeply affects the pollutant removal efficiency.
Consequently, a complete numerical model of the hydraulic behavior of the biofiltration facility is beneficial to

(a) increase system understanding;
(b) provide a valuable prognostic tool to suggest optimal design and maintenance procedures.

The surface surge wave was modeled using the software package WinSRFR (Bautista et al., 2009); subsurface flows were modeled using our originally modified version of the software package Hydrus 2D (Šimůnek et al., 1999). Surface and subsurface flows were coupled implementing the external strategy proposed by Bautista et al., 2010. The numerical protocol here described was completely automated by the implementation of an original Matlab code which allowed to avoid cumbersome, repeated event-specific interactions with the graphical user interfaces provided by WinSRFR and Hydrus packages.
The experience developed during the first phase of this study (Chapter 2) provided appropriate methods for the assessment of the soil parameters of the filter media, and, more specifically, the soil water retention characteristic curve.

Comparative analysis of previous field tests and literature studies yielded to the assessment of the value of the saturated hydraulic conductivity. In particular, issues due to the clogging of the filter media were highlighted.
Field measures recorded from September 2010 to April 2012 provided both input and calibration data.
The results of our numerical model required a deep insight in the peculiar hydraulic behavior shown by the biofiltration trench. Numerical analysis, field observation and literature studies supported the hypothesis of ephemeral hydrophobicity of the filter media. Preferential flow paths are highly common in water repellent soils. Nevertheless, an inverse relationship between soil water content and soil water repellency exists. Based on our numerical analysis and a literature review, two, opposite, flow regimes were diagnosed: (a) unstable, finger flow at very low moisture content values; (b) stable, matrix flow at high, close to saturation, moisture content values. The unstable, finger flow regime is gravity driven; the stable, matrix flow regime is completely described by Richards' equation. A transient regime exist for intermediate soil moisture content values.
Many numerical approaches have been proposed for the modeling of water flow in soils affected by preferential flow paths. Rigorous approaches are based on large computational efforts and require a huge number of parameters, hardly available.
Aiming at a parsimonious, synthetic, yet effective strategy we implemented a lumped model. In particular, we replaced the real, deeply heterogeneous system with an equivalent media encompassing both (a) the time-dependent preferential paths and (b) the soil matrix of the infiltration trench.
This equivalent media was expected to process the inflow hydrographs in the same way as the complex, highly varying real system. Computed outflow hydrographs and average soil moisture content time series had to fit measured data.
According to our analysis, the results of the coupled surface-subsurface numerical model were highly sensitive to the value of the saturated hydraulic conductivity. Partially neglecting its physical character, our simple protocol imposed event-specific bulk values of the saturated hydraulic conductivity.

We then assumed that water flow in the equivalent media could be described with Richards' equation in conjunction with the fictitious value of the saturated hydraulic conductivity.
The bulk value of the saturated hydraulic conductivity had to be adequately changed to account for bidirectional recursive shifts from a preferential flow regime to a matrix flow regime through many transitional regimes.
Soil moisture conditions deeply affected soil water repellency, preferential flow pathways and the flow regime. Antecedent water content of the filter media was a leading parameter. Nevertheless, a further challenge was the modeling of the effects of progressive wetting coupled with the features of the inflow event.
Our analysis yielded to a parsimonious, simple protocol for the assessment of the bulk value of the saturated hydraulic conductivity required by the numerical model.
The overall strategy is based on a few steps:

1) definition of the input data, i.e. (i) the antecedent soil moisture content and (ii) the hydrograph of the inflow event;
2) assessment of the soil water retention curve based on the antecedent soil moisture conditions;
3) assessment of the bulk value of the saturated hydraulic conductivity based on (i) the antecedent soil moisture content; (ii) the volume and the length of the inflow hydrograph (see Eq. 39, 44, 46 in par. 3.6, 3.9);
4) start of the coupled external numerical strategy for surface-subsurface flow computations based on the surface flow package WinSRFR and on an originally modified version of the sub-surface flow package Hydrus 2D.

The 4 steps listed were completely automated in Matlab environment, the only input data required are the (i) antecedent soil moisture content; (ii) the inflow hydrograph; (iii) the geometry of the facility. The protocol was validated trough numerical analysis.
A parsimonious, lumped approach thus proved to adequately model the routing of waves on a spatial and time varying infiltration domain.

Although the proposed protocol was so far employed for the modeling of single events, a short outcoming of this study will be the modeling of the behavior of the infiltration trench during a complete hydrological cycle.

This kind of analysis is beneficial for the definition of optimal design parameters (mainly, geometry, soil type, vegetation type) and management protocols leading quantitative and qualitative treatment of stormwater runoff.
Furthermore, although this protocol was specifically built for the modeling of the biofiltration facility installed at Monash University, the overall strategy is prone to be widely used.

References

Achleitner S., Engelhard C., Stegner U. and Rauch W., 2006, "Local infiltration devices at parking sites. Experimental assessment of temporal changes in hydraulic and contaminant removal capacity", WSUD, Melbourne

Akan, A.O. and Yen, B.C. , 1981, "Mathematical model of shallow water flow over porous media", *Journal of Hydraulic Division*, 107(4), 479-494.

Allaire, SE; Gupta, SC; Nieber, J; et al., 2002, "Role of macropore continuity and tortuosity on solute transport in soils: 1. Effects of initial and boundary conditions", *Journal of Contaminant Hydrology* 58 (3-4), 299-321

Allaire, SE; Gupta, SC; Nieber, J; et al., 2002, "Role of macropore continuity and tortuosity on solute transport in soils:2. Interactions with model assumptions for macropore description", *Journal of Contaminant Hydrology* 58 (3-4), 283-298

Anderson, H., Hoproans E., 1994, "Tomographoy of Soil Water Root Processe, Spec.Publ. 36, *Soil Science Society of America Journal* , Madison,Wis.

Andreu, L., Moreno, F., Jarvis, NJ., 1994," Application of the model macro to water-movement and salt leaching in drained and irrigated marsh soils, marismas, spain ", *Agricultural Water Management* 25(1), 71-88

Annear, T. et al., 2004, "Instream flows for riverine resource stewardship", *Instream Flow Council*, Cheyenne, Wyo.

Archer N., Quintonw , J., Hessw, T., 2002, "Below-ground relationships of soil texture, roots and hydraulic conductivity in two-phase mosaic vegetation in South-east Spain", Journal of Arid Environments (52), 535–553

Asleson, B., Nestingen, R., Gulliver, J et al, 2009, "Performance assessment of rain gardens", Journal of the American Water Resources Association 45(4), 1019-1031

Barber, M. E., King, S. G., Yonge, D. R., and Hathhorn, W. E., 2003, "Ecology ditch: a best management practice for storm water runoff mitigation", Journal of Hydraulic Engineering 8(3), 111-122

Bautista, E.; Zerihun, D.; Clemmens, A. J.; et al., 2010, "External Iterative Coupling Strategy for Surface-Subsurface Flow Calculations in Surface Irrigation" , Journal Of Irrigation And Drainage Engineering-Asce 136, 692-703

Bautista, E.; Clemmens, A. J.; Strelkoff, T. S.; et al., 2009, "Analysis of surface irrigation systems with WinSRFR-Example application", Agricultural Water Management 7, 1162-1169

Bencala,K., Rathbun R., Jackman, P., 1983, "Rhodamine WT dye losses in a mountain stream environment", Water Resources Bullettin 19, 943–950.

Blackwell, P.S., 1993, "Improving sustainable production from water repellent sands", *Western Australia Journal of Agriculture* 34, 160–167.

Bond, R.D., 1969, "The occurrence of water-repellent soils in Australia", *Proceedings of the Symposium on Water-Repellent Soils,* University of California, May 1968..

Bouwer, H.,2002, "Artificial recharge of groundwater: hydrogeology and engineering", Hydrogeology Journal 10, 121–142.

Blecken, G., Zinger, Y., Deletic, A. et al., 2009," Impact of a submerged zone and a carbon source on heavy metal removal in stormwater biofilters", Ecological Engineering 35 (5), 769-778

Braddock R., 2001, "Application of a Soil Water Hysteresis Model to Simple Water Retention Curves", Transport in Porous Media 44, 407–420.

Bratieres, K., Fletcher, T.D., Deletic, A., Zinger, Y., 2008, "Nutrient and sediment removal by stormwater biofilters: a large-scale design optimization study", Water Research, 42(14),3930-3940.

Brooks, R. H. and Corey, A. J.,1964, "Hydraulic Properties of Porous Media", Hydrology Paper 3, Colorado StateUniversity, Fort Collins, CO, pp. 1–27.

Bureau of Meteorology, 2011, "Climate statistics for Australian Locations: monthly climate statistics", data obtained from: Summary Statistics Melbourne Regional Office ww.bom.gov.au/climate/averages/tables/cw_086071.shtml

Burke, J., and Villholth, K., 2007, "Groundwater: a global assessment of scale and significance", in: Molden D. (editor) *Water for Food Water for Life: A Comprehensive Assessment of Water Management in Agriculture*, London: Earthscan, and Colombo: International Water Management institute

Carsel, R; Parrish, R., 1988, "Developing joint probability-distributions of soil-water retention characteristics", Water Resources Research 24(5), 755-769

Castiglione, P.; Mohanty, B. P.; Shouse, P. J.; et al., 2003, "Lateral Water Diffusion in an Artificial Macroporous System: Modeling and Experimental Evidence", *Vadose Zone Journal* 2(2), 212-221

Celia, M; Bouloutas, E; Zarba, R., 1990, "A general mass-conservative numerical-solution for the unsaturated flow equation", Water Resources Research 26 (7), 1483-1496

Chen, C., Wagenet, R.J., 1992, "Simulation of water and chemicals in macropore soils. Part 1. Representation of the equivalent macropore influence and its effect on soil water flow", *Journal of Hydrology* 130, 105–126.

Chua, L., Zhong, Q., 2007, Negative Resistance Curve Tracer, Part II: Manual (M84/53)

Church, M., 1974, "Electrochemical and fluorometric tracer techniques for streamflow measurements", Tech. Bull. 12, Br.Geomorphol. Res. Group, Geo Abstracts Ltd., Univ. of East Anglia, Norwich, UK

Clothier, B., Green, S., Katou, H., 1995, "Multidimensional infiltration - points, furrows, basins, wells, and disks", 59th

Annual Meeting of the Soil Science Society of America, St Louis, MO, oct 29-nov 03, 1995, *Soil Science Society Of America Journal* 59(2), 286-292

Coppola, A.; Gerke, H.; Comegna, A. et al., 2012, "Dual-permeability model for flow in shrinking soil with dominant horizontal deformation", *Water Resources Research* 48(8)

Daly, E., Zinger, Y., Deletic,A., Fletcher, T., 2009, "A possible mechanism for soil moisture bimodality in humid-land environments", Geophysical Research Letters, 36, L07402,

Davis, S. N., G. M. Thompson, H. W. Bentley, and G. Stiles, 1980, "Ground-water tracers—A short review", *Ground Water* 18, 14–23

Davis, A. P., Shokouhian, M., Sharma, H., and Minami, C., 2001, "Laboratory study of biological retention for urban storm water management", Water Environment Research 73 (1), 5-14

Davis, A. P., Shokouhian, M., Sharma, H., Minami, C., and Winogradoff, D., 2003, "Water quality improvement through bioretention: Lead, copper, and zinc removal", Water Environment Research 75 (1), 73-75

Davis, A. P., and McCuen, R. M., 2005, "Stormwater management for smart growth ", Springer, New York.

Davis P., 2007, "Field performance of bioretention: Water quality", Environmental Engineering Sci., 24 (8), 1048-1063

Davis P., 2008, "Field Performance of Bioretention: Hydrology Impacts", Journal of Hydrologic Engineering 13 (2), 90-95

Dekker, L.W., Ritsema, C.J., Oostindie, K., Boersma, O.H., 1998, "Effect of drying temperature on the severity of soil water repellency", Soil Science 163(10) , 780–796.

Dietz, M. , 2007, "Low impact development practices: a review of current research and recommendations for future directions" , Water, Air, Soil Pollution 186(1– 49, 351–363.

Dietz, M. E., and Clausen, J. C., 2005, "A field evaluation of rain garden flow and pollutant treatment" , Water, Air, Soil Pollution 167, 123–138.

Dietz, M. E., and Clausen, J. C., 2006, "Saturation to improve pollutant retention in a rain garden", *Environ. Sci. Technol*. , 40, 1335–1340.

Doerr, S., Shakesby, R., 2000, "Soil water repellency: its causes, characteristics and hydro-geomorphological significance", *Earth-Science Reviews* 51, 33–65

Doerr, S.H. and Thomas, A.D., 2000, "The role of soil moisture in controlling water repellency: new evidence from forest soils in Portugal", *Journal of Hydrology* 231, 134-147

Durner, 1994, "Hydraulic conductivity estimation for soils with heterogenous pore structure", *Water Resources Research* 30, 211–224.

Ela, S., Gupta, S., Rawls, W., 1992, "Macropore and surfaces interactions affecting water infiltration into soil, *Soil Science Society American Journal* 56, 714-721, 1992

Elkins, C., Vansickle, K., 1986, "A tillage concept to enhance soil productivity", *Soil & Tillage Research* 8 (1-4), 375-376

FAWB, 2010. "Adoption Guidelines for Stormwater Biofiltration Systems", Facility for Advancing Water Biofiltration, Melbourne, Australia.

Feng, M. and Fredlund, D.G. ,1999, " Hysteretic influence associated with thermal conductivity sensor measurements", in Proceedings from Theory to the Practice of Unsaturated Soil Mechanics in Association with the 52nd Canadian Geotechnical Conference and the Unsaturated Soil Group, Regina, Sask., 23–24 October 1999. pp. 14:2:14–14:2:20.

Flury, M., Wai, N., 2003, "Dyes as tracers for vadose zone hydrology", *Reviews of Geophysics* 41, 1/1002

Gardenas, A., Šimůnek, J., Jarvis, N., et al, 2006, "Two-dimensional modelling of preferential water flow and pesticide transport from a tile-drained field ", *Journal of Hydrology*, 23 (3-4), 647-660

Gaspar, E., and M. Oncescu, 1972, "Radioactive Tracers in Hydrology", *Elsevier Sci*., New York

Gerke, H.H., van Genuchten, M.T., 1993, "A dual-porosity model for simulating the preferential movement of water and solutes in structured porous media", *Water Resources Research* 29, 305-319.

Gerke, H.H., van Genuchten, M.T., 1993, "Evaluation of a first order water transfer term for variably saturated dual-porosity flow models", *Water Resources Research* 29, 1225–1238.

Gerke, H.H., van Genuchten, M.Th., 1996, "Macroscopic representation of structural geometry for simulating water and solute movement in dual-porosity media", *Advances in Water Resources*, 19, 343– 357.

Germann, P.F., 1985, "Kinematic wave approach to infiltration and drainage into and from soil macropores", *Trans. ASAE* 28, 745-749.

Germann, P.F., Beven, K., 1985, "Kinematic wave approximation to infiltration into soils with sorbing macropores", *Water Resources Research* 21 (7), 990–996.

Govindaraju, R.S., Jones, S.E. and Kavvas, M.L., 1988, "On the diffusion wave model for overland flow 1. Solution for steep slopes" *Water Resources Research*, 24(5), 734- 744.

Govindaraju R.S., Kavvas M.L., 1991, "Dynamics of Moving Boundary Overland Flows Over Infiltrating Surfaces at Hillslopes", *Water Resources Res*earcgh 27, 1885-1898

Greco, R., 2002, "Preferential flow in macroporous swelling soil with internal catchment: model development and applications", *Journal of Hydrology* 269 (3-4), 150-168

Gwo, J.P., Jardine, P.M., Wilson, G.V., Yeh, G.T., 1995, "A multiple-pore-region concept to modeling mass transfer in subsurface media". *Journal of Hydrology* 164, 217–237.

Kastanek, F., 1971, "Numerical simulation technique for vertical drainage from a soil column", Journal of Hydrology 14 , 213-232

Hatt, B., Fletcher, T., Deletic, A., 2009, "Hydrologic and pollutant removal performance of stormwater biofiltration systems at the field scale" , *Journal of Hydrology* 365(3-4), 310-321

Hatt, E.; Fletcher, D.; Deletic, A., 2007, "Hydraulic and pollutant removal performance of stormwater filters under variable wetting and drying regimes" , *Water Science and Technology* 56(12), 11-19

Hogarth, W.L., Hopmans, J., Parlange, J.Y., and Haverkamp, R., 1988, "Application of a simple soil–water hysteresis model", Journal of Hydrology 98, 21–29.

Holzhey, C.S., 1969, "Water-repellent soils in southern California", *Proceedings Symposium Water-Repellent Soils*, University of California, May 1968. pp. 31–42.

Hopmans, JW; Šimůnek, J; Bristow, KL, 2002, "Indirect estimation of soil thermal properties and water flux using heat pulse probe measurements: Geometry and dispersion effects", Water Resources Research 38(1), 1006-1013

Hromadka T.V., Lai C., 1985, "Solving the two-dimensional diffusion flow model", *Proceedings of the Specialty Conf. sponsored by the Hydraulics Div ASCE*, Lake Buena Vista, Fl, Aug 12-19

Hunt, W. F., Jarrett, A. R., Smith, J. T., and Sharkey, L. J., 2006, . "Evaluating bioretention hydrology and nutrient removal at three field sites in North Carolina", *Journal of Irrigation and Drainage Engineering* 132(6), 600– 608.

Hunt, W. F., Smith, J. T., Jadlocki, S. J., Hathaway, J. M., and Eubanks, P. R . , 2008, "Pollutant removal and peak flow mitigation by a bioretention cell in urban Charlotte, NC." , *Journal of Environmental Engineering*, 134, 403–408.

Jarvis, N.J., 1994. "The MACRO Model (Version 3.1). Technical Description and Sample Simulations. Reports and Dissertations", Department of Soil Science, Swedish University of Agricultural Science, Uppsala, Sweden, p. 51.

Kaufman, W. J., and G. T. Orlob, 1956, "An evaluation of groundwater tracers", *Eos Trans. AGU* 37, 297–306

Kasnavia, T., D. Vu, and D. A. Sabatini, 1999, "Fluorescent dye and media properties affecting sorption and tracer selection" , *Ground Water* 37, 376–381

Katterer, T., Schmied, B., Abbaspour, K.C., Schulin, R., 2001, "Single and dual-porosity modelling of multiple tracer transport through soil columns: effects of initial moisture and mode of application", *European Journal of Soil Science*, 52, 1–12.

King, P.M., 1981, "Comparison of methods for measuring severity of water repellence of sandy soils and assessment of some factors that affect its measurement", *Australian Journal of Soil Research* 19, 275–285.

Köhne, J.M., Gerke, H.H., 2005, "Spatial and temporal dynamics of preferential bromide movement towards a tile drain". *Vadose Zone Journal* 4, 79–88.

Kodesova, R.; Kodes, V.; Mraz, A., 2011, "Comparison of Two Sensors ECH2O EC-5 and SM200 for Measuring Soil Water Content", *Soil and Water Research* 6 (2), 102-110

Langergraber, G., Haberl, R., Laber, J., Pressi, A., 2003, "Evaluation of substrate clogging processes in vertical flow constructed wetlands", *Water Science and Technology*, 48 (5), 25-34.

Larsson, M.H., Jarvis, N.J., 1999, "Evaluation of a dual-porosity model to predict field-scale solute transport in a macroporous soil", *Journal of Hydrol*ogy 215, 153–171.

Larsson, M.H., Jarvis, N.J., 1999, "A dual-porosity model to quantify macropore flow effects on nitrate leaching", *Journal of Environmental Quality* 28, 1298–1307.

Le Coustumer, S., Fletcher, T.D., Deletic, A., Barraud, S., Lewis, J.F., 2009, "Hydraulic performance of biofilter systems for stormwater management: influences of design and operation", *Journal of Hydrology*, 376 (1-2), 16-23.

Le Coustumer, S., Fletcher, T., Deletic, A. et al, 2012, "The influence of design parameters on clogging of stormwater biofilters: a large-scale column study ", *Water Research* 46(20), 6743-6752

Letey, J., 1969, "Measurement of contact angle, water drop penetration time, and critical surface tension", *Proceedings of the Symposium on Water-Repellent Soils*, University of California, May 1968, pp. 43–47.

Levenberg, K., 1944, "A Method for the Solution of Certain Non-Linear Problems in LeastSquares", *The Quarterly of Applied Mathematics* 2, 164-168

Lewis, J., Hatt, A., Deletic, T., Fletcher, T., 2008, The impact of vegetation on the hydraulic conductivity of stormwater biofiltration systems", *11th International Conference on Urban Drainage*, Edinburgh, Scotland, UK

Li, H., Sharkey, L., Hunt, W., Davis, A., "Mitigation of impervious surface hydrology using bioretention in North Carolina and Maryland", *Journal of Hydrologic Engineering* 14:407-415.

Liakopoulos, C., "Theoretical solution of the gravity drainage problem", J. Hydraulic Reearch. 2 , 50-74

Lin, W., Gray, D.M. and, Norum, D.I., 1973, "Hydrodynamics of laminar flow over a porous bed", *Water Resources Research*, 9(6), 1637-1644.

Lindsey, G., Roberts, L., Page, W., 1992,"Inspection and maintenance of infiltration facilities", *Journal of Soil and Water Conservation*, 47 (6), 481-486.

Luxmoore, R.., Jardine, J., Wilson, G., Jones, J., and Zelanzy, L., 1990, "Physicaal and chemical controls of preferred path flow through a forested hillslope", 4 *Geoderma* 4(6), 139-154.

MacRae, C. (1992). "The role of moderate flow events and bank structure in the determination of channel response to urbanization." Proc., 45th Annual Conf. of Canadian Water Resources Association, Shrubsole, N.Y., 2.1–12.21.

MacRae, C. (1993). "An alternate design approach for the control of in-stream erosion potential in urbanizing watersheds." Proc., 6th

Int. Conf. on Urban Storm Drainage, H. C. Torno, ed., Vol. 2, Niagara Falls, Ontario, Canada, 1086–1098.

Maqsoud, A., Bussière , B., Mbonimpa, M., 2004, " Hysteresis effects on the water retention curve: a comparison between laboratory results and predictive models", 57th Canadian Geotechnical Conference, 24-27 October 2004, Quebec City, Quebec

McCuen, R. H., 2003, "Smart growth: Hydrologic perspective" , *Journal of Professional Issues in Engineering Education and Practice* , 129 (3), 151–154.

McLaughlin, M. J., 1982, "A review on the use of dyes as soil water tracers", *Water SA* 8, 196–201

Melbourne Water, 2005, "Water Sensitive Urban Design (WSUD) Engineering Procedures: Stormwater", chapter 6: Bioretention basins. CSIRO Publishing, Melbourne, Australia.

Mikulla, C; Einsiedl, F; Schlumprecht, C; et al., 1997, Sorption of uranine and eosine on an aquifer material containing high organic carbon", 7th International Symposium on Water Tracing Portoroz, Slovenia Date: May 26-31, 1997

Mohanty, B.P., Bowman, R.S., Hendrickx, J.M.H., van Genuchten, M.Th., 1997, "New piecewise-continuous hydraulic functions for modeling preferential flow in an intermittent flood-irrigated field", *Water Resources Research* 33, 2049–2063.

Morgan, R.P.C., Quinton, J.N. & Edwards, J. (1995), "Vegetation strategies for combating desertification", MEDALUS II Project 3 Managing Desertification. Contract EV5V-CT920165. Final Report .

Mualem, Y. , 1977, "Extension of the similarity hypothesis used for modeling the soil water characteristics", *Water Resources Research* 13, 773–780.

Mualem, Y. 1984, "Prediction of the soil boundary wetting curve", *Journal of Soil Science* 137, 379–390.

Mualem, Y. 1984, "A modified dependent domain theory of hysteresis", *Journal of Soil Science* 137, 283–291.

Panguluri, S; Jennings, A., 1994, "A software package to calibrate preferential flow models", *Environmental Software* 9 (4), 233-245

Parker, G., 1973, "Tests of Rhodamine WT dye for toxicity", *J. Res. U.S. Geological Survey* 1, 499.

Parlange, J.-Y, 1976, "Capillary hysteresis and the relationship between drying and wetting curves", *Water Resources Research* 12, 224–228

Paul, MJ; Meyer, JL, 2001, "Streams in the urban landscape", *Annual Review Of Ecology And Systematics*

Pham, Q.H., Fredlund, D.G., and Barbour, S.L. , 2003, "A practical hysteresis model for the soil-water characteristic curve for soils with negligible volume change", *Géotechnique* 53, 293–298.

Philipp, A., Schmitz, G. H., and Liedl, R. (2010). "An analytical model of surge flow in non-prismatic permeable channels and its application in arid regions", *Journal of Hydraulic Engineering*, 136(5), 290–298.

Philipp, A.; Liedl, R., Woehling, T., 2012, "Analytical Model of Surface Flow on Hillslopes Based on the Zero Inertia Equations", *Journal of Hydraulic Engineering* 138 (5), 391-399

Quinton, J.N., 1996, "Influence of plant roots on infiltration, water redistribution and water use", Mediterranean Desertification and Land Use. MEDALUS III. Contract EVN4CT95-0115 First Annual Report.

Read, J., Wevill, T., Fletcher, T., Deletic, A., 2008, "Variation among plant species in pollutant removal from stormwater in biofiltration systems", *Water Research* 42, 893-902.

Richards, L.A., 1931, "Capillary conduction of liquids through porous media", *Physics* 1, 318-333.

Rigon, R., G. Bertoldi, and T. M. Over , 2006, "GEOtop: a distributed hydrological model with coupled water and energy budgets", *Journal of Hydrometeorology* 7, 371–388.

Sabatini, D. A., and T. A. Austin, 1991, "Characteristics of Rhodamine WT and Fluorescein as adsorbing ground-water tracers", *Ground Water* 29, 341–349

Sansalone, J., and Teng, Z., 2004, "In situ partial exfiltration of rainfall runoff. I: Quality and quantity attenuation", *Journal of Environmental Engineering* 130 (9), 990-1007

Sansalone, J., and Teng, Z., 2005, "Transient rainfall-runoff loadings to a partial exfiltration system: Implications for urban water quantity and quality", *Journal of Environmental Engineering* 131 (8), 1155-1167

Schaap, M.G., F.J. Leij, & M.Th. Van Genuchten, 1998, "Neural network analysis for hierarchical prediction of soil hydraulic properties", *Soil Science Society American Journal* 62, 847-855.

Schneebeli M., Sokratov S., 2004. "Tomography of temperature gradient metamorphism of snow and associated changes in heat conductivity", *Hydrological Processes Journal* 18:3655–3665

Schueler, T.R., Kumble, P.A., Heraty. M.A., 1992., "A current assessment of urban best management practices, techniques for reducing non-point source pollution in the coastal zone" , Metropolitan Washington Council of Governments, Washington DC.

Scott, P.S., Farquhar, G.J., and Kouwen, N. ,1983, " Hysteretic effects on net infiltration", Advances in infiltration. *American Society of Agricultural Engineers Publication* 11-83, St. Joseph, Mich. pp. 163–170

Shah T., 2007, "The groundwater economy of South-Asia: an assessment of size, significance and socio-ecological impacts", In: Giordano M, Villholth KG (eds) The agricultural groundwater revolution: opportunities and threat to development. CABI, Wallingford, pp 7–36

Shiklomanov, I., 1993, "World fresh water resources" in Peter H. Gleick (editor), *Water in Crisis: A Guide to the World's Fresh Water Resources* (Oxford University Press, New York).

Si,B. C. , Kachanoski, R. G., 2000, "Unified solution for infiltrationand drainage with hysteresis; theory and field test", *Soil Science Society American Journal* 64, 30–35.

Šimůnek, J., Kodesova, R., Gribb , M., van Genuchten, M., 1999, "Estimating hysteresis in the soil water retention function from cone permeameter experiments", *Water Resources Research* 35 (5), 1329–1345

Šimůnek, J., Van Genuchten, M., 1999, "The HYDRUS-2D software package for simulating two-dimensional movement of water, heat, and multiple solutes in variably-saturated media, version 2.0", *Rep. IGWMC-TPS-53, 251 pp., Int. Ground Water Model. Cent., Colo. Sch. of Mines, Golden.*

Šimůnek, J., Jarvis, N.J., van Genuchten, M.Th., Gardenas, A., 2003, "Review and comparison of models for describing non equilibrium and preferential flow and transport in the vadose zone", *Journal of Hydrology*, 272, 14–35.

Šimůnek, J. and van Genuchten, M. Th., 2012, "The Dual Perm Module for HYDRUS (2D/3D). Simulating Two-Dimensional Water Movement and Solute Transport in Dual-Permeability Porous Media, Version 1.0", PC Progress, Prague, Czech Republic, 32 pp., 2012.

Singh, P., Kanwar, R., and Thompson, M., 1991, "Macropore characterization for two tillage systems using resin-impregnatio technique", *Soil Science Society of America Journal*, 55, 1674-1679

Singh, P., Kanwar, R., and Thompson, M., 1991, "Measurement and characterization of macropores by using AUTOCAD and automatic image analysis", *Journal of Environmental Quality*, 20, 289-294

Smart, P, Laidlaw N., 1977, "An evaluation of some fluorescent dyes for water tracing" , *Water Resources Research* 13,15–33.

Schmitz, G. H., Liedl, R., and Volker, R. (2002). "Analytical solution to the zero-inertia problem for surge flow phenomena in non-prismatic channels." *J. Hydraul. Eng*., 128(6), 604–615.

Schmitz, G. H., and Seus, G. (1990). "Mathematical zero-intertia modeling of surface irrigation: Advance in borders." *J. Irrig. Drain. Eng.*, 116(5), 603–615.

Schmitz, G. H., and Seus, G. (1992). "Mathematical zero-intertia modeling of surface irrigation: Advance in furrows." *J. Irrig. Drain. Eng.*, 118(1), 1–18.

Smith, R.E. and Woolhiser, D.A., 1971, "Overland flow on an infiltrating surface". *Water Resources Research* 7(4), 899-913

Steenhuis, T. S., Boll, J., Shalit, G., Selker, J. S., and Merwin, I. A., 1994, ''A simple equation for predicting preferential flow solute concentrations", *Journal of Environmental Quality*, 23, 1058–1064.

Sunada, K. and Hong, T.F., 1988, "Effects of slope conditions on direct runoff characteristics by the interflow and overland flow model", *Journal of Hydrology*, 102, 323-334

Tayfur, G., Kavvas, M.L., Govindaraju, R.S. and Storm, D.E., 1993, "Applicability of St. Venant equations for 2-D overland flow over rough infiltrating surfaces", *Journal of Hydraulic Engineering*, 119(l), 51-63

Taylor, R.; Scanlon, B.; Rodell, M et al., 2012 Ground water and climate change. *Nature Climate Change*, 1-8.

Todini, E., Venutelli, M., 1991, "Overland flow: A two-dimensional modeling approach", *Recent Advances in the Modeling of Hydrologic System*. Kluwer Academic Publishers, The Netherlands, pp. 153-166

Topp, G. C., 1969, "Soil-water hysteresis measured in a sandy loam and compared with the hysteretic domain model", *Soil Science Society American Processes* 33, 645–65

Topp, G; Zebchuk, W; Dumanski, J, 1980, "The variation of insitu measured soil-water - properties within soil map units", *Canadian Journal Of Soil Science* 60(3), 497-509

Tschapek, M., 1984, "Criteria for determining the hydrophilicity of soils", *Zeitschrift fur Pflanzenernaehrung und Bodenkunde* 147, 137–149.

United States Department of Agriculture-Soil Conservation Service USDA-SCS, 1986, "Urban hydrology for small watersheds" , *Technical Release No. 55* , Washington, D.C.

U.S. Environmental Protection Agency (USEPA), 1996 , "Managing urban runoff", EPA 841-F-96-004G

VanDerMolen, W., Torfs,P., DeLima, J., 1995, "Water depths at the upper boundary for overland-flow on small gradients", *Journal of hydrology* 17(1-2), 93-102

Van Genuchten, M. Th., 1980, "A closed form equation for predicting the hydraulic conductivities of unsaturated soils", *Soil Science Society American Journal* 44, 892–898.

Viaene, P., Vereecken, H., Diels, J., and Feyen, J. , 1994, "A statistical analaysis of six hysteresis models for the moisture retention characteristic", *Journal of Soil Science* 157, 345–355.

Vogel, T., K. Huang, R. Zhang, and M. T. van Genuchten, 1996, "The HYDRUS code for simulating one-dimensional water flow, solute transport, and heat movement in variably-saturated media, version 5.0", *Res. Rep. No 140*, U.S. Salinity Lab., U.S. Dep. of Agric., Riverside, Calif., 1996.

Vogel, T., Cıslerova, M., 1988, "On the reliability of unsaturated hydraulic conductivity calculated from the moisture retention curve", *Transport in Porous Media* 3, 1–15.

Wallis, M.G., Horne, D.J., 1992, "Soil water repellency" , Advances in Soil Science, Vol. 20 Springer, New York, pp. 91–146.

Wallis, M.G., Scotter, D.R., Horne, D.J., 1991, "An evaluation of the intrinsic sorptivity water repellency index on a range of New Zealand soils", *Australian Journal of Soil Resear*ch 29, 353–362.

Wang, L., Lyons, J., Kanehl, P., and Bannerman, R. ,2001, "Impacts of urbanization on stream habitat and fish across multiple spatial scales" , *Journal of Environmental Planning and Management*, 28 (2), 255–266.

Williams, R. T., and J. W. Bridges, 1964, "Fluorescence in solution", *J. Clin. Pathol*. 17, 371–394

Wilson, J. T., L. E. Leach, M. Henson, and J. N. Jones,1986, " In situ biorestoration as a ground water remediation technique", *Ground Water Monitoring Review* 6,56–64

Winter, K.-J., Goetz, D., 2003, "The impact of sewage composition on the soil clogging phenomena of vertical flow constructed wetlands.", *Water Science and Technology* 48 (5), 9–14.

Whisler , F., Watson K., 1968, "One-dimensional gravity drainage of uniform columns of porous materials", *Journal of Hydrology* 277

Wöhling, T., Singh, R., and Schmitz, G. H. (2004). "Physically based modeling of interacting surface-subsurface flow during furrow irrigation advance", *J. Irrig. Drain. Eng*., 130(5), 349–356.

Wöhling, Th.; Froehner, A.; Schmitz, G. H.; et al., 2006, "Efficient solution of the coupled one-dimensional surface - Two-dimensional subsurface flow during furrow irrigation advance", *Journal of Irrigation and Drainage Engineering* 132(4), 380-388

Wöhling, Th.; Mailhol, J. C., 2007,"Physically based coupled model for simulating 1D surface-2D subsurface flow and plant water uptake in irrigation furrows. I: Model development", *Journal of Irrigation and Drainage Engineering*, 6: 538-547

Wong, T.H.F., Fletcher, T.D., Duncan, H.P., Jenkins, G.A., 2006, "Modelling urban stormwater treatment – a unified approach", *Ecological Engineering* 27 (1), 58–70

Zinger, A., Deletic, T. and Fletcher, D. , 2007, "The effect of various intermittent dry-wet cycles of nitrogen removal capacity in biofilter systems", *13th International Rainwater Catchment Systems Conference and 5th International Water Sensitive Urban Design Conference*, Sydney, ustralia, 21–23 August 2007.

Zisman, W.A., 1964, "Relation of the equilibrium contact angle to liquid and solid constitution", Gould, R.F. Ed., *American Chemical Society. Advances in Chemistry Series* Vol. 43, 1–51.